Reactor Support Structure

Yankee Nuclear Power Station
Structural Analysis Report

For: Yankee Atomic Electric Company
By: Cygna Energy Services

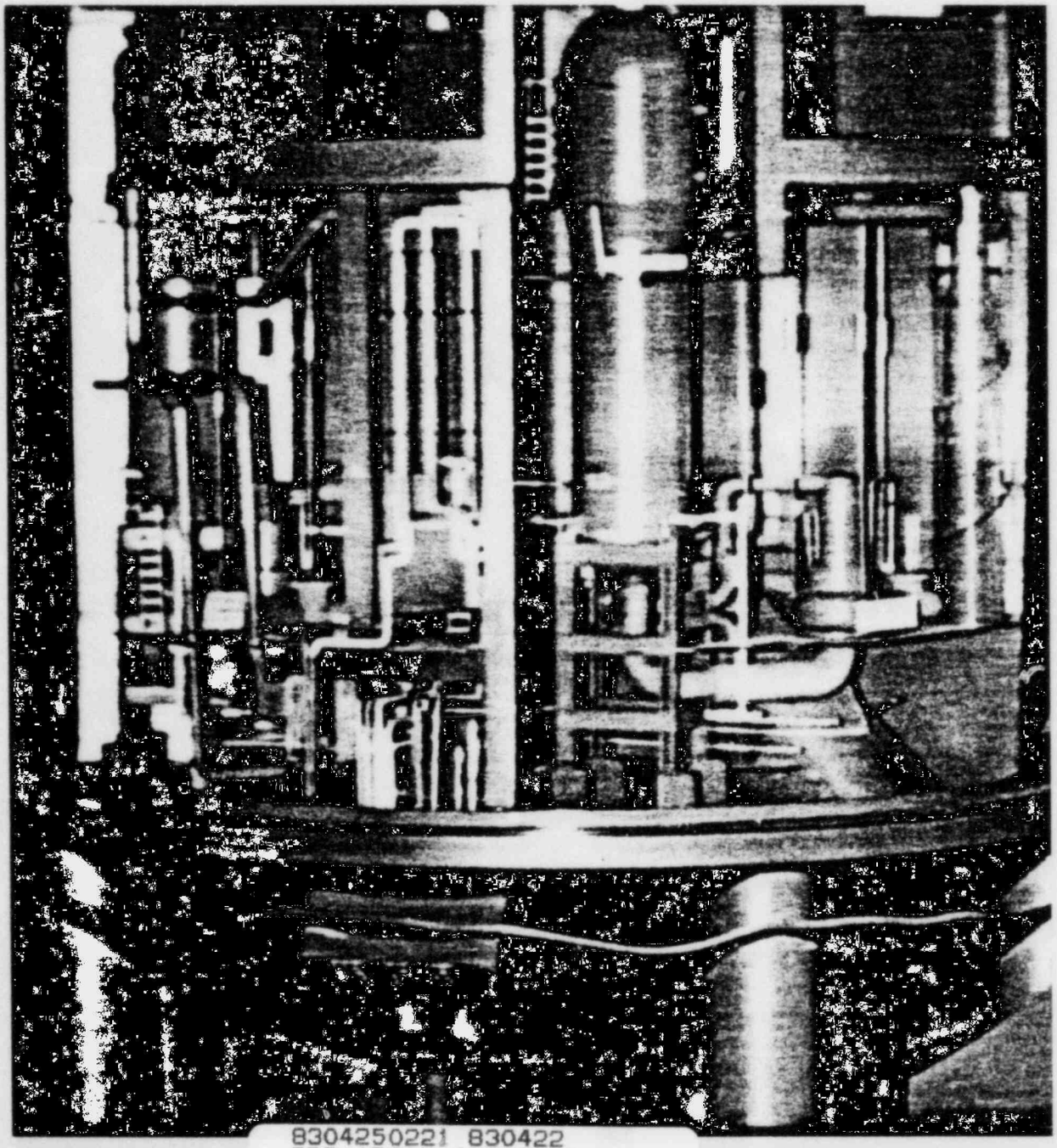

March 1983 Rev. 3

Job No. 80023
Report No. EY-YR-80023-6
March, 1983
Rev. 3

Seismic Analysis of Reactor Support Structure

Yankee Nuclear Power Station

Rowe, Massachusetts

Prepared by: Tsan-yuan Wang
T. Y. Wang

Prepared by: Bilgin Atalay
Bilgin Atalay

Reviewed by: J. Vallenas 3/8/83
Jose Vallenas

Approved by: Eric van Stijgeren
Eric van Stijgeren

Job No. 80023
Report No. EY-YR-80023-6
March, 1983
Rev. 3

Seismic Analysis of Reactor Support Structure

Yankee Nuclear Power Station

Rowe, Massachusetts

Prepared by: Tsampean Wang
T. Y. Wang

Prepared by: Bilgin Atalay
Bilgin Atalay

Reviewed by: J. Vallenas 3/8/83
Jose Vallenas

Approved by: Eric van Stijgeren
Eric van Stijgeren

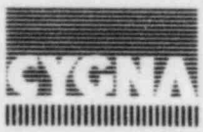

TABLE OF CONTENTS

TABLE OF CONTENTS (cont'd.)

APPENDICES

I. EXECUTIVE SUMMARY

I.1 Purpose

The purpose of this report is to summarize the results of the structural analyses performed by Cygna Energy Services* (Cygna) for Yankee Atomic Electric Company (YAEC). The results described in this report pertain to the Reactor Support Structure (RSS) at the Yankee Nuclear Power Station (YNPS) at Rowe, Massachusetts.

I.2 Scope

As requested by YAEC, Cygna has performed detailed structural analyses of the RSS. These analyses were based on the following input data for YNPS:

- Existing structural drawings (See Appendix A)
- Design Criteria (See Section III)
- Seismic ground motion (See Appendix C)

I.3 Conclusion

The RSS with the six newly installed steel collars can withstand Yankee Composite Spectra. Under NRC response spectra, the columns and ring foundaton of the RSS will yield. However, the results of nonlinear time history analyses on the RSS indicate that the structure as built can functionally withstand the NRC spectrum. The steel collars have sufficient strength to comply with the performance criteria described in Chapter III.

*Cygna Energy Services is the new name for EES, Inc.
Ownership, philosophy and staffing of the firm remains the same.

II. DESCRIPTION OF STRUCTURE

The RSS is constructed of reinforced concrete and consists of two concentric cylinders supported by six exterior columns and two interior columns as shown in Figs. A.1 through A.8. The total height of the structure is 122'-5" and its weight is calculated to be 26860 kips.

The two cylinders are connected at the base by a semi-conical slab 5'-0" thick. The outer cylinder is 82'-6" in diameter, 77'-0" in height and its wall thickness is 5'-0" for the lower half and 2'-0" for the upper half. The inner cylinder is 28'-6" in diameter, 55'-6" in height and its wall thickness is 5'-0" for the lower half and 4'-6" for the upper half. In addition to the 5'-0" base slab, these two cylinders are connected by six radial walls with thicknesses ranging from 1'-6" to 5'-0" (Fig. A.2). Since these walls were primarily designed as radiation shields, their load resistance capacity exceeds the requirement by a wide margin. For this reason, the cylindrical part of the structure is considered rigid in the analyses.

The exterior columns are 7'-0" in diameter and they are supported by a ring foundation as shown in Figs. A.1 and A.5 through A.8. These columns have a steel shell which is 3/8" thick and are connected to the upper cylindrical structure through 44 - #14 dowels. The embedment lengths of the #14 dowels at the base of the upper structure range from 2'-6" to 3'-6". The 3/8" thick shell is welded to a 3" thick baseplate which is in turn connected to the foundation through twelve 1-1/4" bolts (Fig. A.8). Since the capacity of the baseplate-to-foundation connection is much weaker than that of the column, it has been strengthened by a steel collar as shown in Fig. A.9. The ring foundation is 7'-0" thick and its inside radius and outside radius are 30'-3" and 43'-3", respectively.

The interior columns are 7'-6" in diameter and are supported by a 43'-0" x 43'-0" x 8'-6" mat foundation as shown in Figs. A.1 and A.5 through A.8.

These columns are covered by 1/2" thick steel shells and are connected to the base of the upper cylindrical structure through 64 - #14 dowels. The embedment lengths of the #14 dowels range from 2'-7" to 3'-2". The interior columns have the same baseplate-to-foundation connection as the exterior columns.

III. PERFORMANCE CRITERIA

III.1 Materials

The ultimate compression strength of the concrete is 4 ksi for the upper structure and columns and 3 ksi for the foundations. The yield stress of all the reinforcing bars is 40 ksi and that of the steel shell is 32 ksi.

The 2'-6" embedment length of the #14 dowels is less than the 4'-6" development length specified by Section 2612(f) of 1979 UBC for 40 ksi reinforcing steel. The adequacy of the shorter development length will be thoroughly investigated in Section V.7.

The allowable soil bearing pressure is 20 ksf as specified by client documentation [17].

III.2 Earthquake Loadings

The RSS is analyzed for two earthquake spectra, Yankee Composite Spectra (YCS) and NRC Spectra (Fig. C.1). For linear elastic analysis, the critical damping ratios selected for YCS and NRC spectra are 7% and 10%, respectively, as per Ref. 1. The acceleration values at the fundamental frequencies of the structure are shown in Table C.1.

The nonlinear time-history analyses of the RSS were performed only for NRC spectra. The critical damping ratio used in the analyses was conservatively selected as 7% and 10%. For more on the choice of damping ratios used, see Section V.3.

III.3 Combination of Earthquake Directional Components

The RSS is required to be evaluated for the earthquake ground motions applied simultaneously in two perpendicular horizontal directions and the vertical direction. The earthquake ground motions are assumed to be stochastically independent. It is unlikely that the peak acceleration of these ground motions will occur at the same time. To deal with this problem, Newmark and Hall [2] recommend that the direction effects be combined by taking 100% of the effects due to motion in one direction and 40% of the effects from the two remaining principal directions of motion. If the two horizontal load components are approximately equal and the vertical component is negligible, this method will produce an increase of about 8% for a circular structure. This combination method is conservative because Ref. 3 has shown that under two stochastically independent motions applied in two perpendicular directions, the expected response of a simple, linear system is a maximum or a minimum when its degree-of-freedom is parallel to either one of the directions of the motions.

As will be discussed in Section V.1, the RSS has only one effective horizontal mode and one vertical. The dynamic characteristics of the RSS are similar to a concentrated mass supported by a circular shaft. The effect of the two horizontal earthquake loads will be conservatively included as a 10% increase of one horizontal load. The effects due to the vertical earthquake load will be combined with those due to the horizontal earthquake loads by the absolute sum method.

IV. ANALYSIS PROCEDURES

IV.1 General

The RSS and its foundations were analyzed separately. The dynamic characteristics and seismic responses of the structure under YCS loads were obtained by using linear elastic methods. Nonlinear dynamic analyses were performed to determine the RSS response to seismic excitation levels consistent with the NRC spectra. The amplified floor response spectra at two different locations of the structure were also generated for piping analyses. Foundations were analyzed employing the equivalent soil springs which can only take compression.

IV.2 Computer Programs

Six computer programs were used to perform the entire analyses. RCCOLA [4] determined the ultimate strength and the moment-curvature relationship of the different column sections. ANSYS Revision 3 [5] was used for the linear dynamic analyses of the RSS and the linear static analyses of the steel collar. Nonlinear dynamic analyses of the RSS was carried out using the computer program PRA [6]. The time-history analyses of the structure were carried out using MOST2 [7] and the amplified floor response spectra were generated with INSPEC [8]. ANSYS Revision 4 [9] was used for the nonlinear static analysis of the ring foundation.

IV.3 Linear Dynamic Model of Reactor Support Structure

The RSS was analyzed using linear methods to study its dynamic characteristics and maximum member forces under different earthquake loads. As discussed in Chapter I, the column base connections were modified. A mathematical model was used to represent the existing structure as shown in Fig. B.1.

As shown in Fig. B.1, the exterior column-to-foundation connections are modeled as fixed at the top of the steel collars. Since the moment capacity of the column baseplate-to-foundation connection is very small as compared with the moment capacity of the column (see M-Ø diagrams of the various column sections shown in Figs. E.1a and E.1b), it was modeled as a hinge. The upper cylindrical part of the structure was modeled by a rigid region as discussed in Chapter I.

IV.4 Nonlinear Dynamic Model of Reactor Support Structure

Fig. B2 shows the finite element model of the Reactor Support Structure (RSS). The model is a two dimensional one. The six exterior columns are represented by three columns (each representing two columns of the RSS) extending from nodes 1 to 7, 8 to 14, and 15 to 21. The two interior columns are represented by one column extending from node 22 to 29. The darker lines in Fig. B2 represent rigidly modeled elements. Nonlinear properties of the model are considered explicitly with yielding elements.

IV.5 Nonlinear Static Model of Ring Foundation

Fig. B.3 shows the finite element model of the ring foundation. Since the structure and the loading are symmetric with respect to the X-axis, only one-half of the structure is employed. The ring foundation and the exterior columns are modeled by elastic beam elements. The soil is modeled by the spring elements which can only take compression.

As will be discussed in Section V.4, after studying the responses of the ring foundation to the NRC spectrum loads, it was found that Beam Elements 141 and 148 [Fig. B.3(C)] will yield. To investigate the effect of the yielding of the ring foundation on the distribution of the soil pressures, a plastic hinge element was inserted at Node 37 and the analysis was repeated.

IV.6 Linear Static Model of Steel Collar

Fig. B.4 shows the mathematical model of the steel collar. The cross-section of the various elements of the collar are shown in Fig. B.4(C). The cross-section of the collar has the shape of a channel. The location of the shear center of the channel section is also shown in this figure. Since any force which is not applied at the shear center of a section will introduce a torsion in that section, the channel was modeled as a beam running along its shear center to accurately apply the torsion to the channel section. The rock bolts were modeled by spring elements [Nodes 101 and 201, Fig. B.4(B)]. The friction mechanism between the collar and the foundation was modeled by rigid springs [Nodes 252 and 352, Nodes 252 and 452, Fig. B.4(B)]. Since the collar and the loading are symmetric with respect to the Y-axis, only one-half of the collar was modeled.

V. ANALYSIS RESULTS

V.1 Structural Characteristics

The upper part of the RSS was modeled as a rigid region. The structure has only two effective modes of vibration which included more than 96% of the total mass. Table D.1 lists the horizontal and vertical fundamental frequencies of the structure. The distributed masses of the structure at the top of the interior column are also shown in this table.

V.2 Linear Dynamic Analyses of Reactor Support Structure

Tables E.1 and E.2 show the linear responses of the RSS to different earthquake inputs in three directions. Since the dynamic properties of the structure are almost identical in two horizontal directions, the structure was only analyzed for earthquake input in one horizontal and one vertical direction. The effect of the earthquake in the other horizontal direction was considered by multiplying the results due to the earthquake input in one horizontal direction by a factor of 1.10, as discussed in Section III.3. The vertical earthquake input was equal to 2/3 (two-thirds) of the horizontal input.

As shown in Table E.1, the column shears developed under dead load and YCS loads are much smaller than the corresponding shear capacities. The column moments are also smaller than the corresponding yield moment. Therefore, it can be concluded that the RSS can withstand the dead load and YCS loads.

Under the dead load and NRC spectra loads, the column shears are still much smaller than the corresponding shear capacities (Table E.2). However, all the columns yield. Since the column shears are relatively small, ductile behavior of the RSS can be expected. The next section describes the results of a nonlinear time-history analysis of the RSS performed to evaluate its behavior in the inelastic range.

Table E.3 shows the maximum displacement at the top of the interior column obtained from the linear dynamic analyses. The maximum displacement due to NRC spectra creates a minimal P-Δ effect of 0.111/28 = 0.4%, where 28'-0" is the height of the structure at the top of the interior columns. As discussed in Section V.3, the maximum displacement resulting from the nonlinear time-history analyses is 0.13 ft, which creates a P-Δ effect of 0.5%. Therefore, the P-Δ effect was neglected.

V.3 Nonlinear Dynamic Analyses of Reactor Support Structure

The nonlinear model of the RSS described in Section IV.4 and shown in Fig. B.2 is analyzed under a number of artificial and real earthquake time histories. The purpose of the analyses is to quantify the extent of the nonlinear behavior, if any, of the top dowel sections of RSS columns when the structure is subjected to NRC spectra level ground motions. The six analyses performed are designated herein as A07, A10, R07, R10, A07.1 and R07.1 (see Table E.4 for parameters of the analyses). The letter 'A' indicates that the horizontal and vertical excitations are artificial, whereas 'R' (real) indicates that they are actual records. The numbers 07 and 10 correspond to damping values of 7% and 10% of critical, respectively, in the first mode. The choice of damping values follows NRC Guideline NUREG/CR-0098 for reinforced concrete just below yield point. Furthermore, the above damping values are consistent with those experimentally measured at nuclear power plant facilities (see Table 7 of Ref. 18). It should be noted that considerable energy absorption capacity is available through inelastic actions at the RSS columns, the ring foundation, and soil-structure interaction. Analyses with suffix '.1' have damping ratios in the second mode equal to damping ratios in the first mode. The time histories of horizontal and vertical components of the artificial time histories used as excitation in analyses A07 (or A07.1) and A10 (or A10.1) are shown in Figs. E.2 through E.5. The response spectra corresponding to time-histories shown in Figs. E.2 and E.3 are shown in Figs. E.6 and E.7, respectively. Also shown in Figs. E.6 and E.7 is the NRC spectra, which is

seen to be conservatively enveloped by the spectra of the time-histories used as excitation. The time histories given in Figs. E.2 through E.5 are multiplied by the factors shown in Table E-4 prior to their application as excitation in the analyses. The factor '1.1' is used to account for the combination of two perpendicular horizontal components (see Section III.3).

Time-history record Real 1 is shown in Fig. E.8. The 7% and 10% damping ratio response spectra of the record scaled to a PGA = 0.188g envelope the NRC spectra over the frequency range of interest as shown in Figs. E.9 and E.10. Time history of the record Real 2 used in the analyses is shown in Fig. E.11, and its response spectrum with 7% and 10% damping ratios in Fig. E.12.

The horizontal displacement response time-history of node 7 for the six analysis cases listed in Table E.4 are given in Figs. E.13 through E.18. It can be seen that the maximum relative displacement of the top dowel sections of the columns is about 0.13 ft. (1.56 in.) (occurring for analysis case 'A10', see Fig. E.14). It should be noted that displacements for nodes 14 and 21 are almost identical to those of node 7.

The plastic hinge rotation time-histories at sections at nodes 7, 14, 21, and 29 are given in Figs. E.19 through E.24 for the six analysis cases listed in Table E.4. The information given in Figs. E.19 through E.24 is summarized in Table E.5. It can be seen that the maximum plastic hinge rotation is 3.63×10^{-4} rad occurring at Section 29 (interior columns) under analysis case 'A10'. Furthermore, it can be observed that in all cases the inelastic action takes place during the strong motion portion of the excitations, and after some time no further inelastic action takes place. The largest number of inelastic cycles any section undergoes is four and takes place at Section 29 under analysis case 'A07'.

Figs. E.25 through E.28 show the axial force - bending moment interaction variation through time at Sections 7, 14, 21, and 29 for analysis cases A07,

A10, R07, and R10, respectively. Also included in Figs. 25 through 28 are the yield surfaces corresponding to effective yield of tensile reinforcement. It can be seen that excursions beyond the yield surfaces are limited both in number and extent, and columns rarely experience net tensile axial load.

In addition to the six nonlinear analyses described above, the RSS model shown in Fig. B.1 was subjected to a number of additional real earthquake time histories as part of the Yankee Rowe Probabilistic Seismic Risk Assessment Project performed by Cygna. A summary of the relevant findings of that project are given in Table E.6. The quantity appearing as $\overline{SV}$ in Table E.6 is an average spectral velocity which provides a measure of the effect of a particular ground motion on a structure in the frequency range f_s and f_e. The average spectral velocity, $\overline{SV}$, is defined as:

$$\overline{SV} = \int_{fs}^{fe} W(f)SV(f,\xi)df$$

where:

f = frequency

f_s = softened frequency = 0.87 cps for the RSS

f_e = fundamental elastic frequency = 1.27 cps for the RSS

$W(f)$ = linear weighting function satisfying $\int_{f_s}^{f_e} W(f)df=1$

= 12.5 (1.27-f) for the particular case

$SV(f,\xi)$ = spectral velocity of a single degree-of-freedom oscillator with frequency f, and damping ratio ξ,

ξ = critical damping ratio = 0.07 for the RSS

The average spectral velocity, $\overline{SV}$ of the NRC spectrum is approximately 12.5 in/sec. Noting that the analyses summarized in Table E.6 have average spectral velocities in the neighborhood of 12.5 in/sec it can be seen that the additional analyses summarized in Table E.6 result in limited inelastic action at the top dowel sections under NRC spectrum level excitations.

The above presented results indicate that the inelastic demand on the RSS and in particular the top dowel sections of the RSS is fairly limited. Based on experimental evidence presented in Appendix H, the critical dowel sections have sufficient inelastic deformation capacity to safely withstand ground motions of the NRC spectrum type.

V.4 Nonlinear Static Analyses of Ring Foundation

Because of the different arrangements of the reinforcement, the capacities of the ring foundation vary along its length as shown in Fig. E.29. The interaction between the torsion and shear capacities of the various sections of the ring foundation is shown in Fig. E30.

As shown in Fig. B.3(a), the horizontal earthquake force was applied to the RSS by an equivalent static force, Fx. The effect of the vertical earthquake was combined with the gravitational force and applied to the RSS by an equivalent static force, Fz. The vertical earthquake force can act either upward or downward. Six load cases were studied. Case 1 combines the dead load, horizontal YCS loads and vertical YCS load acting upward. Case 2 is similar to Case 1 except the vertical YCS load is acting downward. Cases 3 and 4 are similar to Cases 1 and 2 except the YCS loads are replaced by the NRC spectrum loads. Cases 5 and 6 are similar to Cases 3 and 4 except a plastic hinge is inserted at Node 37 [Fig. B.3(b)].

The soil pressure, moment, shear and torsion diagrams of the ring foundation under the six load cases are shown in Figs. E.31 to E.36. The forces developed in the ring foundation are also shown in Tables E.7 to E.12.

As shown in Fig. E.31, when the vertical YCS load acts upward, the maximum soil pressure is 10.92 ksf and, if the vertical YCS load acts downward, the maximum soil pressure increases to 12.65 ksf (Fig. E.12). For these two load cases, the forces developed in the ring foundation are smaller than the corresponding capacities.

If the YCS loads are replaced by the NRC spectra loads (Load Cases 3 and 4), the maximum soil pressure reaches 17.16 ksf (Fig. E.34). The moments developed in Beam Elements 141 and 148 exceed the yield moment (Tables E.9 and E.10).

To study the change in the distribution of soil pressure due to yielding of the ring foundation, a plastic hinge element was inserted at Node 37. The moment capacity of this plastic hinge is limited to 12,666 k-ft (Fig. E.29). The analytical results are shown in Figs. E.35 and E.36 as well as Tables E.11 and E.12. As shown in Fig. E.36, the maximum soil pressure increases to 18.13 ksf. Comparing Table E.9 with E.11 and Table E.10 with E.12, it can be seen that the forces developed in the ring foundation with or without the plastic hinge are similar except in Beam Elements 141 and 148. All the beam forces shown in Tables E.11 and E.12 are less than the corresponding capacities of the ring foundation.

Therefore, it can be concluded that under the dead load and YCS loads, the ring foundation is structurally adequate and the soil stresses are less than the allowable soil bearing pressure of 20 ksf. Under the dead load and NRC spectrum loads, the ring foundation is expected to yield but not fail.

A preliminary study [20] indicates the existence of a liquefaction potential under the ring foundation under NRC spectrum (see Fig. E.37), assuming the water table to be at ground surface. This will reduce the passive earth pressure and the stiffness of the soil springs shown in Fig. B.3a used in the

previous analyses. The analysis of the ring foundation is repeated without considering the passive earth pressure and it is seen that the results do not change noticeably [20].

V.5 Linear Static Analysis of Mat Foundation

In the analysis of the mat foundation the soil pressure distribution was assumed to vary linearly. This assumption is accurate if the maximum soil pressure is less than the allowable pressure of 20 ksf. Under combined dead load and YCS loads, the maximum soil pressure is 6.00 ksf, which is less than the allowable pressure. If the YCS loads were replaced by the NRC Spectrum loads, the maximum soil pressure increases to 7.98 ksf, also less than the allowable pressure.

Table E-12 lists the maximum forces developed in the various locations due to the combination of dead load and earthquake loads. Restricted by the moment capacity of the baseplate-to-foundation connection of the interior columns, the maximum forces developed in the mat foundation are identical for the two different earthquake loads investigated. It can be seen that the moment capacity of the mat foundation is more than adequate to take the loads and its shear capacity is marginal. No functional failure is expected.

V.6 Linear Static Analyses of Steel Collar

The collar was constructed and anchored to the foundation through 20 rock bolts in the inner ring. These rock bolts were post-tensioned to 180 kips and anchored on the bottom plate of the collar.

Restricted by the moment capacity of the exterior column, only a maximum moment of 19,730 k-ft can be applied to the collar. To guarantee the integrity, the collar was analyzed against this maximum moment although this moment was not reached as shown in the results of linear analyses (Tables E-1

and E-2) or nonlinear time-history analysis. The analytical results are shown in Table E.14. The yield stress of the steel collar is 60 ksi. The maximum stress developed in the collar was 18.8 ksi, or 0.31 fy. The maximum stress developed in the bottom plate was 42.7 ksi, or 0.71 fy. The rock bolts have a yield stress of 80 ksi. The maximum stress developed in the rock bolts was 71.8 ksi, or 0.90 fy. Therefore, it can be concluded that the collar is capable of resisting 19,730 k-ft moment and it is acceptable under both YCS loads and NRC Spectra loads.

V.7 Dowel Embedment Analysis

The RSS nonlinear model shown in Fig. B.2 assumes that a plastic hinge forms at that top dowel section without pull-out in any of the reinforcing dowels. The formation of the plastic hinge, in turn, depends on the dowel's ability to slip with respect to the surrounding concrete. Also, before bond failure is reached, the dowel must be able to displace sufficiently at the section of crack opening to allow the maximum rotations experienced in the RSS model without complete bond failure.

To assess the capacity of the dowel sections the following factors are considered:

a) shortest dowel development length, l_d

The plastic hinge is assumed to form at the construction joint near the top of the RSS columns. Therefore, l_d is 30" for an exterior column and 30.75" for an interior column (Fig. A5, SW DWG 9699-FC-58B).

b) average bond stress, μ

Monotonic pull-out tests of #14 bars [12] show average bond stresses between 1 ksi and 2 ksi (Fig. E-38). Cyclic tests of smaller

diameter bars (#6, #8, #10) [13, 14] show average bond stresses in excess of 1 ksi (Table E-15). For this analysis a base value for average bond stress of 1 ksi is used. Considering a reduction for closely spaced (bundled) bars (17% per ACI '77, Sec. 12.4 [15]), it is conservatively assumed that μ=0.7 ksi for the analysis of dowel capacity. The bond stress value of μ = 0.7 is also suggested for use by NRC consultants [19].

c) Stress-strain diagram for dowel

For simplicity, a bilinear diagram is assumed (Fig. E-39). This diagram approximates the behavior of ASTM A15-54T intermediate grade reinforcing steel. Note that the A15-54T specification does not cover #14 reinforcing bars. However, client documentation [16] shows that the #14 dowels were special ordered to conform to ASTM A15-54T and A305-56T.

Note that the reinforcing dowels are well confined by the steel shell, the circular hoops, and the slab reinforcement so that no adjustments are necessary for lack of confinement as suggested by Ref. 12.

The capacity of the dowels is determined as follows:

$$\sigma_{max} = \frac{l_d \mu \ell_o}{A_b} \qquad (1)$$

where σ_{max} is the maximum dowel stress capacity before bond failure, ℓ_o (= 5.5") is the dowel perimeter and A_b (= 2.25 in^2) is the cross-sectional area of the dowel. The resulting maximum dowel capacity stresses, for μ = 0.7 ksi, are

- Exterior column, l_d = 30" $\quad \sigma_{max}$ = 51 ksi > f_y = 40 ksi

- Interior column, l_d = 30.75" σ_{max} = 53 ksi > f_y = 40 ksi

The plastic rotational capacities of these columns are determined as below,

$$l_y = \frac{f_y A_b}{\mu \Sigma_o} \quad (2)$$

$$\varepsilon_{max} = \frac{f_y}{E} + \frac{\mu \Sigma_o}{A_b E_{sh}} (l_d - l_y) \quad (3)$$

$$\delta = \frac{1}{2} \varepsilon_y l_y + \left(\frac{\varepsilon_{max} + \varepsilon_y}{2}\right) (l_d - l_y) \quad (4)$$

$$\phi = \frac{\delta}{D_b} \quad (5)$$

where l_y is the development length necessary to yield the dowel (= 23.4"), f_y is the dowel yield stress (=40 ksi), ε_{max} is the maximum strain developed at σ_{max}, ε_y is dowel yield strain, E is Young's modulus (= 29000 ksi), and E_{sh} is the strain hardening modulus (151 ksi) of the bilinear stress-strain curve for the dowel, δ is the dowel displacement at cracked (plastic) section, ϕ is the plastic hinge rotation, and D_b is the diameter of the dowel ring in the column (= 75" for an interior column and 69" for an exterior column).

The plastic rotational capacities of these columns, as determined by Eqs. 2 through 5, above, are shown in Table E-16. The capacity exceeds the maximum nonlinear model rotation by a factor of 20 for an exterior column and by a factor of 12 for an interior column. Therefore, the anchorage capacity of the dowels is sufficient to withstand the rotations experienced by the RSS nonlinear model. Further discussion of the dowel issue is presented in Appendix H.

Furthermore, note that the maximum plastic hinge rotation of 3.63×10^{-4} rad would result in a maximum slip of (90")(3.63×10^{-4}) ≅ 0.033 inches, where the neutral axis is conservatively assumed equal to the depth of the column. It

can be seen that this maximum slip may result in visible cracks but is not of concern from a functional safety point of view.

V.8 Stud Bolt Analysis

Welded headed studs are embedded in the concrete column and attached to the steel shell that confines the exterior and interior columns of the RSS. The stud bolts are 7/8" in diameter and their numbers are 350 and 500 for exterior and interior columns, respectively. The spacing between studs is 8" vertically and circumferencially. The length of the studs is estimated to be 5" using the construction photographs (see Fig. E.40). The studs transmit load between the concrete column and the steel shell, primarily through shearing action. The location of the studs is shown in Fig. A.5. To estimate the capacity of the studs, an analysis consisting of the following steps is performed.

a. It is assumed that the critical loading condition for the studs occurs when a plastic hinge forms during a large seismic event. For the purpose of this calculation, the plastic hinge is assumed to occur at the construction joint near the top of a column. Yielding in the column's reinforcing dowels occurs and strain hardening of the dowels produces a stress which is estimated to be 1.1 fy. This approximation is made in the absence of the actual stress-strain relationship, and is based on limited maximum plastic hinge rotations.

b. The maximum force in a dowel ($1.1\ fy \times A_s$) is transferred to the neighboring shear studs along the length of the column where stud bolts are located. The length of shear transfer varies around the column circumference as the embeded length of the dowel varies. The minimum length of shear transfer is approximately 30" for an exterior column and 104" for an interior column.

c. The shear force uniformly distributed along a vertical row of studs is calculated as a multiple of the force in one dowel; the multiple being the ratio of the number of dowels to the number of vertical stud bolt rows. The resulting maximum shear force in a stud bolt is 23.4 kips and 13.6 kips for exterior and interior columns, respectively. This compares favorably with the allowable value of 27.1 kips obtained using Eq. 6.14 of Ref. 21, based upon a stud yield stress of 60 ksi.

d. The distortion of concrete due to the pulling-out movement of the dowel at the plastic hinge causes a higher shear demand on stud bolts nearest the construction joint where the plastic hinge is assumed to form. A displacement of the studs consistent with the maximum plastic rotation is computed to account for the higher shear demand. The maximum rotations for the columns are taken from the 2-D nonlinear RSS analysis (see Section V.3), and are reproduced in Table E.16. The amount of rotation and the neutral axis location determine the maximum crack opening and pulling-out movement of the dowel on the tension side of the column. The bending moment and the axial force at maximum plastic hinge rotation that are used to calculate the neutral axis location are shown as point P in Fig. E.25 for an exterior column, and as point Q in Fig. E.26 for an interior column. A movement of the dowel and the resulting distortion of the concrete causes a movement in the stud bolt head. That movement is conservatively assumed to be equal to the pull-out movement. The resulting shear force induced by this displacement is 0.2 kips and 0.3 kips for the exterior and interior columns, respectively. Bending moment stress at the base of the stud due to concrete distortion is found to be a maximum of 23 ksi in an interior column. This stress is well below yield stress of the stud.

The above shows that the studs are able to sustain loads produced during plastic hinge formation, even when shear due to distortions in the concrete near the plastic hinge location are considered in a conservative manner.

VI. GENERATION OF AMPLIFIED RESPONSE SPECTRA

VI.1 Amplified Response Spectra Due to YCS and NRC Spectra

The amplified response spectra (ARS) were generated for the analysis of the piping systems attached to the RSS. These spectra were generated at Elev. 1122'-2", Radius 34'-7" and Elev. 1087'-6", Radius 29'-9". Since the RSS is symmetric with respect to two horizontal directions, only one set of horizontal spectra and one set of vertical spectra were generated at each location. The critical damping ratios selected were 2% and 3%. All spectra were broadened by 15% in accordance with Regulatory Guide 1.122.

The ARS due to YCS are shown in Figs. F.1 through F.3. Since the vertical spectra are almost identical at the two locations considered, only the plot of vertical spectra located at Elev. 1122'-2", Radius 34'-7" is provided (Fig. F.2). The ARS due to NRC spectra are shown in Figs. 4 through 6. Similarly, only the plot of vertical spectra located at Elev. 1122'-2", Radius 34'-7" was provided (Fig. F.5).

VI.2 Comparison of Spectra Generated by Different Synthetic Time-Histories

The ARS shown in Figs. F.1 through F.6 were generated by using the synthetic time-histories of the corresponding earthquake spectra. To measure the accuracy and the reliability of these generated ARS, a comparative study was performed.

Four synthetic time-histories corresponding to YCS were randomly constructed. The time-history HIST 107A.TH is the one used in Section VI.1 to generate the horizontal spectra. The three additional spectra used for comparison were generated by using time-histories HIST 107.TH, HIST 107B.TH and HIST 107C.TH. These spectra were located at Elev. 1122'-2", Radius 34'-7" and their critical damping ratio was 2%. The model of the RSS had six collar fixes.

Fig. F.7 shows the comparison of the four spectra. It can be seen that these spectra have similar shapes. However, their peak acceleration vary by as much as 26%. Note that the spectra employed for piping analyses (using time-history HIST 107A.TH) is the most conservative one.

The amplified response spectra corresponding to nonlinear time-history analysis case A07.1 described in Section V.3 is shown in Fig. F.8. Also shown in Fig. F.8 for comparison is the ARS corresponding to the linear elastic analysis for 10% damping NRC spectra. It can be seen that the spectra corresponding to case A07.1 (the nonlinear analysis) are enveloped by the ARS resulting from a linear elastic analysis with 10% damping.

VII. SUMMARY OF REVIEW

(1) The embedment length of the #14 dowels is sufficient to develop the maximum rotations experienced at the connections between the upper cylindrical structure and the top of the interior and exterior columns when the structure is subjected to the NRC spectra.

(2) Under combined dead load and YCS loads, the forces developed in the columns and their ring and mat foundations will not exceed the corresponding ultimate capacities specified by ACI 318-77. The maximum soil pressure under the mat and ring foundations are smaller than the allowable pressure.

(3) Under combined dead load and NRC spectra loads, all the columns and the ring foundation will yield. The forces developed in the mat foundation, however, will not exceed ultimate capacities. The maximum soil pressure under the mat and ring foundation are less than the allowable pressure.

(4) The steel collar anchored by 20 rock bolts can resist 19,730 kips-ft moment. This moment capacity is adequate to resist both the YCS loads and NRC spectra loads.

(5) Based on the analyses described herein, no additional modifications are necessary to satisfy the design criteria for the YCS spectra. In addition, the RSS will not collapse and no functional failure is expected when subjected to the NRC Spectra.

APPENDIX A

BUILDING PLANS

APPENDIX A

BUILDING PLANS

Figure No.	Contract Drawing No.
Fig. A.1	S&W DWG 9699-FC-56A
A.2	RC-56B
A.3	FC-56D
A.4	RC-58A
A.5	FC-58B
A.6	FC-58C
A.7	FC-59A
A.8	FC-59B
A.9	CYGNA DWG SPD 80023-CF-1002

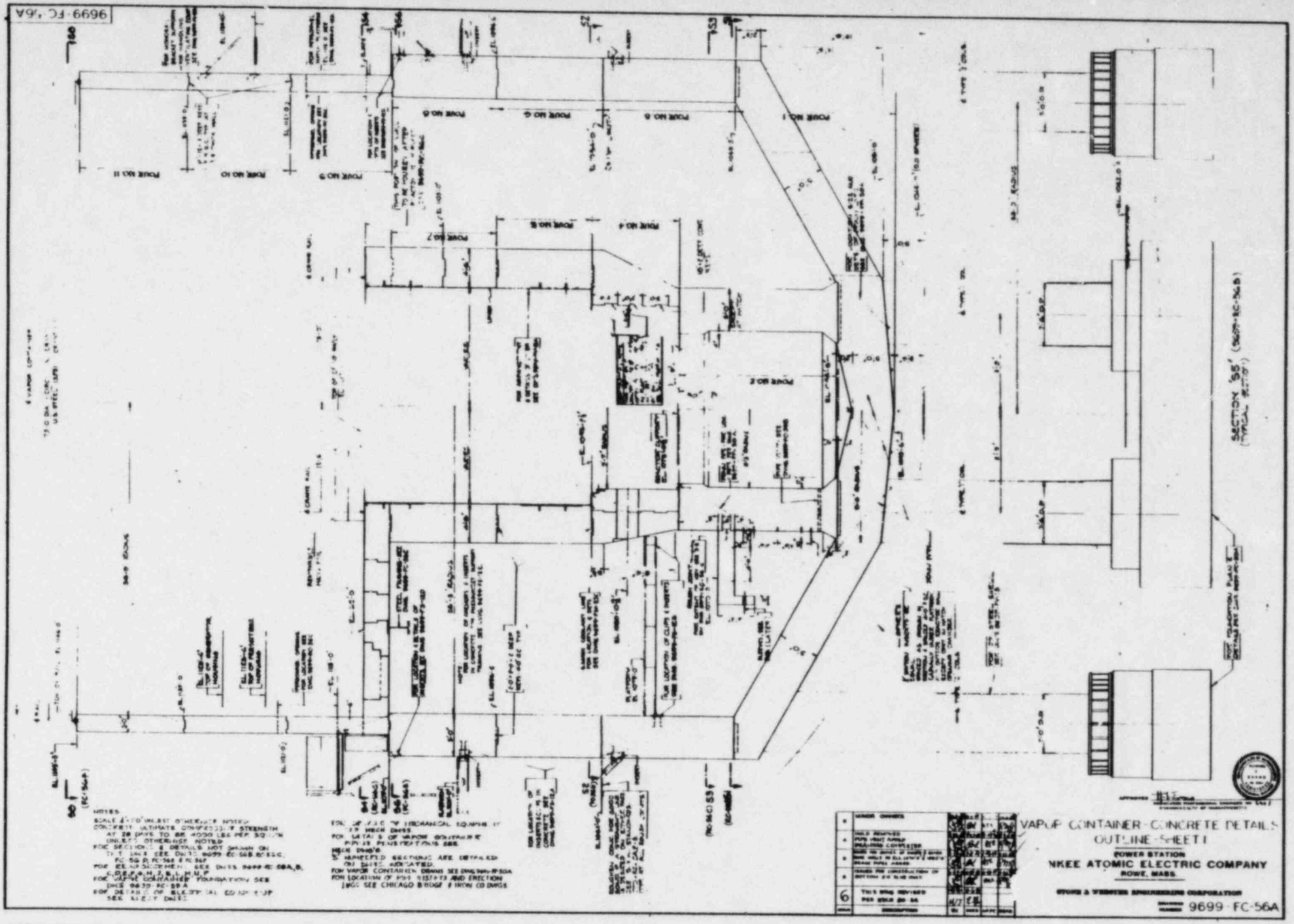

Yankee Atomic Electric Company
Reactor Support Structure
80023; EY-YR-80023-6; Rev. 3

FIG. A.1

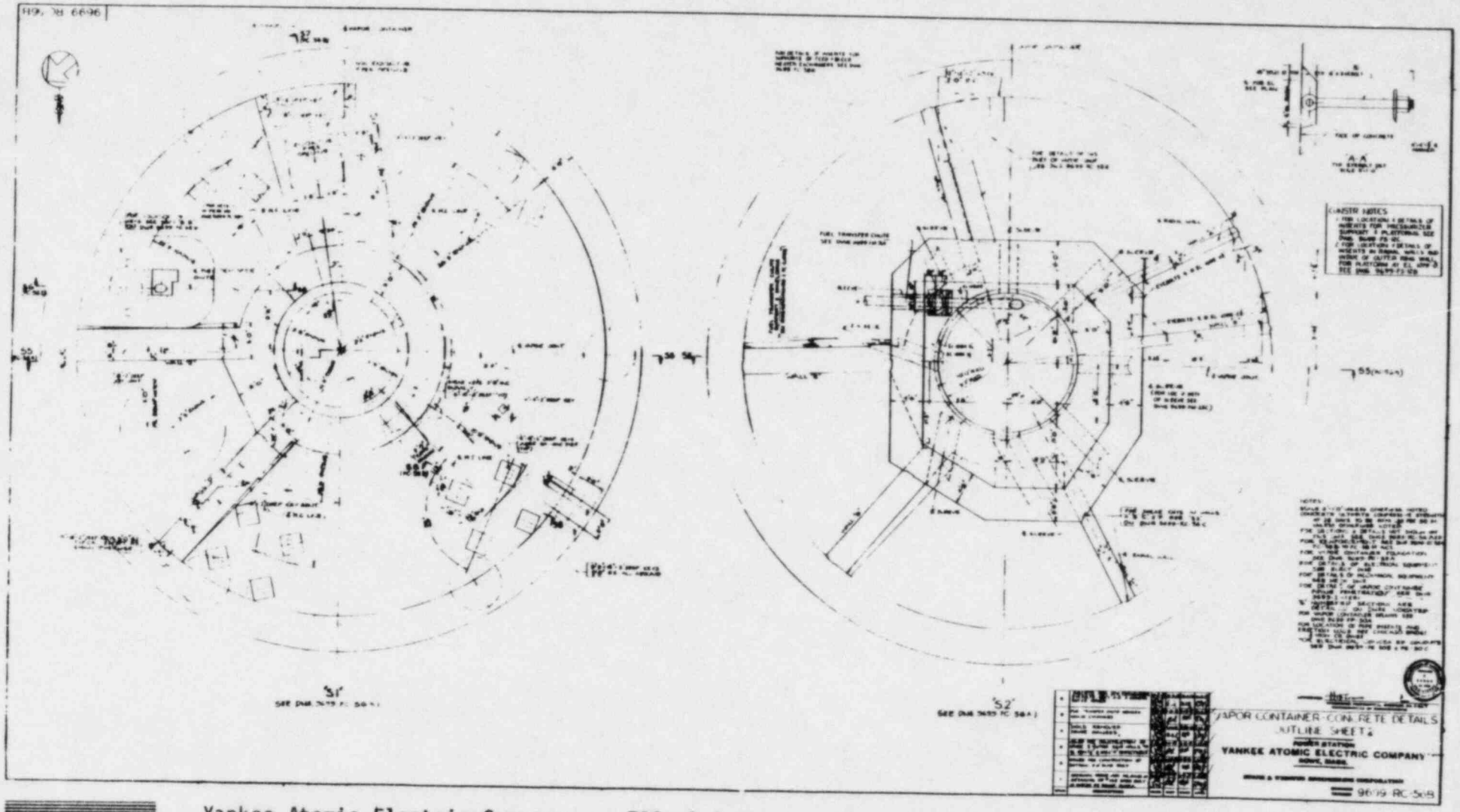

Yankee Atomic Electric Company
Reactor Support Structure
80023; EY-YR-80023-6; Rev. 3

FIG. A.2

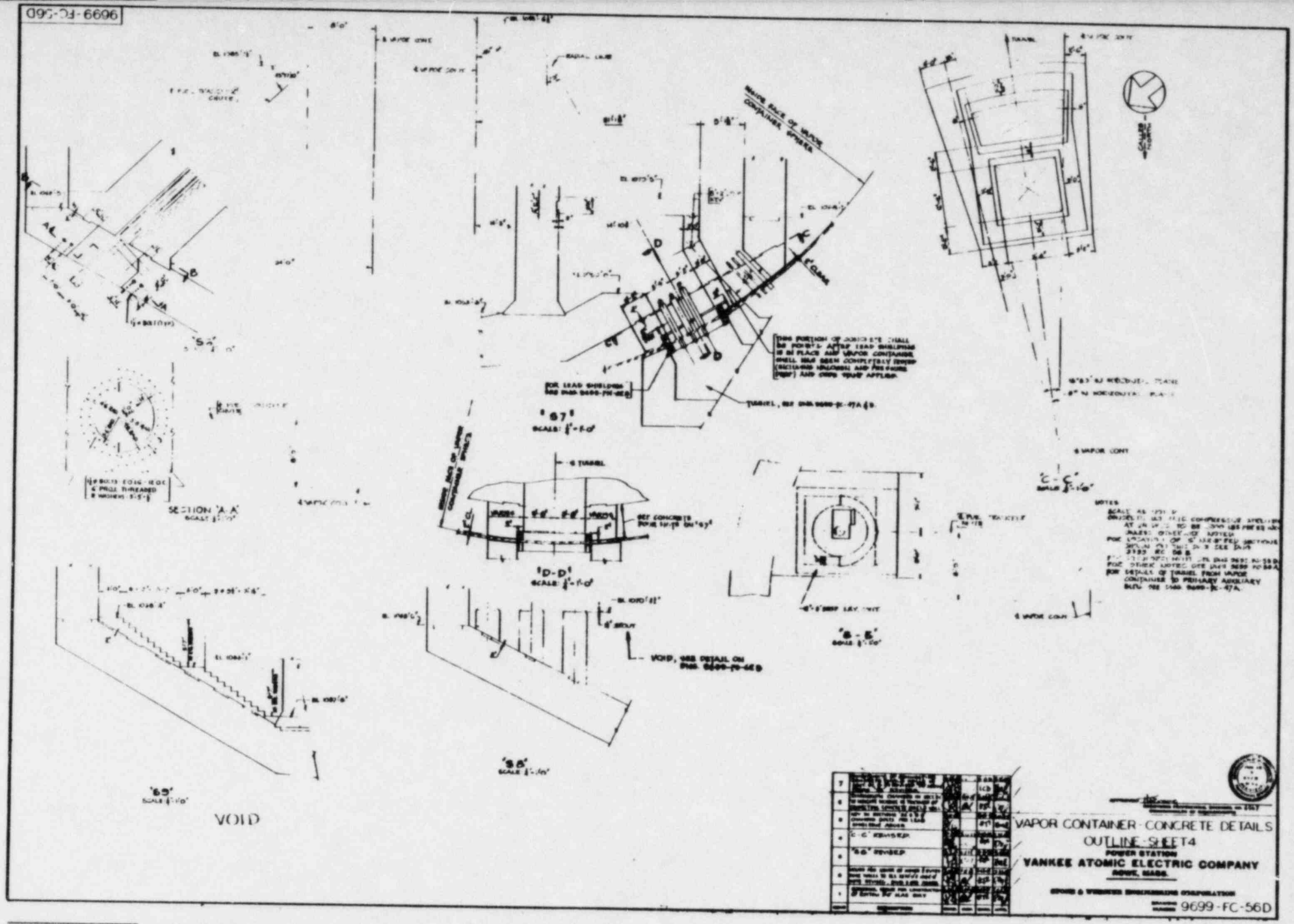

Yankee Atomic Electric Company
Reactor Support Structure
80023; EY-YR-80023-6; Rev. 3

FIG. A.3

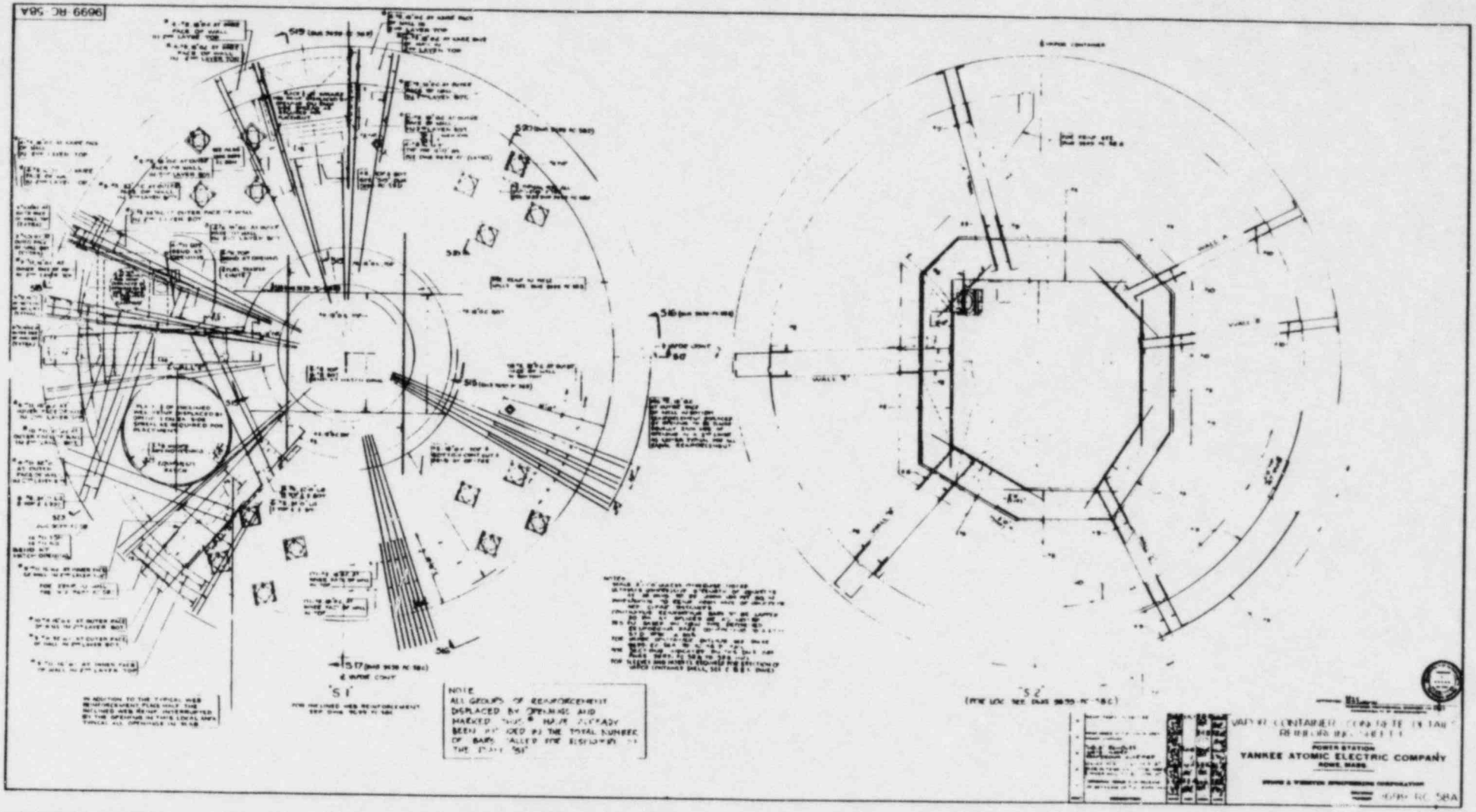

Yankee Atomic Electric Company
Reactor Support Structure
80023; EY-YR-80023-6; Rev. 3

FIG. A.4

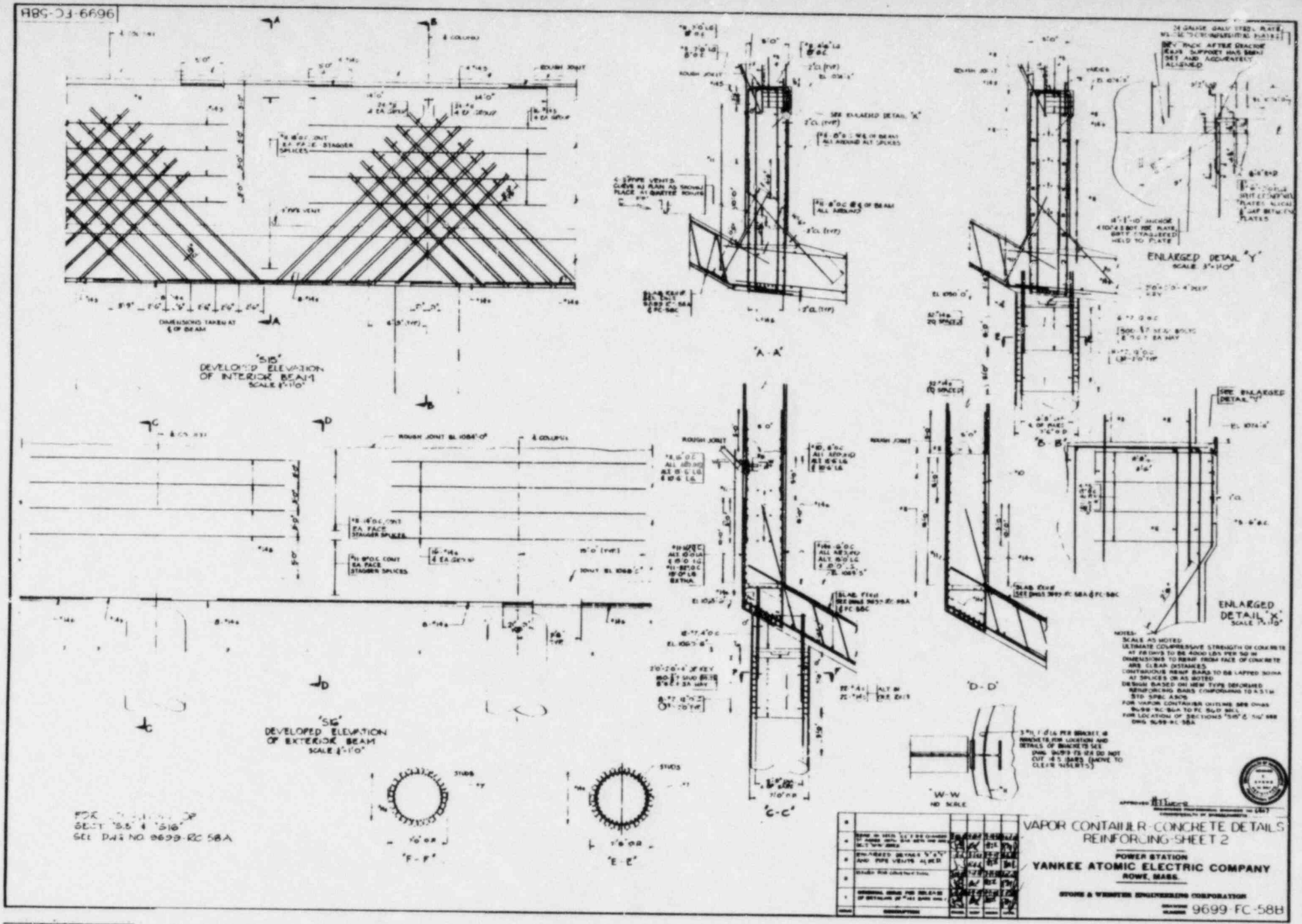

Yankee Atomic Electric Company
Reactor Support Structure
80023; EY-YR-80023-6; Rev. 3

FIG. A.5

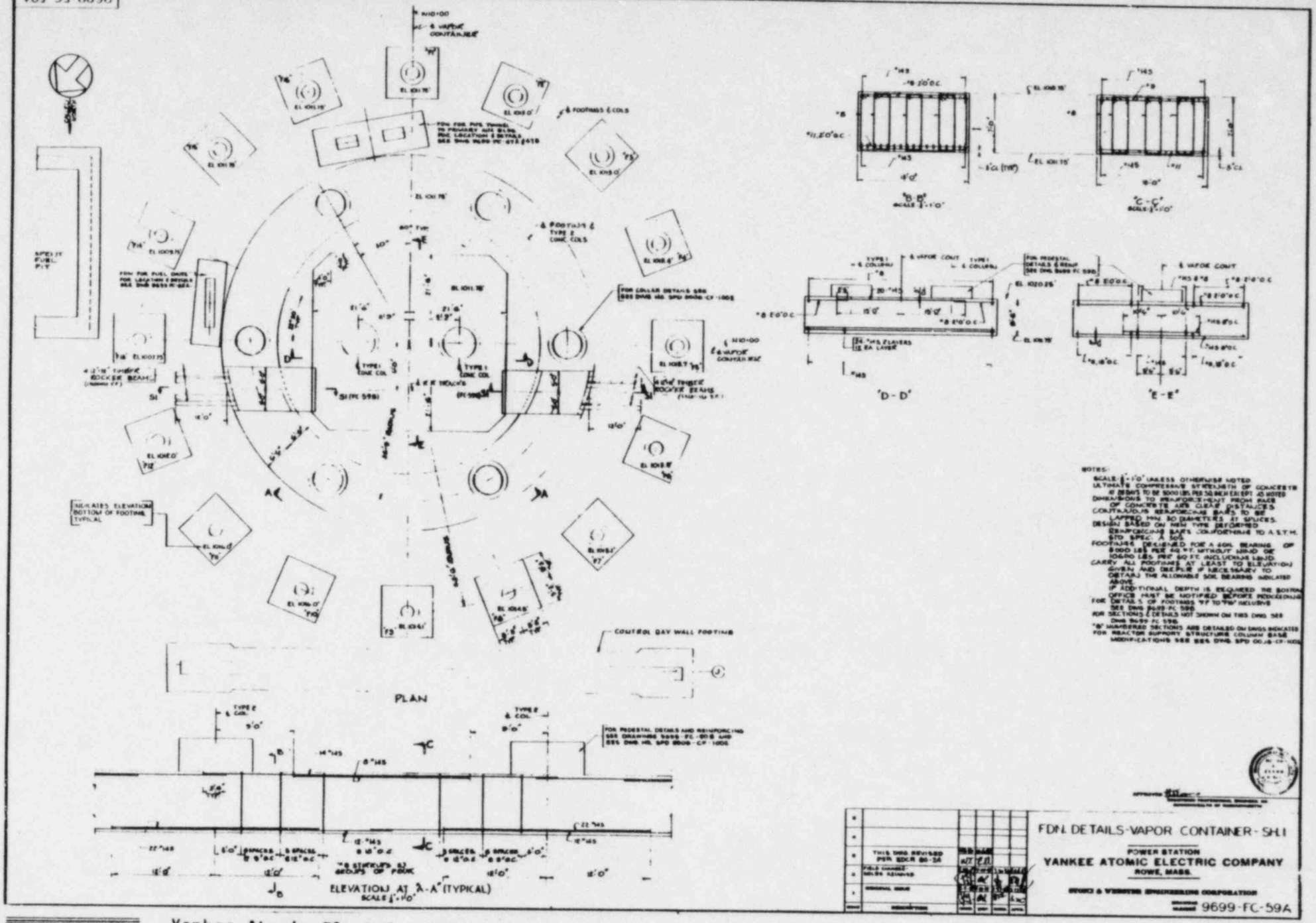

Yankee Atomic Electric Company
Reactor Support Structure
80023; EY-YR-80023-6; Rev. 3

FIG. A.6

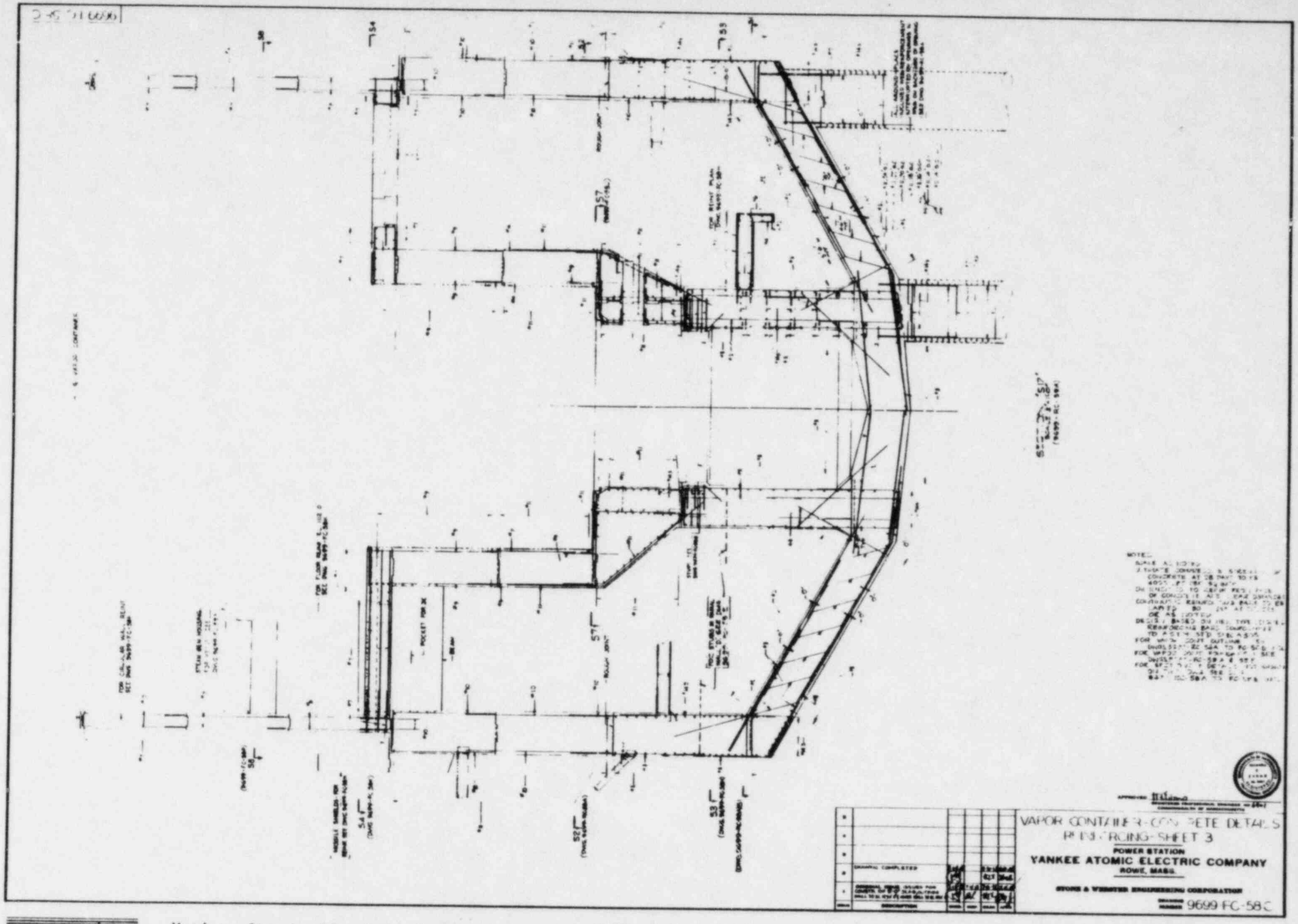

Yankee Atomic Electric Company
Reactor Support Structure
80023; EY-YR-80023-6; Rev. 3

FIG. A.7

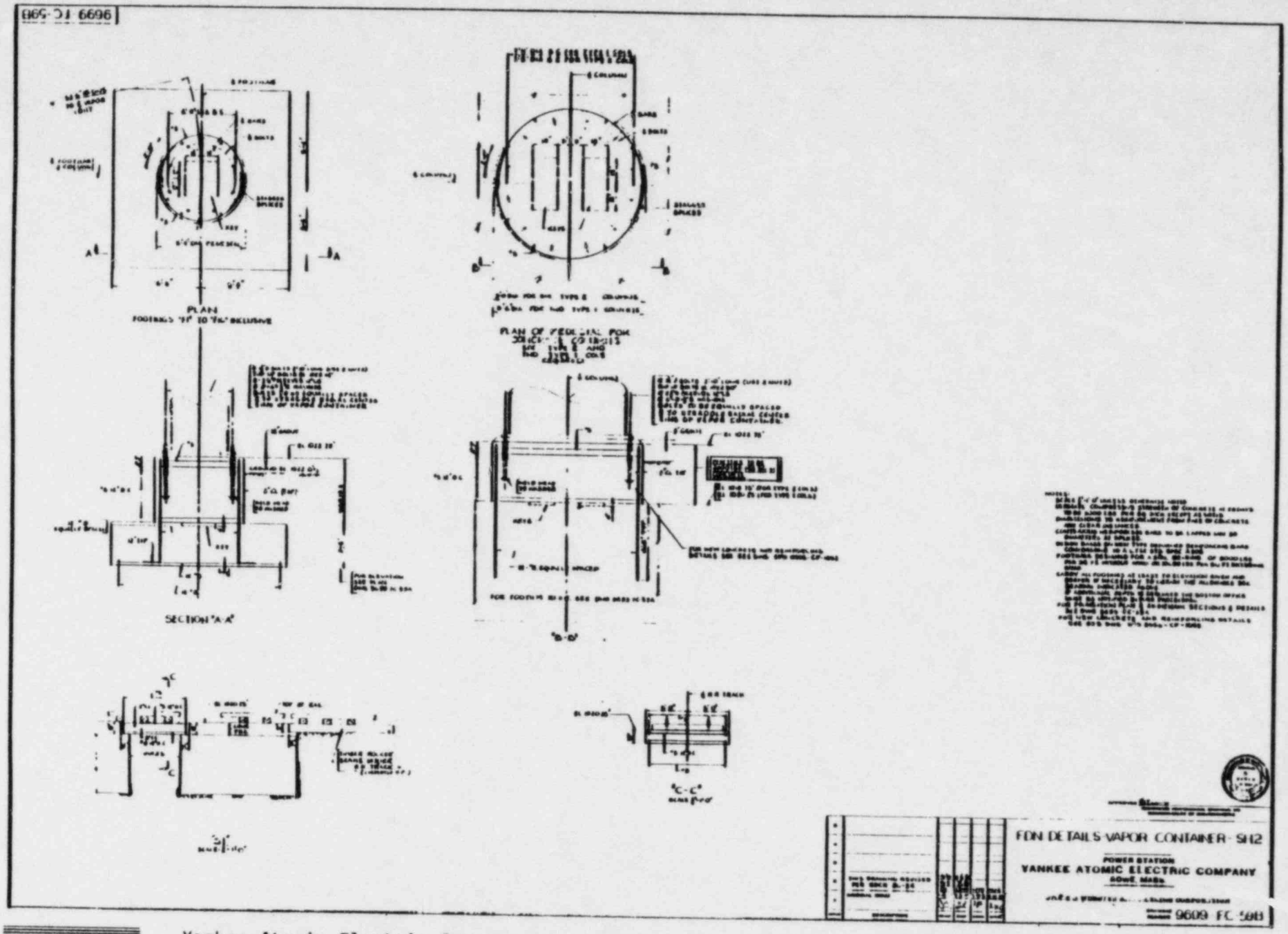

Yankee Atomic Electric Company
Reactor Support Structure
80023; EY-YR-80023-6; Rev. 3

FIG. A.8

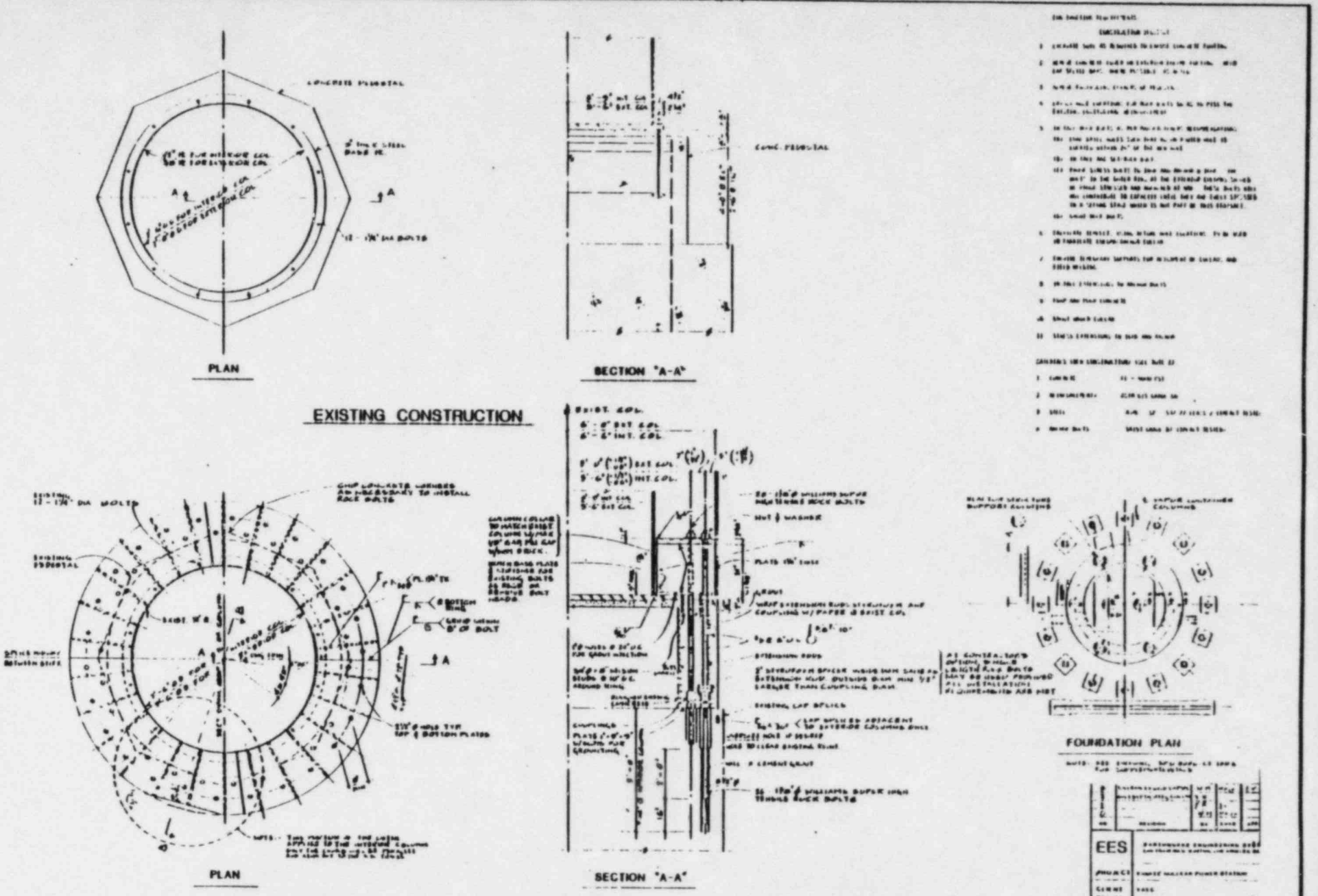

Steel Collar Modification

Yankee Atomic Electric Company
Reactor Support Structure
80023; EY-YR-80023-6; Rev. 3

FIG. A.9

APPENDIX B

COMPUTER MODELS

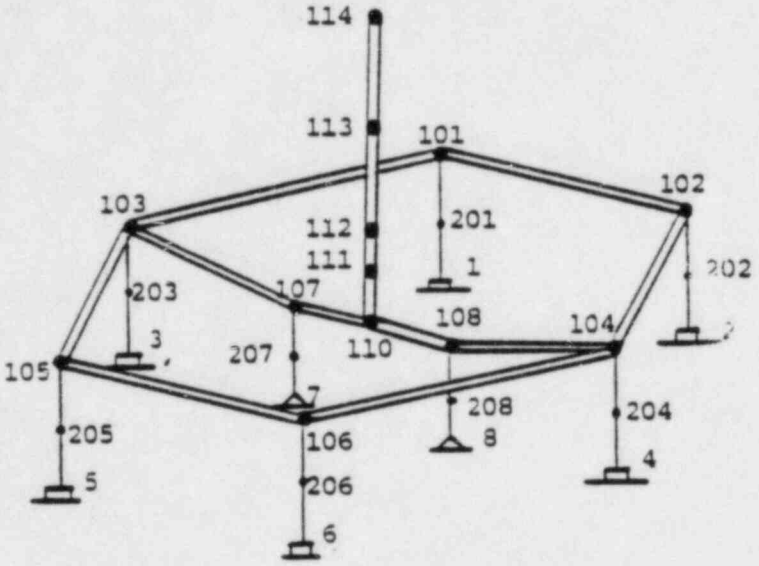

SIX EXT. COLUMNS HAVE COLLAR

FIG. B.1 LINEAR MODEL OF REACTOR SUPPORT STRUCTURE

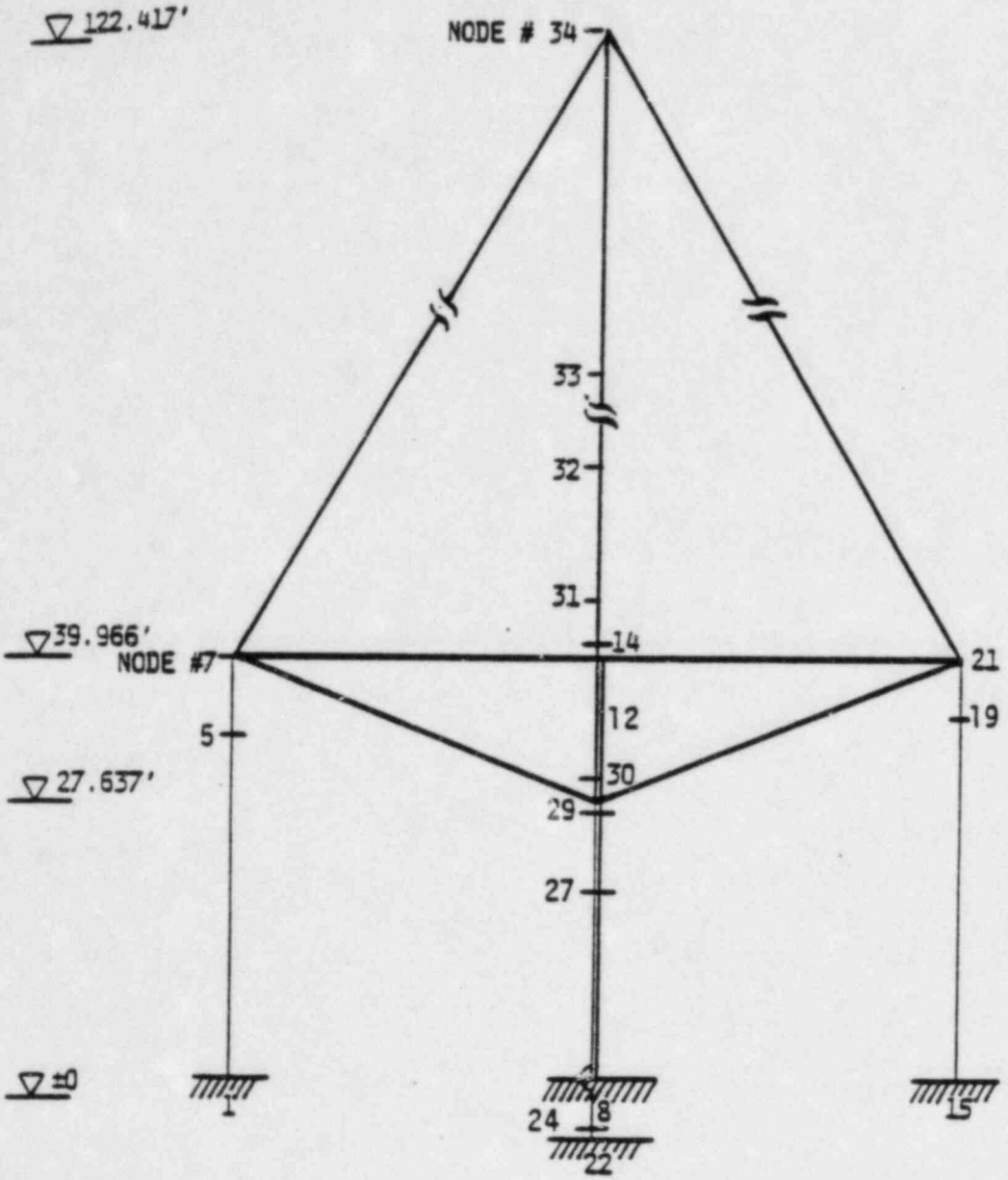

FIG. B.2 NON-LINEAR MODEL

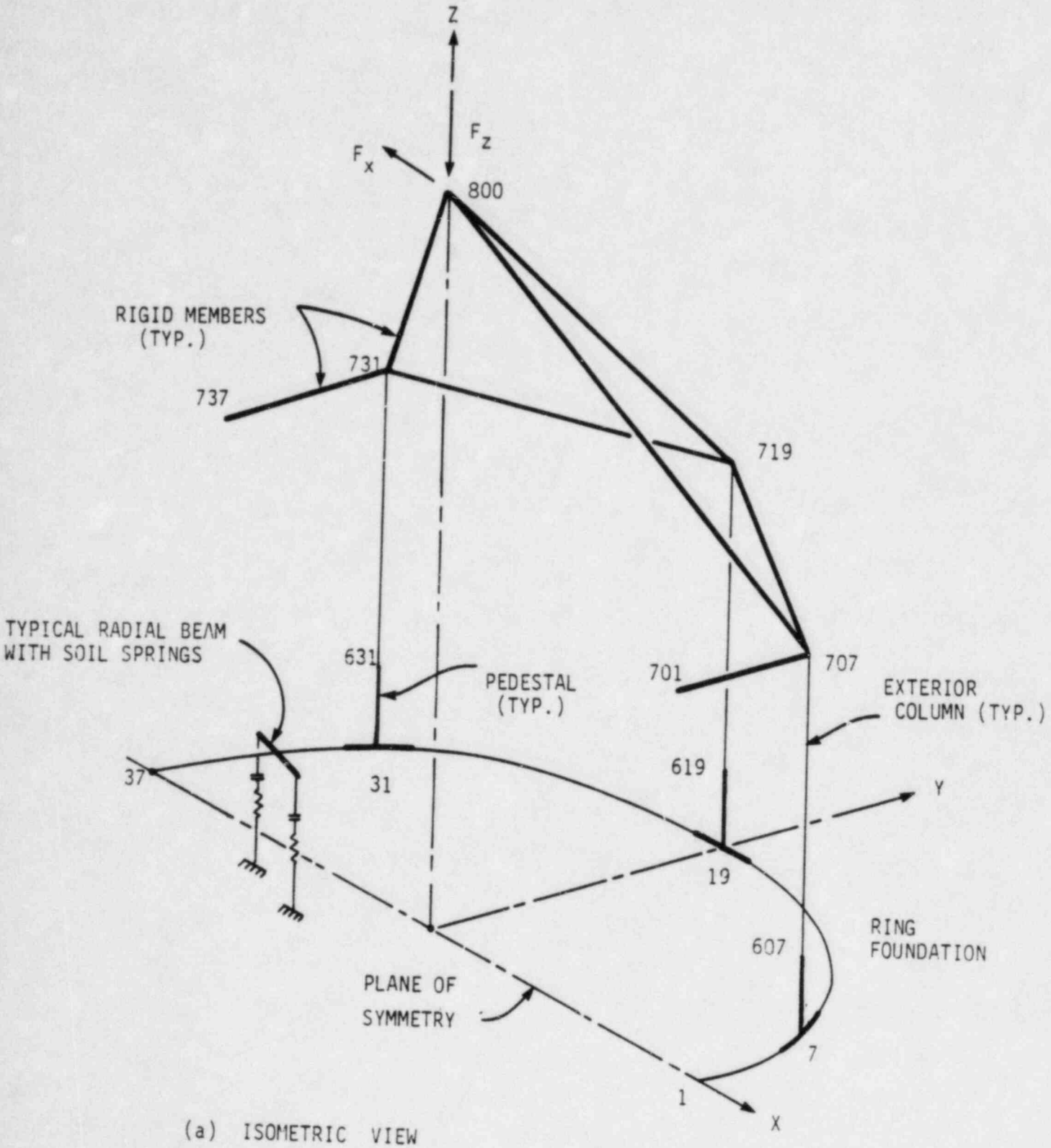

FIG. B.3 FINITE ELEMENT MODEL OF RING FOUNDATION

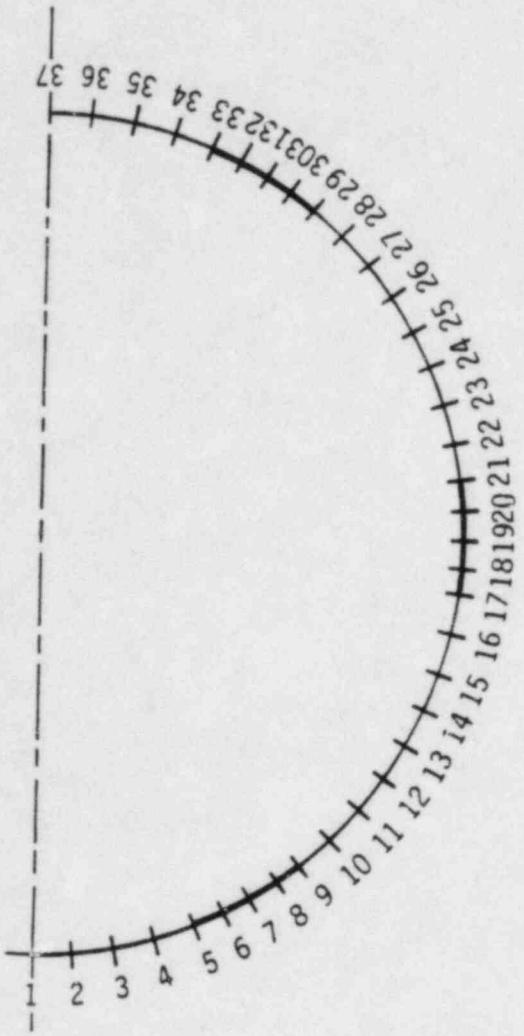

(b) Node Numbers of Ring Foundation

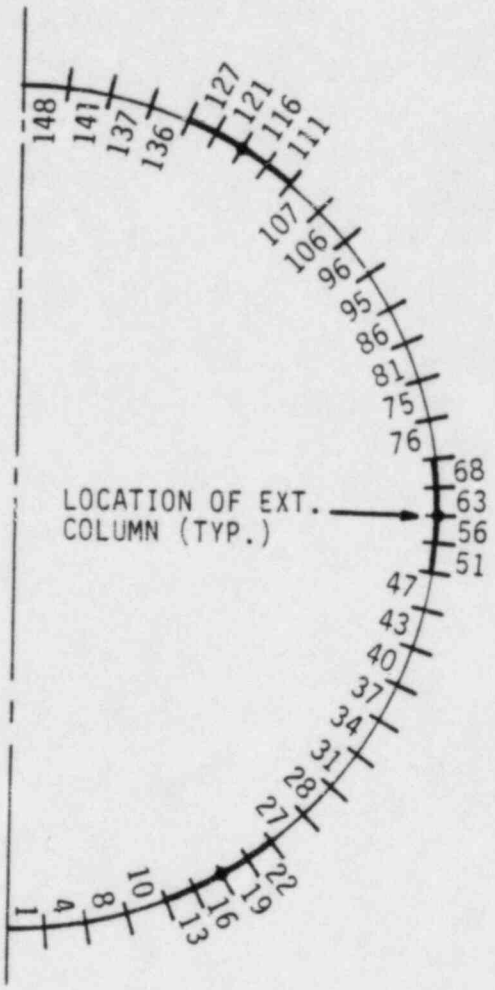

(c) Element Numbers of Ring

FIG. B.3 (continued)

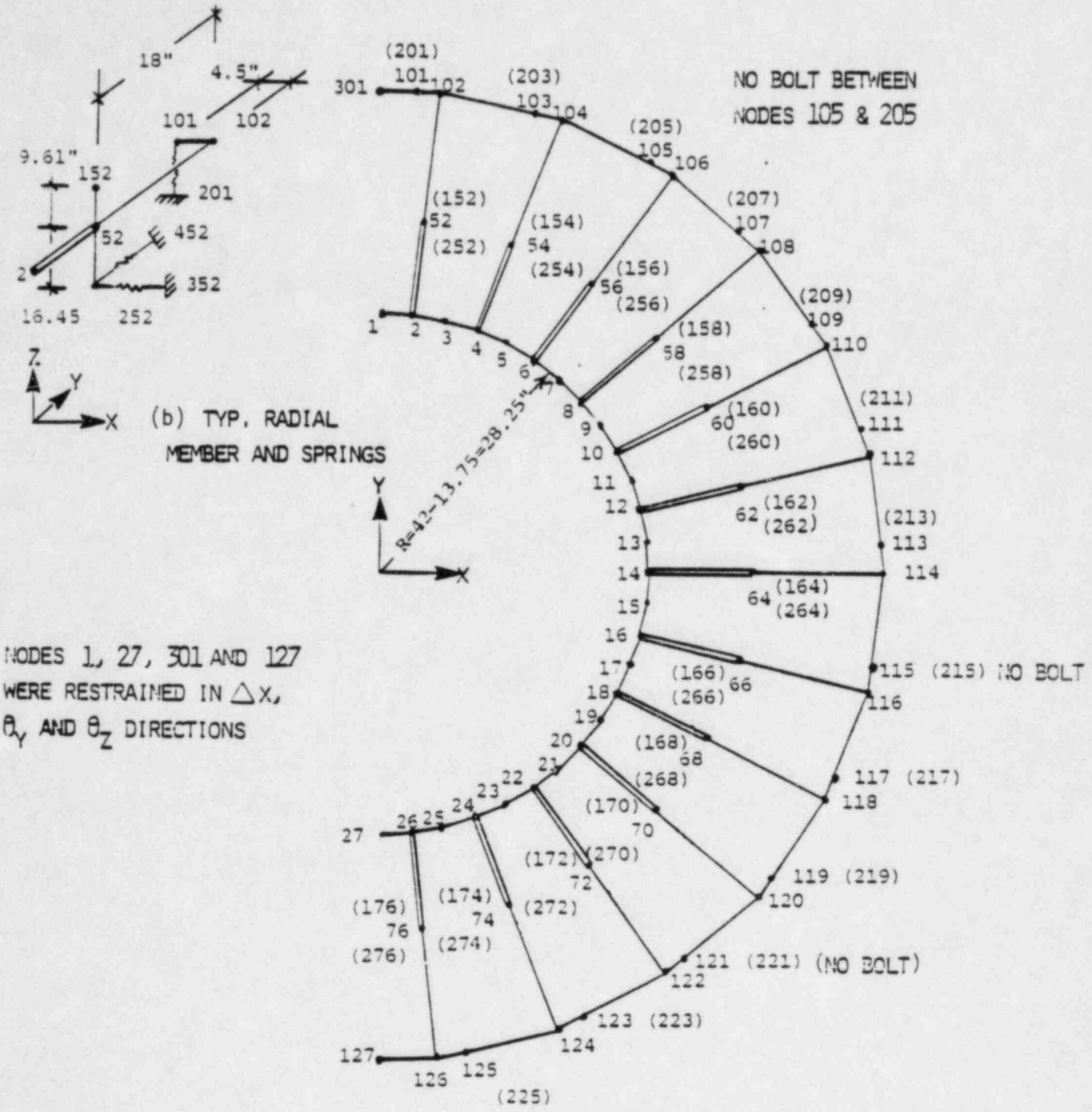

FIG. B.4a & B.4b FINITE ELEMENT MODEL OF COLLAR

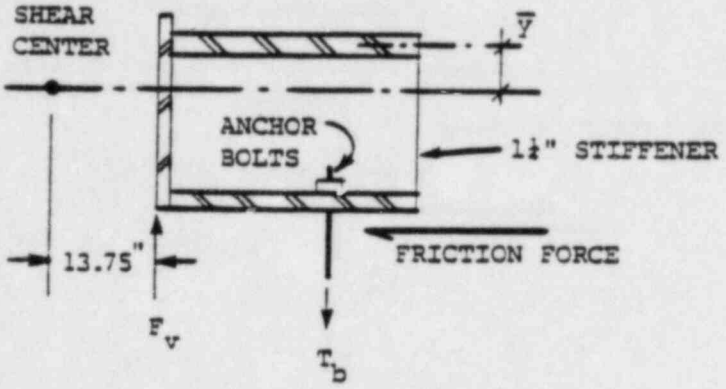

CHANNEL SECTION

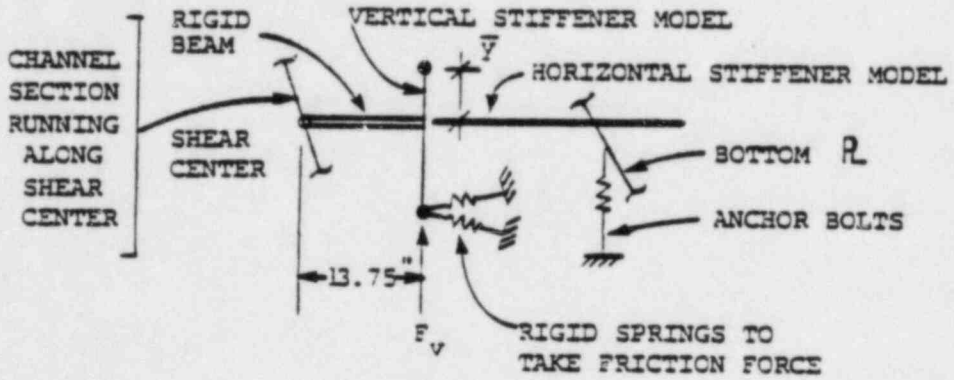

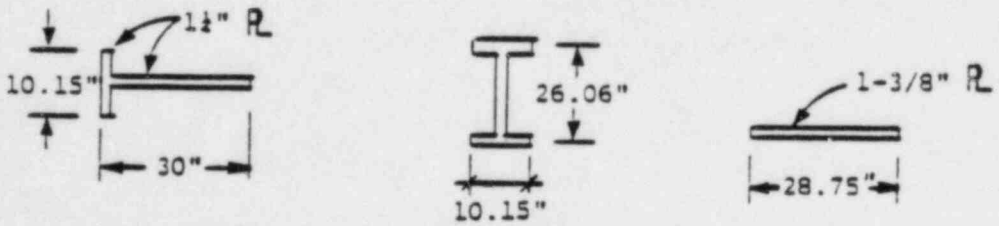

VERT. STIFFENER MODEL

HORIZ. STIFFENER MODEL

BOTTOM PLATE

FIG. B.4c FINITE ELEMENT MODEL OF COLLAR

APPENDIX C

EARTHQUAKE LOADINGS

TABLE C-1

EARTHQUAKE INPUT

Frequency (HZ)	Spectral Acceleration (G)	
	YCS 7% Damping	NRC 10% Damping
1.27 (6 Collar Fixes)	0.115	0.235
12.32 (Vertical)	0.155	0.237

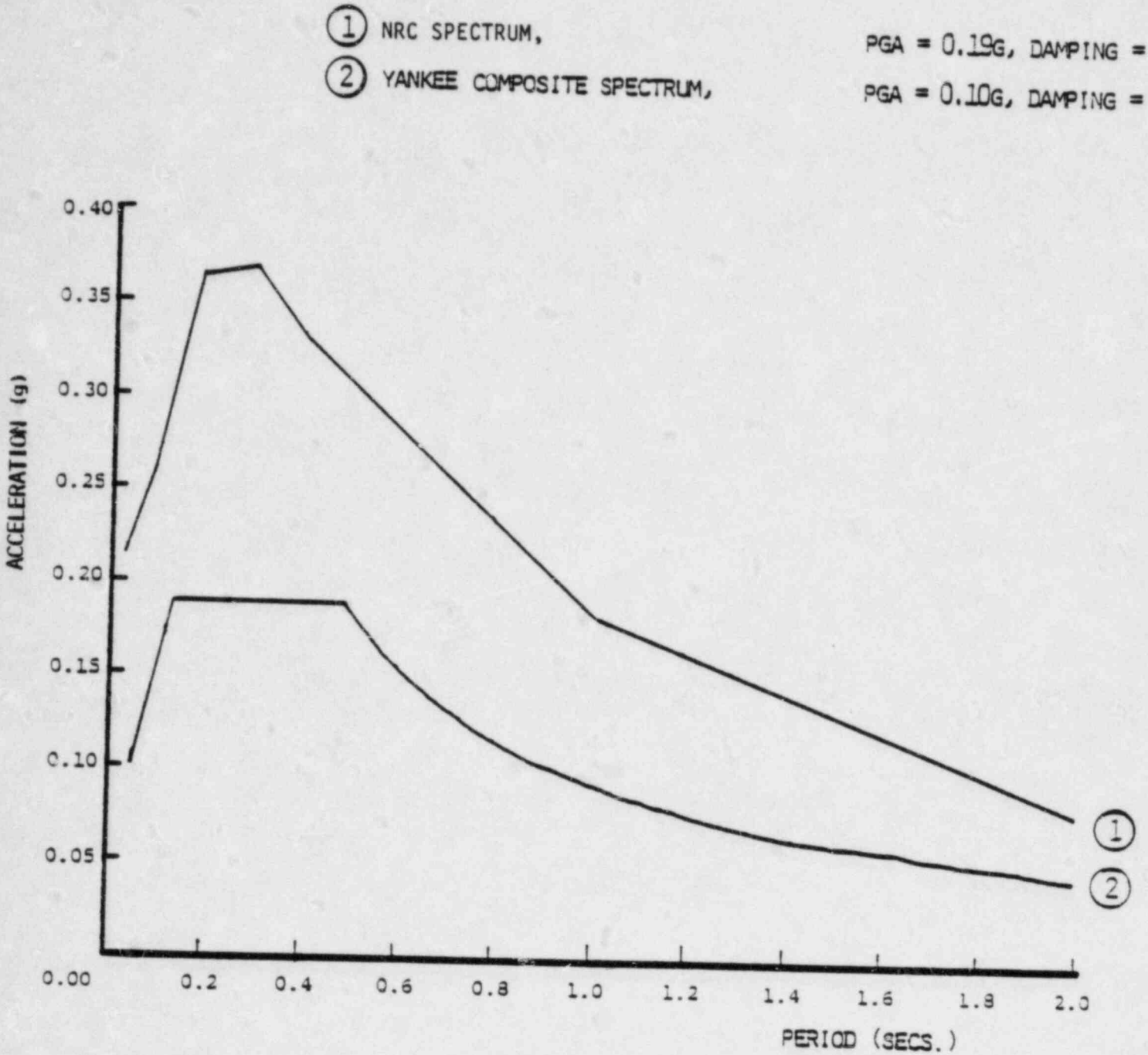

FIG. C.1 EARTHQUAKE SPECTRA

APPENDIX D

TABLE OF DYNAMIC CHARACTERISTICS

TABLE D-1

DYNAMIC CHARACTERISTICS OF RSS

Repair Stage	First Frequency (H_z)		Distributed Mass ($\frac{k\text{-}sec^2}{ft}$)	
	Horizontal	Vertical	Horizontal	Vertical
6 collar fixes	1.27	12.32	815.4	811.5

Total Mass = 850.34 $\frac{k - sec^2}{ft}$; W = 27,381^k

APPENDIX E

TABLES AND PLOTS OF ANALYTICAL RESULTS

TABLE E-1

3-D LINEAR ELASTIC MODEL UNDER YCS WITH 7% DAMPING

				Interior Column			Exterior Column		
				Top	Bottom		Top	Bottom	
				Dowel	Shell	Collar	Dowel	Shell	Collar
CAPACITIES	My	P = DL		19721.	18066.	* 38095.	12470.	11630.	* 34590.
		P = DL - Ev - Eh		17638.	16096.		9345.	8521.	
	Mu	P = DL		24980.	23225.	* 56460.	16275.	15530.	* 50590.
		P = DL - Ev - Eh		23206.	21466.		13145.	12181.	
	Vu	P = 0		2991.	3042.	5885.	2088.	2252.	5885.
ACTION	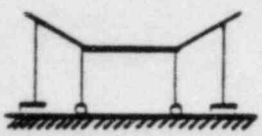		M	13980.	0.	--	7100.	7229.	7982.
	6 Collar Fixes F = 1.27 Hz		V	508.	508.	--	378.	378.	378.
	Dead Load (DL)			4700.			2910.		
	Vert. EQ Load (EV)			451.			278.		
	Vert. Load Due to Horizontal EQ (EH)			737.			1416.		

(Units in kips and ft)

*Moment capacity evaluated at zero axial load

TABLE E-2

3-D LINEAR ELASTIC MODEL UNDER NRC SPECTRUM WITH 10% DAMPING

				Interior Column			Exterior Column		
				Top	Bottom		Top	Bottom	
				Dowel	Shell	Collar	Dowel	Shell	Collar
CAPACITIES	My	P = DL		19721.	18066.	*	12470.	11630.	*
		P = DL - Ev - Eh		15738.	13155.	38095.	6201.	5320.	34590.
	Mu	P = DL		24980.	23225.	*	16275.	15330.	*
		P = DL - Ev - Eh		21415.	19668.	56460.	9807.	8478.	50590.
	Vu	P = 0		2991.	3042.	5885.	2088.	2252.	5885.
ACTION	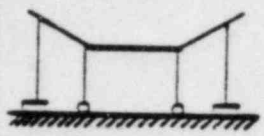 6 Collar Fixes F = 1.27 Hz		M	28570.	0.	--	14510.	14773.	16312.
			V	1038.	1038.	--	772.	772.	772.
	Dead Load (DL)			4700.			2910.		
	Vert. EQ Load (EV)			690.			425.		
	Vert. Load Due to Horizontal EQ (EH)			1507.			2894.		

(Units in kips and ft)

*Moment capacity evaluated at zero axial load

TABLE E-3

MAXIMUM DISPLACEMENT FROM LINEAR DYNAMIC ANALYSES

Repair Stage	Displacement at Top of Interior Column	
	YCS 7 % Damping	NRC 10% Damping
6 Collar Fixes F = 1.27 Hz	0.543'	0.111'
6 Collar Fixes F = 1.27 Hz	0.543'	0.111'

TABLE E-4

PARAMETERS OF THE NONLINEAR ANALYSES PERFORMED

Analysis	Horizontal Component			Vertical Component			Damping Ratio	
	Time History	PGA g	Factor	Time History	PGA g	Factor	Mode 1	Mode 2
A07	Artificial 1	0.227	1.1	Artificial 2	0.213	0.75	0.07	0.
A10	Artificial 3	0.205	1.1	Artificial 4	0.208	1.0	0.10	0.
R07	Real 1†	0.188*	1.1	Real 2††	0.113**	1.0	0.07	0.
R10	Real 1	0.188	1.1	Real 2	0.113	1.0	0.10	0.
A07.1	Artificial	0.227	1.1	Artificial	0.213	0.75	0.07	0.07
R07.1	Real 1	0.188	1.1	Real 2	0.113	1.0	0.07	0.07

† Real 1 time history is the S00E component of El Centro record of Imperial Valley earthquake of 5/18/40

††Real 2 time history is the vertical component of El Centro record of Imperial Valley earthquake of 5/18/40

* Response spectrum of Real 1 time history scaled to a PGA = 0.188 g envelops the NRC spectrum over $0.87 < f < 1.27$ hz for damping ratios = 0.07 and 0.10.

**Recorded PGA's are 0.348 g and 0.210 g for Real 1 and Real 2 time histories. Real 1 time history is scaled by 0.188 g/0.348 g = 0.539. Similarly, scaling Real 2 time history by 0.539, PGA = 0.539 (0.210g) = 0.113 g.

TABLE E.5

EXTENT OF INELASTIC ACTION OCCURING AT TOP DOWEL SECTIONS

Analysis	Max. Absolute Plastic Hinge Rotation at Section				Number of Inelastic Cycles at Section			
	7	14	21	29	7	14	21	29
	(10^{-4} RAD)							
A07	1.31	0.74	2.00	2.79	1.	1.	1.	4.
A10	1.86	1.11	0.30	3.63	0.5	0.5	0.5	1.5
R07	0.37	0.35	1.15	2.64	0.5	1.	1.	2.
R10	0.	0.05	0.79	1.98	0.	0.5	0.5	1.5
A07.1	0.16	0.12	0.98	2.41	0.5	0.5	0.5	1.5
R07.1	0.02	0.12	0.94	2.30	0.5	0.5	0.5	1.5

TABLE E-6

SUMMARY OF NONLINEAR ANALYSES PERFORMED ON RSS FOR THE PROBABILISTIC SEISMIC RISK ASSESSMENT PROJECT

Earthquake	Date	Recorded At	Comp.	PGA g	$\overline{SV}$ in/sec	Max. $\lvert\theta_{ph}\rvert$ at Section (10^{-4})				Number of Inelastic Cycles at Section			
						7	14	21	29	7	14	21	29
San Francisco	3/22/57	Golden Gate Park	N10E	0.45	9.37	0.	0.	0.	0.	0.	0.	0.	0.
"	"	"	S80E	0.45	13.07	0.	0.	0.	0.	0.	0.	0.	0.
"	"	"	"	0.60	17.43	0.	0.	0.3	1.0	0.	0.	0.5	0.5
Lytle Creek	9/12/70	Colton	South	0.40	12.08	0.	0.	0.	0.1	0.	0.	0.	0.5
"	"	"	"	0.45	13.59	<0.05	0.	0.	0.7	0.5	0.	0.	2.
"	"	"	East	0.45	13.42	0.5	0.	<0.05	1.7	0.5	0.	0.5	1.
Imperial Valley	5/18/40	El Centro	S00E	0.16	12.11	0.	0.	0.	<0.05	0.	0.	0.	0.5
"	"	"	"	0.20	15.14	0.5	0.	0.3	1.2	0.5	0.	0.5	1.5
NW California	10/7/51	Ferndale	N46W	0.20	9.16	0.	0.	0.	0.	0.	0.	0.	0.
"	"	"	"	0.30	13.74	<0.05	0.	0.3	1.0	0.5	0.	0.5	1.5
San Luis Obispo	11/21/52	San Luis Obispo	N36W	0.20	11.11	0.8	<0.05	0.	2.0	0.5	0.5	0.	1.
"	"	"	"	0.25	13.88	1.6	1.0	6.8	3.2	0.5	0.5	1.	1.5
NW California	2/9/41	Ferndale	S45E	0.26	11.46	0.1	0.	0.1	1.1	0.5	0.	0.5	1.
"	"	"	"	0.32	14.33	1.8	0.1	1.1	3.6	0.5	1.	1.	3.
Parkfield	6/27/66	San Luis Obispo	S54W	0.30	11.51	0.3	0.	0.	1.3	0.5	0.	0.	0.5
"	"	"	"	0.37	14.38	1.9	1.2	0.4	3.9	0.5	0.5	1.	1.5

TABLE E-7

CASE 1: RING FOUNDATION FORCES DUE TO DEAD LOAD PLUS YCS HORIZONTAL AND VERTICAL (UPWARD) LOADS

ELEMENT	SHEAR (K)	TORSION (K)	BENDING MOMENT (K-FT)	
1	44	168	1799	-1954
4	131	518	1921	-2386
8	222	909	2318	-3104
10	318	1369	2994	-4117
27	-820	-4046	7022	-4130
28	-687	-3515	4484	-2069
31	-549	-3211	2392	-455
34	-404	-3080	758	667
37	-250	-3104	-369	1252
40	-83	-3205	-948	1242
43	101	-3337	-928	572
46	306	-3441	-246	-833
76	-1409	-1914	7180	-2211
75	-1124	-1870	2393	1570
81	-837	-2206	-1374	4327
86	-546	-2822	-4085	6012
95	-246	-3580	-4808	5677
96	-70	-4382	-5294	5046
106	410	-5095	-3141	1692
107	778	-5606	-1178	1566
136	-1362	2950	3888	916
137	-957	2426	-1174	4550
141	-567	1582	-4743	6744
148	-188	549	-6846	7513

TABLE E-8

CASE 2: RING FOUNDATION FORCES DUE TO DEAD LOAD PLUS YCS HORIZONTAL AND VERTICAL (DOWNWARD) LOADS

ELEMENT	SHEAR (K)	TORSION (K)	BENDING MOMENT (K-FT)	
1	70	124	1142	-1390
4	211	396	1365	-2111
8	357	734	2056	-3316
10	509	1186	3223	-5021
27	-1010	-3859	7931	-4366
28	-821	-3335	4712	-1816
31	-628	-3083	2124	90
34	-429	-3040	203	1312
37	-223	-3140	-1015	1802
40	-3	-3318	-1492	1503
43	236	3502	-1175	343
46	498	-3612	-1	1754
76	-1601	-1739	8078	-2430
75	-1259	-1705	2595	1846
81	-918	-2093	-1664	4902
86	-574	-2790	-4668	6695
95	-222	-3637	-5484	6868
96	147	-4520	-5877	5357
106	542	-5284	-3336	1423
107	967	-5797	-890	2521
136	-1554	3135	4788	691
137	-1091	2603	-967	4818
141	-647	1706	-5025	7306
148	-215	594	-7417	8177

TABLE E-9

CASE 3: RING FOUNDATION FORCES DUE TO DEAD LOAD PLUS NRC HORIZONTAL AND VERTICAL (UPWARD) LOADS

ELEMENT	SHEAR (K)	TORSION (K)	BENDING MOMENT (K-FT) NODE (I)	BENDING MOMENT (K-FT) NODE (J)
1	-35	445	9281	-9155
4	-106	1321	9070	-8694
8	-178	2148	8527	-7899
10	-249	2895	7657	-6778
27	-670	-14455	14454	-12089
28	-741	-13230	13419	-10803
31	-813	-12134	12021	-9154
34	-871	-11148	10272	-7200
37	-915	-10296	8230	-5002
40	-945	-9603	5958	-2623
43	-962	-9087	3521	-126
46	-926	-8917	991	2274
76	-2180	-7180	12300	-4609
75	-1884	-6942	5287	1358
81	-1556	-7350	-672	6162
86	-1198	-8289	-5410	9636
95	-803	-9568	-7280	10112
96	-363	-11055	-9122	10404
106	128	-12559	-6880	6427
107	678	-13913	-5155	2762
136	-2198	6693	3255	4497
137	-1545	5302	-5073	10524
141	-916	3388	-10941	14172*
148	-304	1166	-14391*	15467*

*Exceeds flexural capacity.

TABLE E-10

CASE 4: RING FOUNDATION FORCES DUE TO DEAD LOAD PLUS NRC HORIZONTAL AND VERTICAL (DOWNWARD) LOADS

ELEMENT	SHEAR (K)	TORSION (K)	BENDING MOMENT (K-FT) NODE (I)	NODE (J)
1	-17	449	6564	-6504
4	-50	1338	6418	-6241
8	-81	2206	6071	-5784
10	-108	3041	5532	-5149
27	-989	-10421	12580	-9090
28	-969	-9081	10027	-6609
31	-918	-8067	7433	-4194
34	-840	-7364	4935	-1973
37	-733	-6946	2660	-74
40	-596	-6782	733	1369
43	-427	-6828	-715	2210
46	-211	-7028	-1545	2292
76	-2419	-5215	12527	-3994
75	-2012	-5097	4489	2607
81	-1589	-5661	-2090	7695
86	-1148	-6763	-7099	11149
95	-680	-8153	-8278	10678
96	-174	-9677	-9821	10437
106	379	-11128	-6476	5136
107	989	-12318	-4010	519
136	-2364	6150	5196	3141
137	-1662	4951	-3674	9535
141	-985	3192	-9926	13401*
148	-327	1103	-13607*	14763*

*Exceeds flexural capacity.

TABLE E- 11

CASE 5: RING FOUNDATION FORCES DUE TO DEAD LOAD PLUS NRC HORIZONTAL AND VERTICAL (UPWARD) LOADS -- WITH PLASTIC HINGE AT NODE 37

ELEMENT	SHEAR (K)	TORSION (K)	BENDING MOMENT (K-FT) NODE (I)	NODE (J)
1	-35	447	9308	-9183
4	-106	1325	9098	-8721
8	-178	2155	8554	-7926
10	-249	2904	7683	-5804
27	-667	-14306	14431	-12078
28	-738	-13082	13394	-10790
31	-809	-11988	11994	-9139
34	-864	-10990	10243	-7194
37	-905	-10126	8209	-5017
40	-932	-9420	5956	-2668
43	-946	-8889	3547	-210
46	-905	-8706	1055	2137
76	-2156	-6742	12371	-4766
75	-1857	-6480	5401	1149
81	-1527	-6854	-508	5894
86	-1165	-7753	-5192	9304
95	-758	-8984	-7057	9767
96	-326	-10416	-8835	9986
106	168	-11819	-5788	5193
107	721	-13024	-4000	1457
136	-2154	5689	4547	2138
137	-1505	4561	-2630	7938
141	-884	2929	-8298	11418
148	-290	1008	-11607	12632

TABLE E-12

CASE 6: RING FOUNDATION FORCES DUE TO DEAD LOAD PLUS NRC HORIZONTAL AND VERTICAL (DOWNWARD) LOADS -- WITH PLASTIC HINGE AT NODE 37

ELEMENT	SHEAR (K)	TORSION (K)	BENDING MOMENT (K-FT) NODE (I)	NODE (J)
1	-17	449	6593	-6532
4	-50	1339	6446	-6266
8	-82	2207	6096	-5805
10	-110	3042	5553	-5163
27	-993	-10467	12604	-9101
28	-974	-9124	10042	-6605
31	-925	-8109	7433	-4170
34	-848	-7407	4915	-1924
37	-742	-6993	2616	3
40	-606	-6836	661	1477
43	-435	-6892	-818	2352
46	-222	-7107	-1680	2466
76	-2424	-5422	12358	-3810
75	-2013	-5327	4326	2773
81	-1586	-4914	-2233	7826
86	-1139	-7039	-7204	11223
95	-665	-8449	-8333	10679
96	-151	-9988	-9793	10328
106	411	-11437	-6153	4702
107	1029	-12604	-3547	-83
136	-2308	5550	6635	1505
137	-1610	4493	-1987	7666
141	-944	2899	-8021	11345
148	-309	999	-11541	12632

TABLE E-13

MAXIMUM FORCES DEVELOPED IN MAT FOUNDATION

Force	Load Combination		Ultimate Strength
	D.L. + YCS	D.L. + NRC	
Shear	4094^{k}	4094^{k}	4630.^{k}
Moment	36774$^{k\text{-}ft}$	36774$^{k\text{-}ft}$	92441.$^{k\text{-}ft}$

TABLE E.14

BEAM ELEMENT STRESS DUE TO F_V (FROM 15500 K-FT), F_H = 1948^K AND V = 794^K

Elem. No.	Node I	Node J	Section	Axial Force (kips)	M_{major} (k-in)	M_{minor} (k-in)	$\frac{M_{maj}}{S_{maj}}$ $\frac{M_{min}}{S_{min}}$ (ksi)	Torsion (k-in)	Shear Stress Due To Torsion (k-in)	V_y (kips)	V_y (kips)
1	1	2	Collar	59.3	3729.	1366.	5.06	0.	0.	0.	0.
2	2	3		58.3	3812.	1039.	4.71	1117.	12.5	118.	47.7
4	4	5		90.6	3499.	4353.	8.81	126.	1.41	52.6	14.7
25	25	26		40.5	8297.	1582.	8.84	11.2	0.13	9.6	78.1
26	26	27	Collar	428.	11836.	5152.	18.6	0.	0.	0.	0.
60	74	274	Vert. Stiff.	0.	2307.	2441.	12.1	0.	0.	148.	140.
64	72	272	Vert. Stiff.	0.	1304.	3281.	14.8	0.	0.	199.	79.3
40	52	102	Horiz. Stiff.	6.1	3001.	240.	9.13	139.	4.03	12.7	170.
41	54	104	Horiz. Stiff.	2.6	2690.	401.	10.7	363.	10.5	22.8	149.
43	58	108	Horiz. Stiff.	0.4	3395.	93.	7.74	173.	5.02	4.2	189.
80	101	102	Bottom Plate	--	362.	--	40.9	--	--	--	--
82	103	104	Bottom Plate	--	387.	--	42.7	--	--	--	--
107	103	203	Rock Bolt	198.2	--	--	71.8	--	--	--	--
108	107	207	Rock Bolt	189.1	--	--	68.5	--	--	--	--

TABLE E.15 STRESSES AND END DISPLACEMENTS [13]

(a) Monotonic Loading*

Specimen No.	Bar Size	Block Width (in.)	Maximum Stress (ksi)	Average Bond Stress (ksi)	Displacement at Maximum Stress	
					Pulling End (in.)	Pushing End (in.)
2	# 6	15	77	2.42	.104	-.037
3	# 8	25	102	1.14	.98	-.065
5	# 6	15	80	2.19	.123	-.052
7	# 8	15	56	2.09	.06	-.048
10	# 6	20	89	2.10	.35	-.035
13	# 8	25	95	2.13	.45	-.096
16	#10	25	87	2.34	.169	-.060

*Except for specimen no. 3 which is subjected to pull on one end only, the rest are under pull and push with pull equal to push.

(b) Cyclic Loading

For pull equal to push.

Specimen No.	Bar Size	Block Width (in.)	Max. Stress (ksi)	Average Bond Stress (ksi)	End Displacement at Max. Stress (in.)	
					δ_1	δ_2
4	# 6	15	55	1.73	.067	-.065
6	# 6	15	64	1.6	.048	-.041
8	# 8	15	51	1.52	.039	-.034
9	# 8	15	50	1.67	.040	-.031
11	# 6	20	67	1.58	.062	-.027
12	#16	20	72	1.35	.054	-.025
14	# 8	25	72	1.283	.060	-.030
15	# 8	25	74	1.49	.071	-.032
17	#10	25	68	1.62	.052	-.033
18	#10	25	66	1.86	.054	-.038

TABLE E-16

PLASTIC HINGE ROTATIONS OF DOWEL SECTIONS

	Max. $\lvert\theta_{ph}\rvert$ Capacity 10^{-4} RAD.	θ_{ph} in RSS Nonlinear Model 10^{-4} RAD.
Exterior Col.	39.6	2.00*
Interior Col.	44.4	3.63**

*Model run A07
**Model run A10

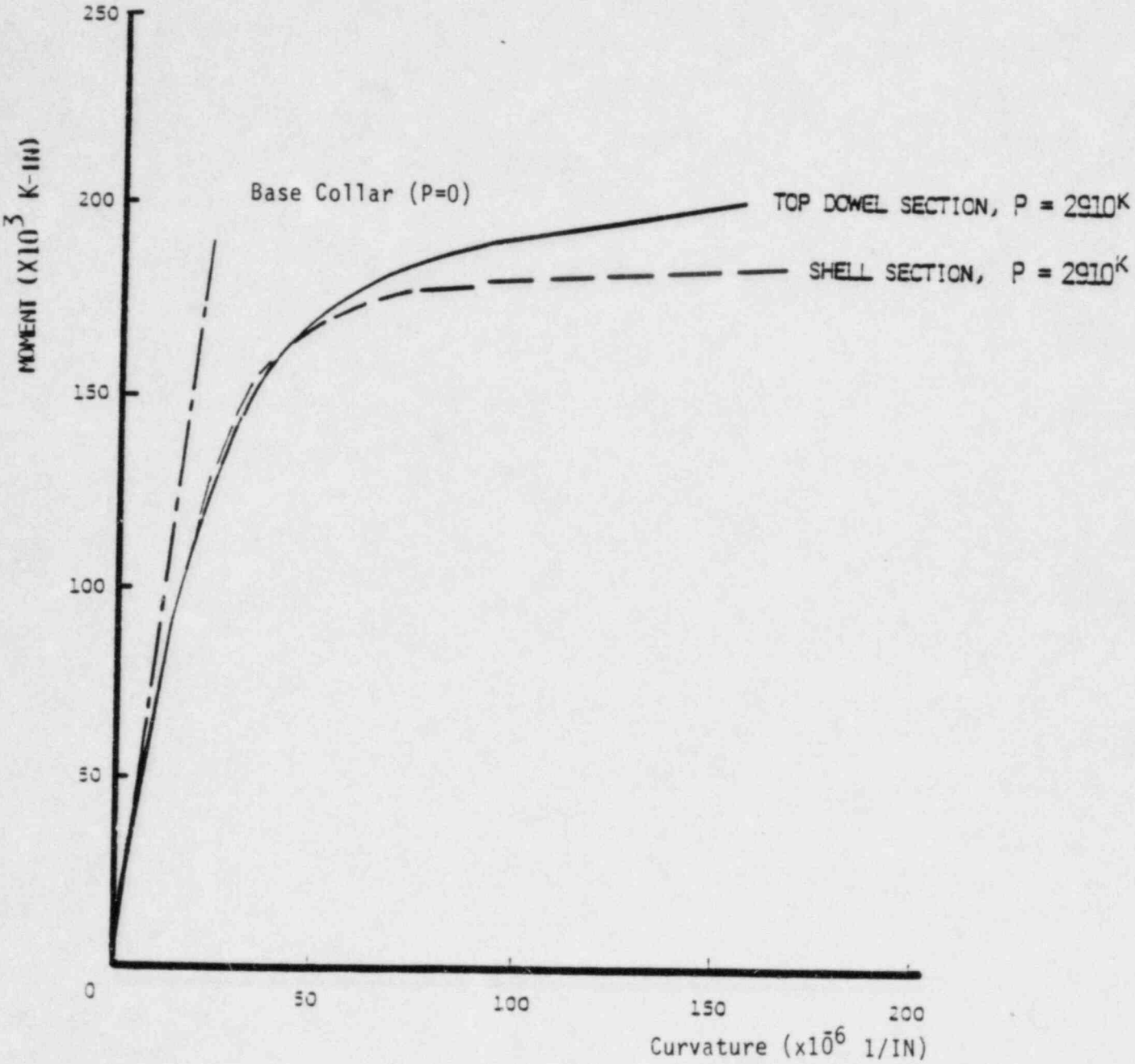

FIG. E.1a MOMENT-CURVATURE DIAGRAMS OF EXTERIOR COLUMN

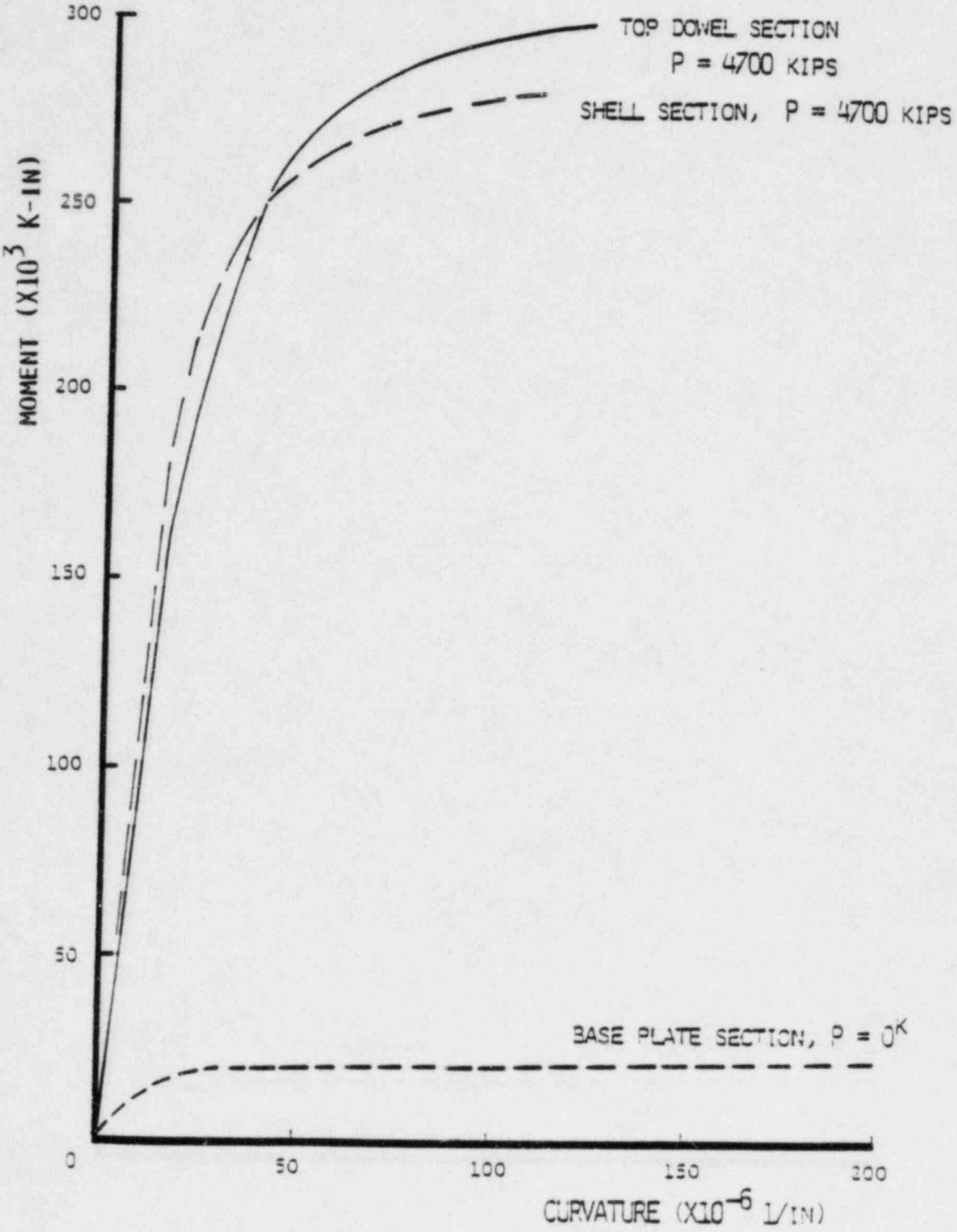

FIG. E.1b MOMENT-CURVATURE DIAGRAMS OF INTERIOR COLUMN

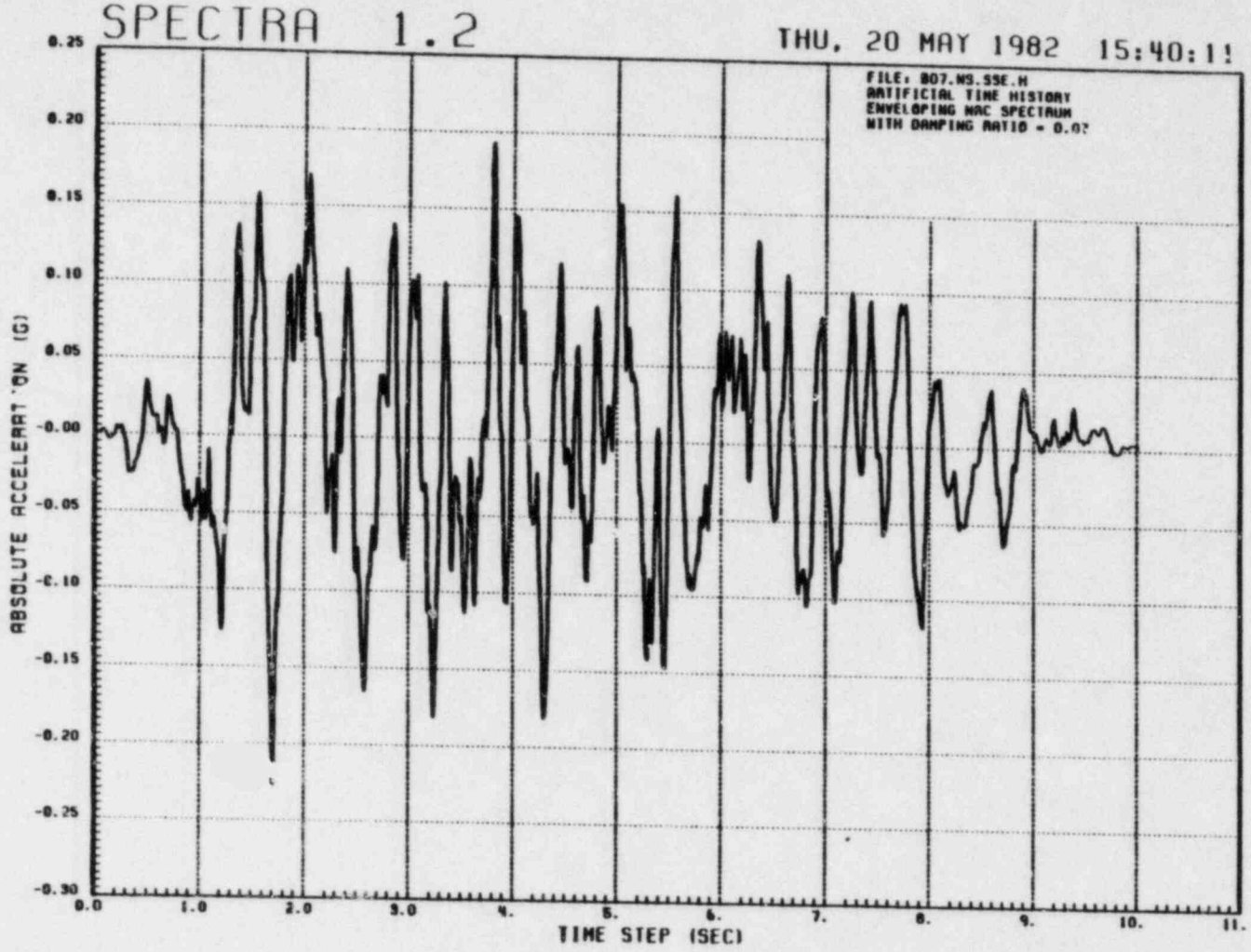

FIG. E.2 ARTIFICIAL TIME HISTORY 1

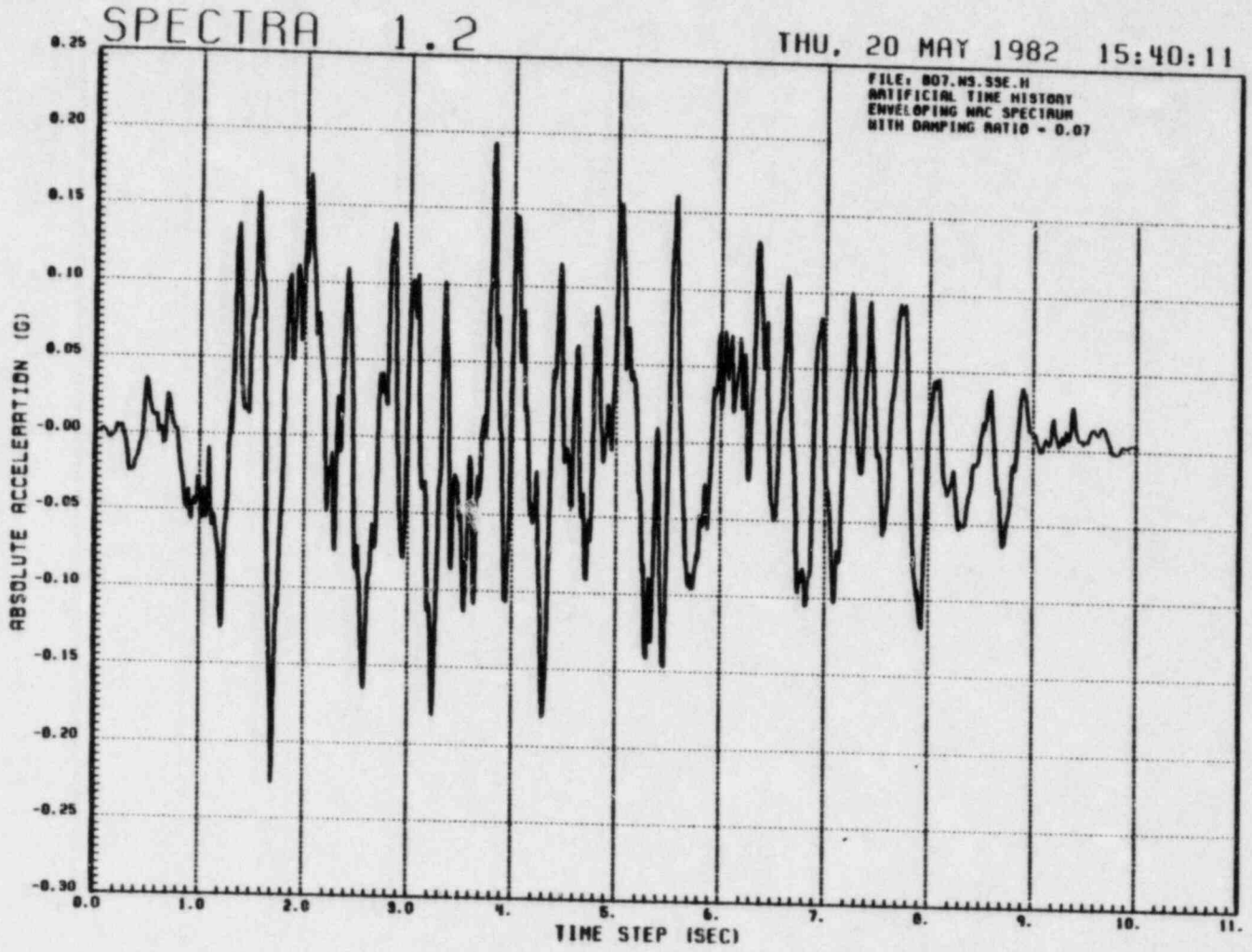

FIG. E.3 ARTIFICIAL TIME HISTORY 2

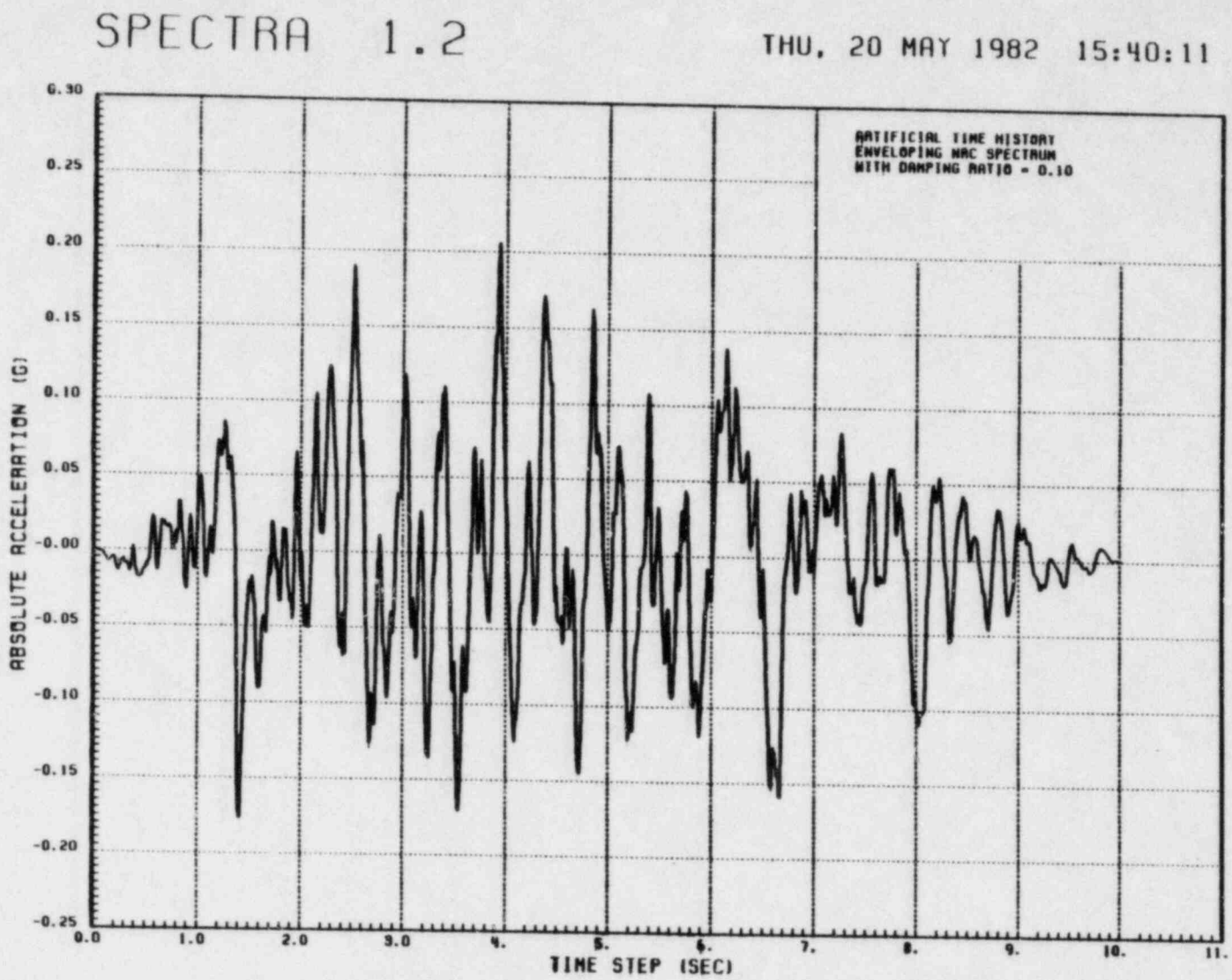

FIG. E.4 ARTIFICIAL TIME HISTORY 3

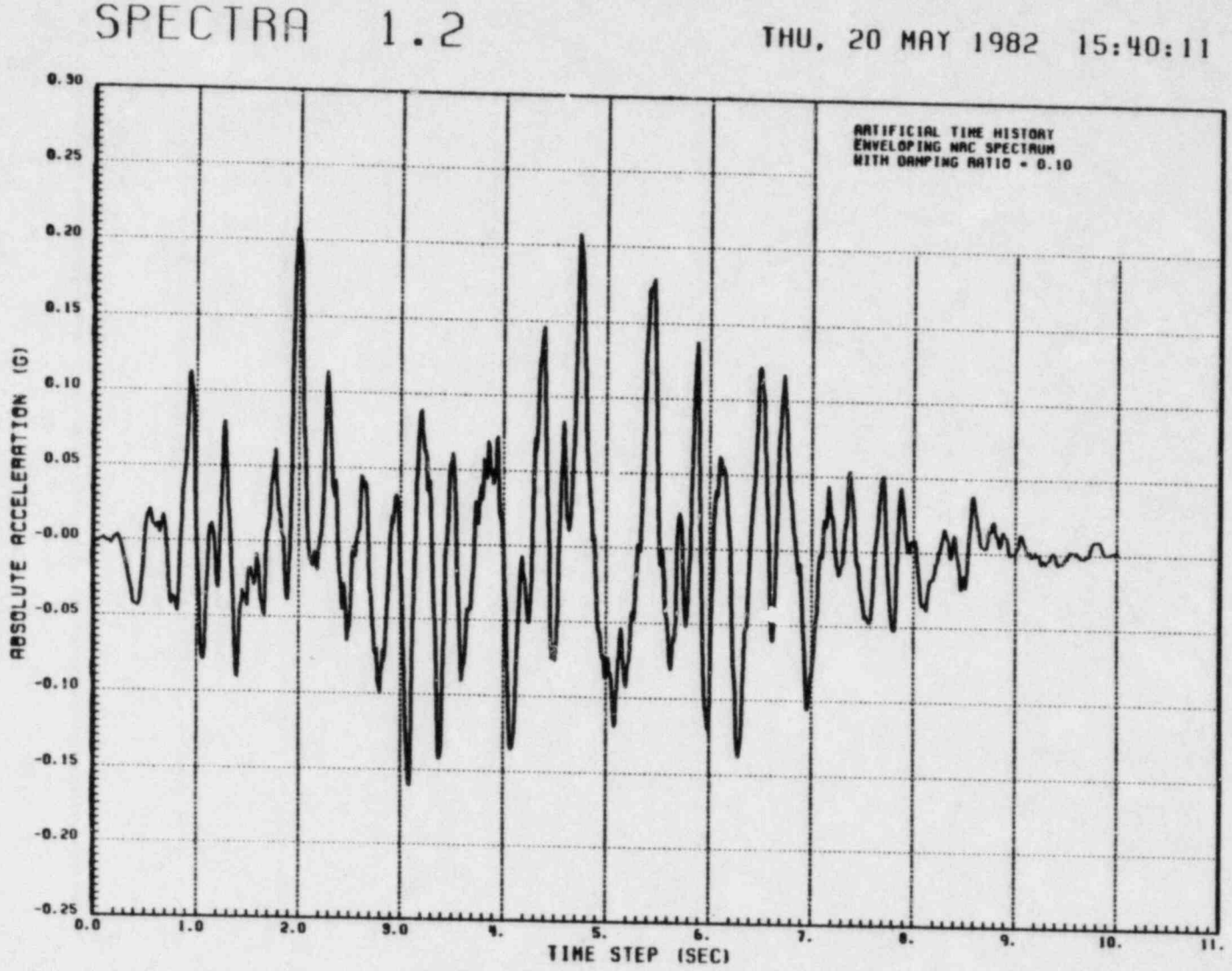

FIG. E.5 ARTIFICIAL TIME HISTORY 4

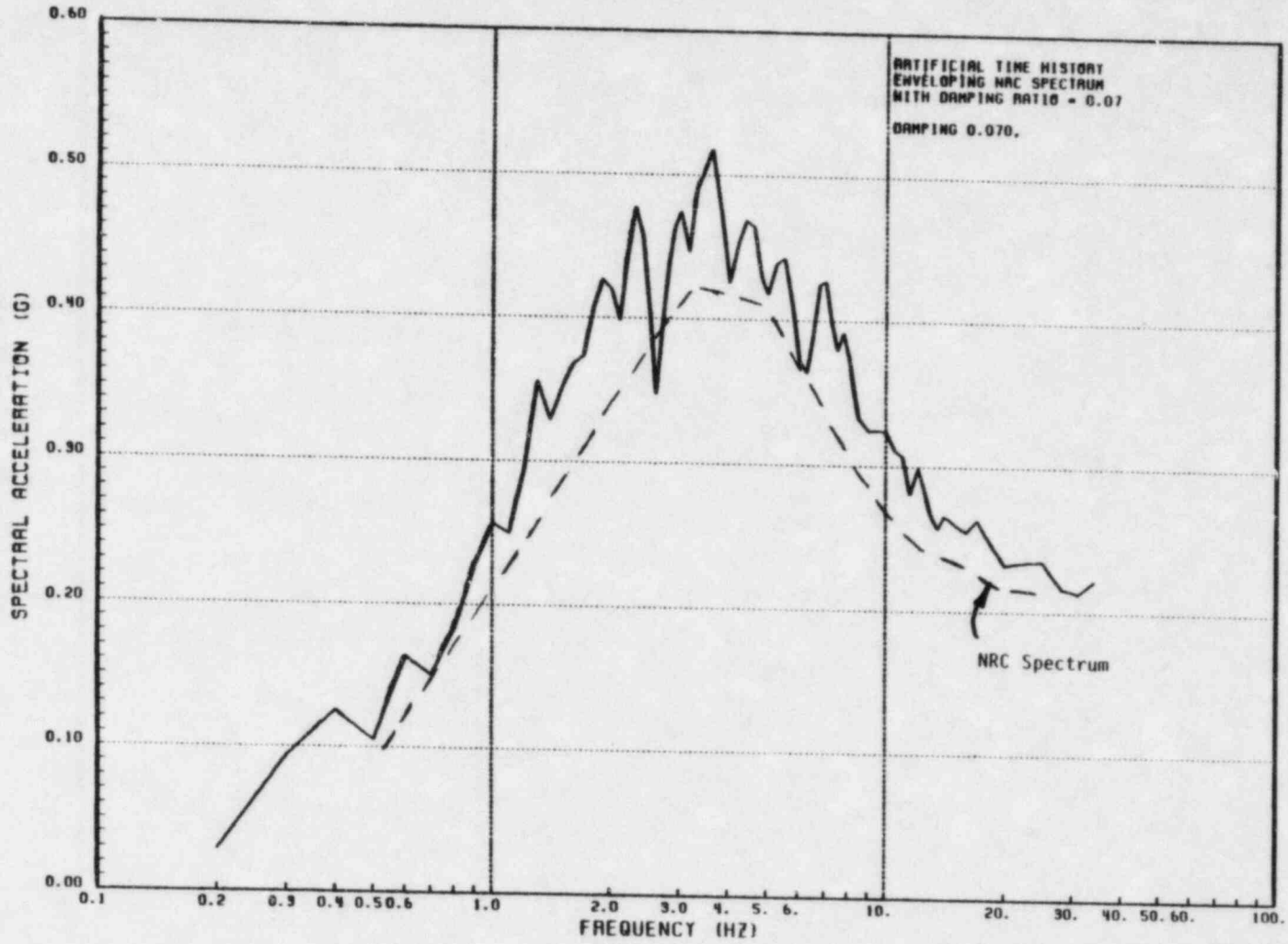

FIG. E.6 RESPONSE SPECTRUM OF ARTIFICIAL TIME HISTORY 1

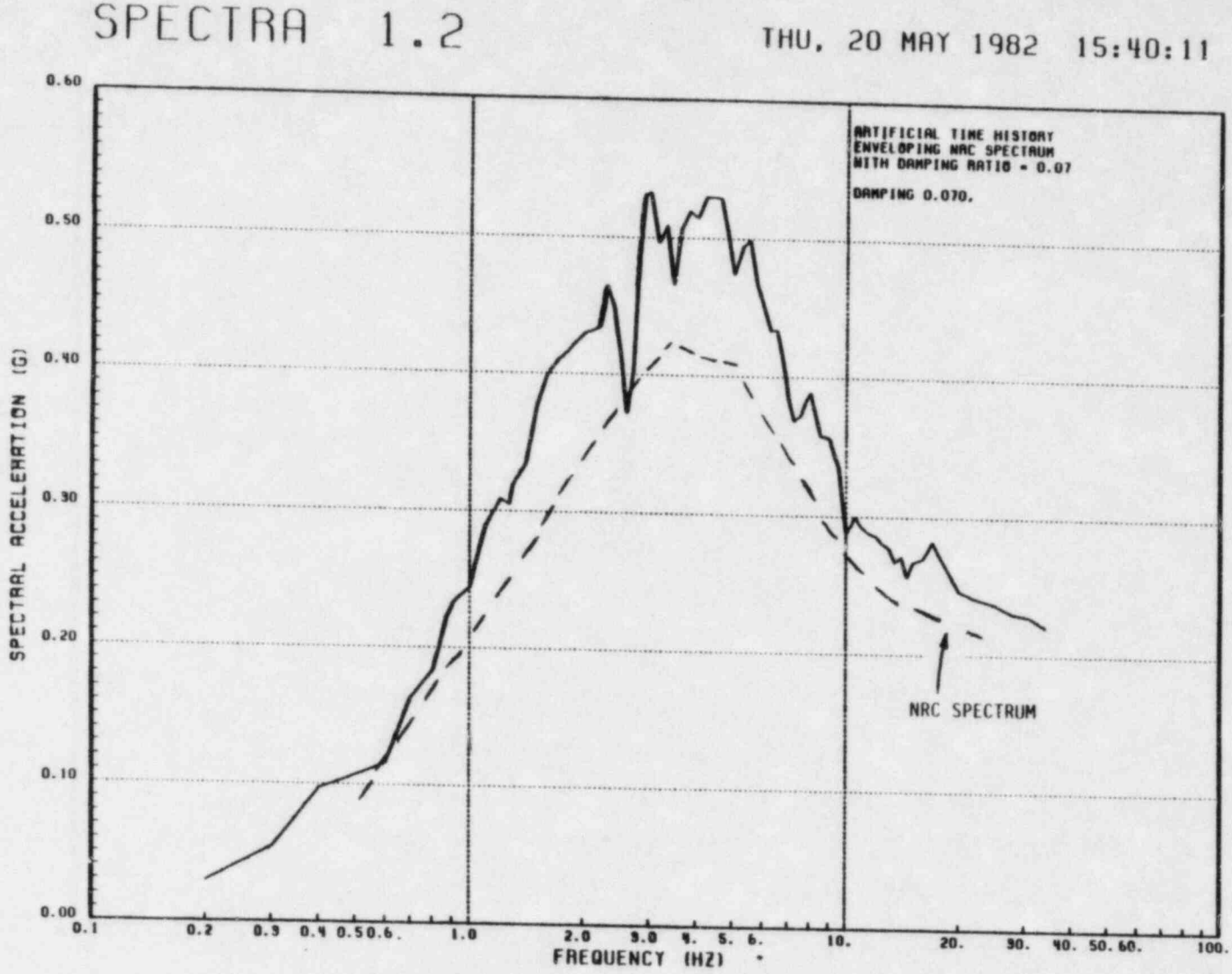

FIG. E.7 RESPONSE SPECTRUM OF ARTIFICIAL TIME HISTORY 2

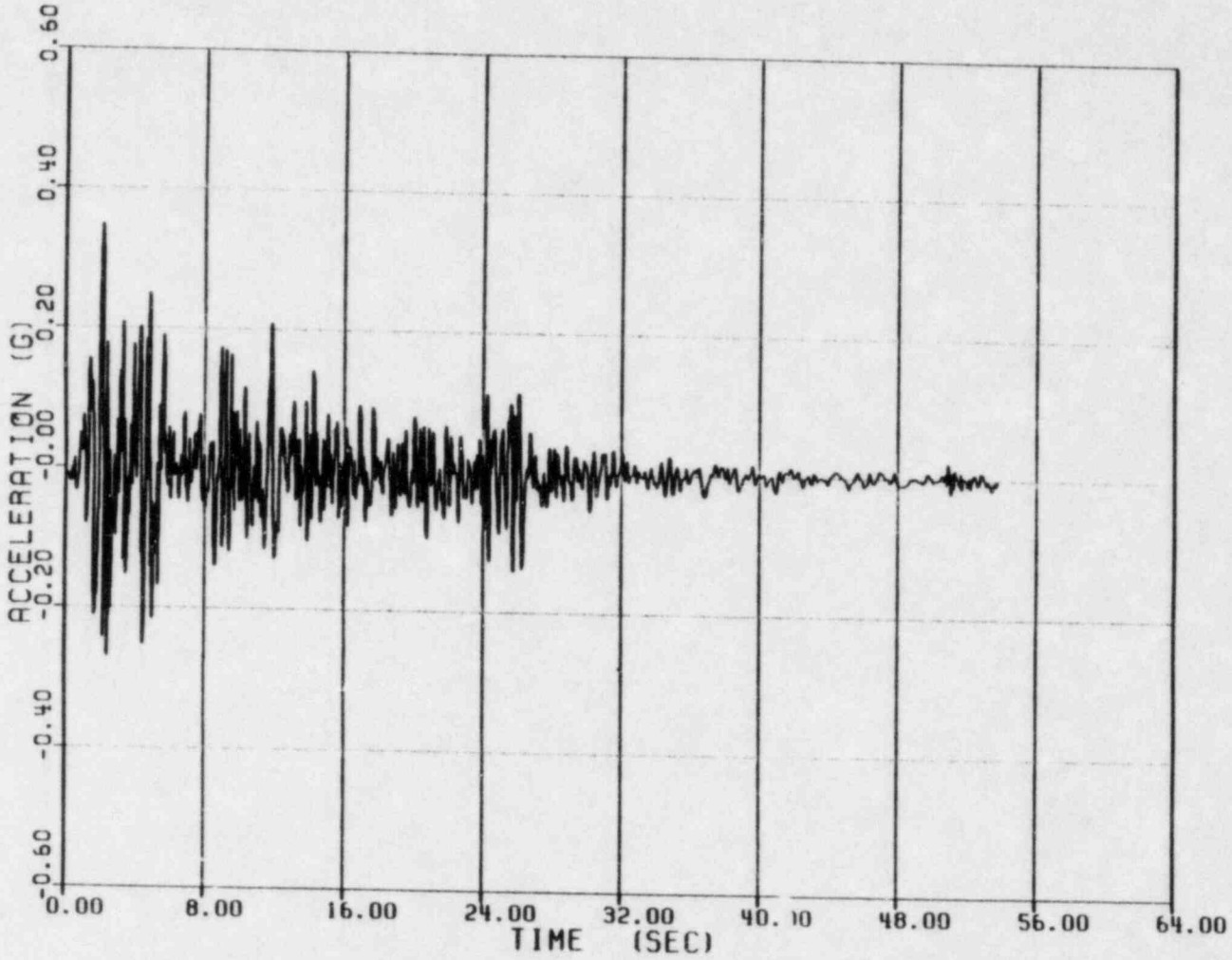

FIG. E.8 IMPERIAL VALLEY E/Q. OF 5/18/40 RECORDED AT EL CENTRO, SOOE COMPONENTS

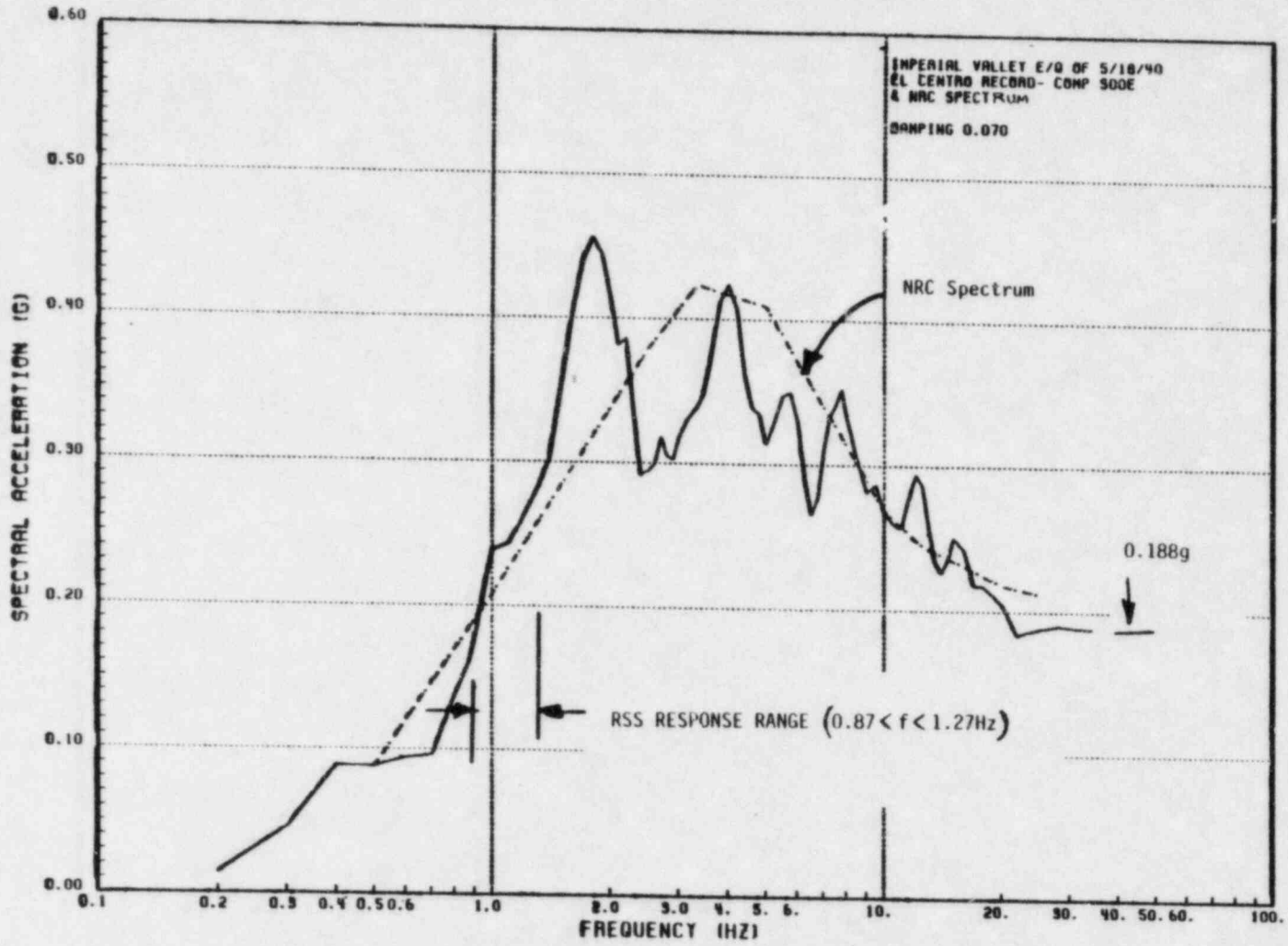

FIG. E.9 RESPONSE SPECTRUM OF EL CENTRO RECORD, S00E COMPONENT, DAMPING = 0.07

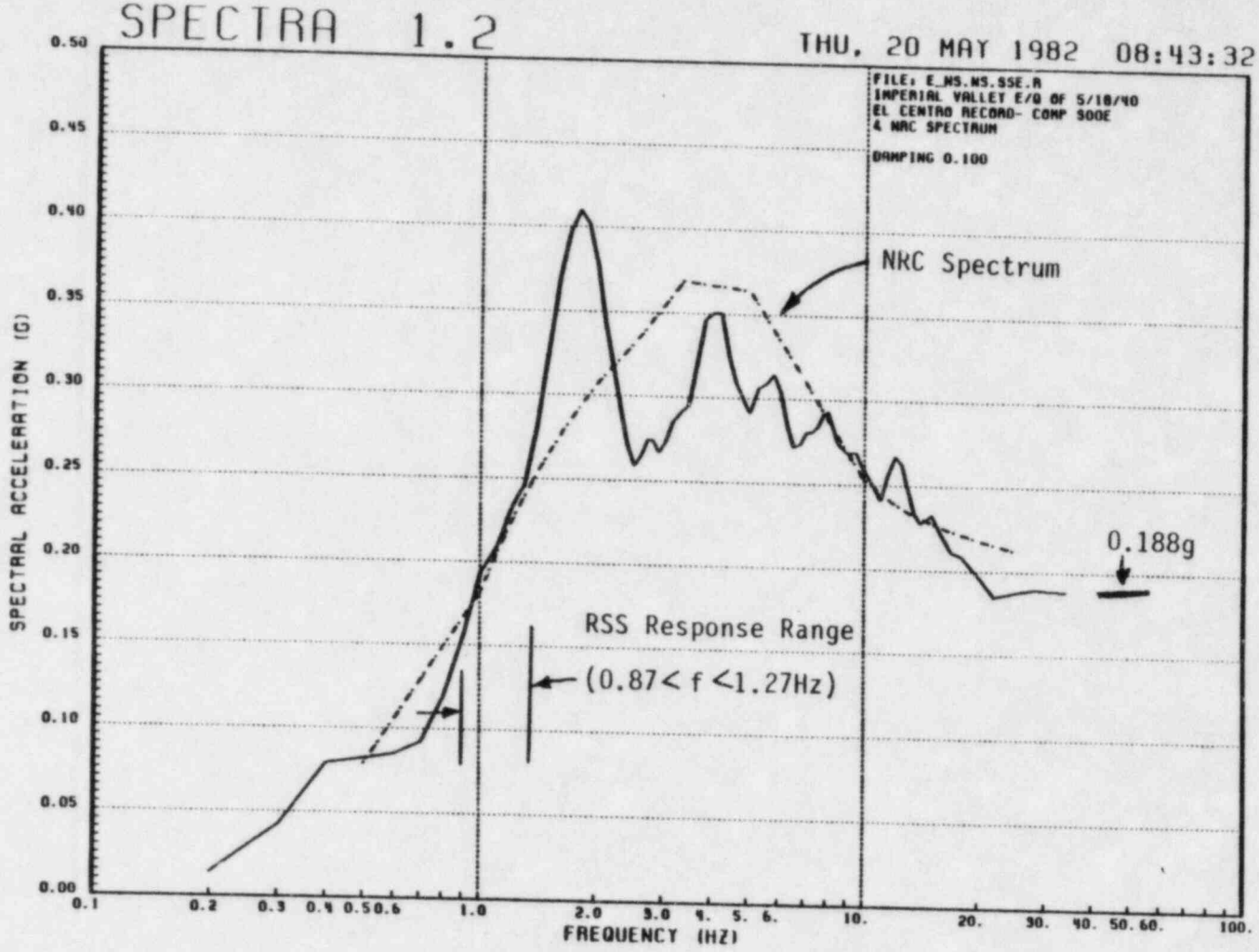

FIG. E.10 RESPONSE SPECTRUM OF EL CENTRO RECORD, S00E COMPONENT, DAMPING: =0.10

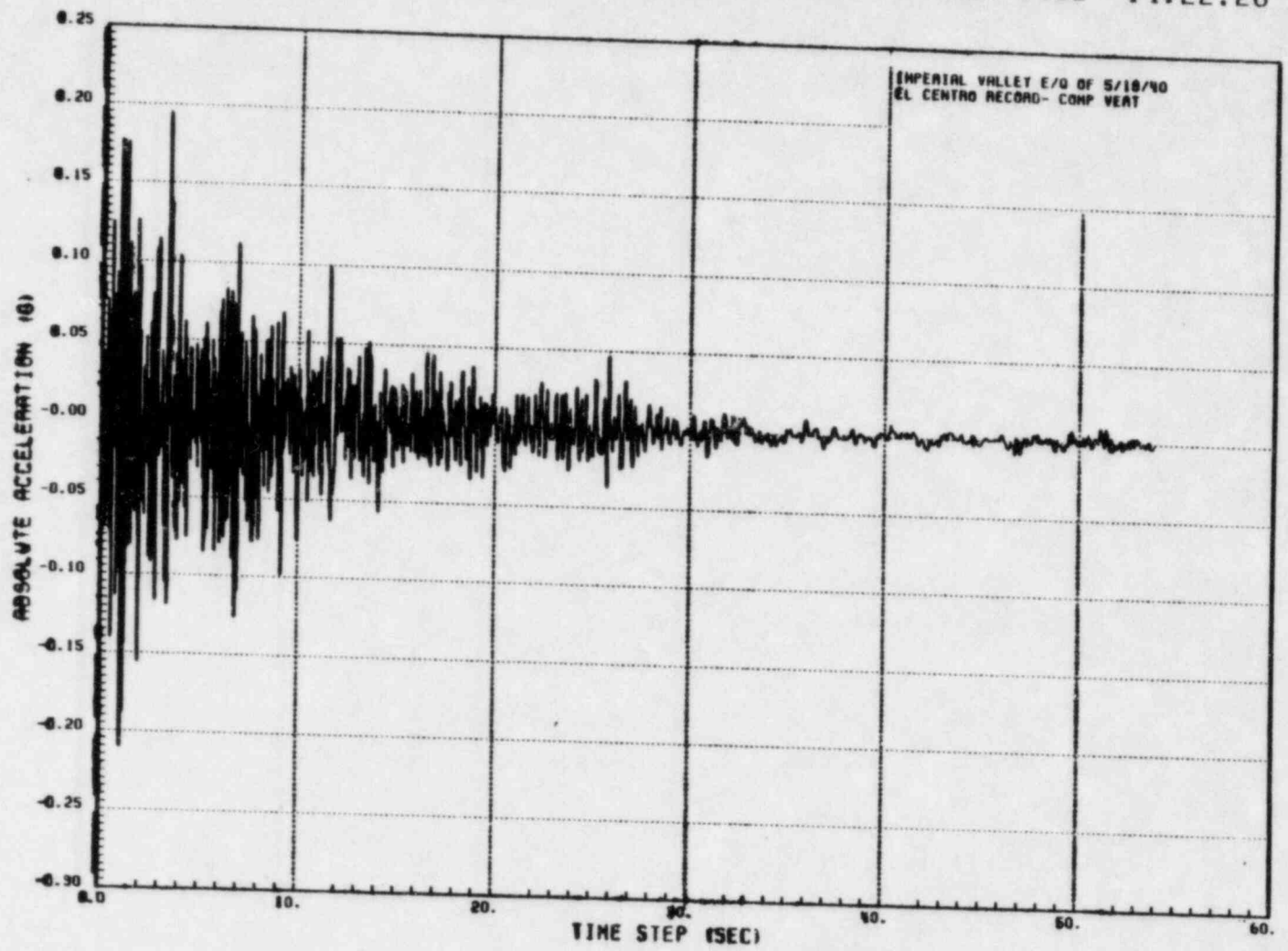

FIG. E.11 IMPERIAL VALLEY E/Q. OF 5/13/40 RECORDED AT EL CENTRO, VERTICAL COMPONENT

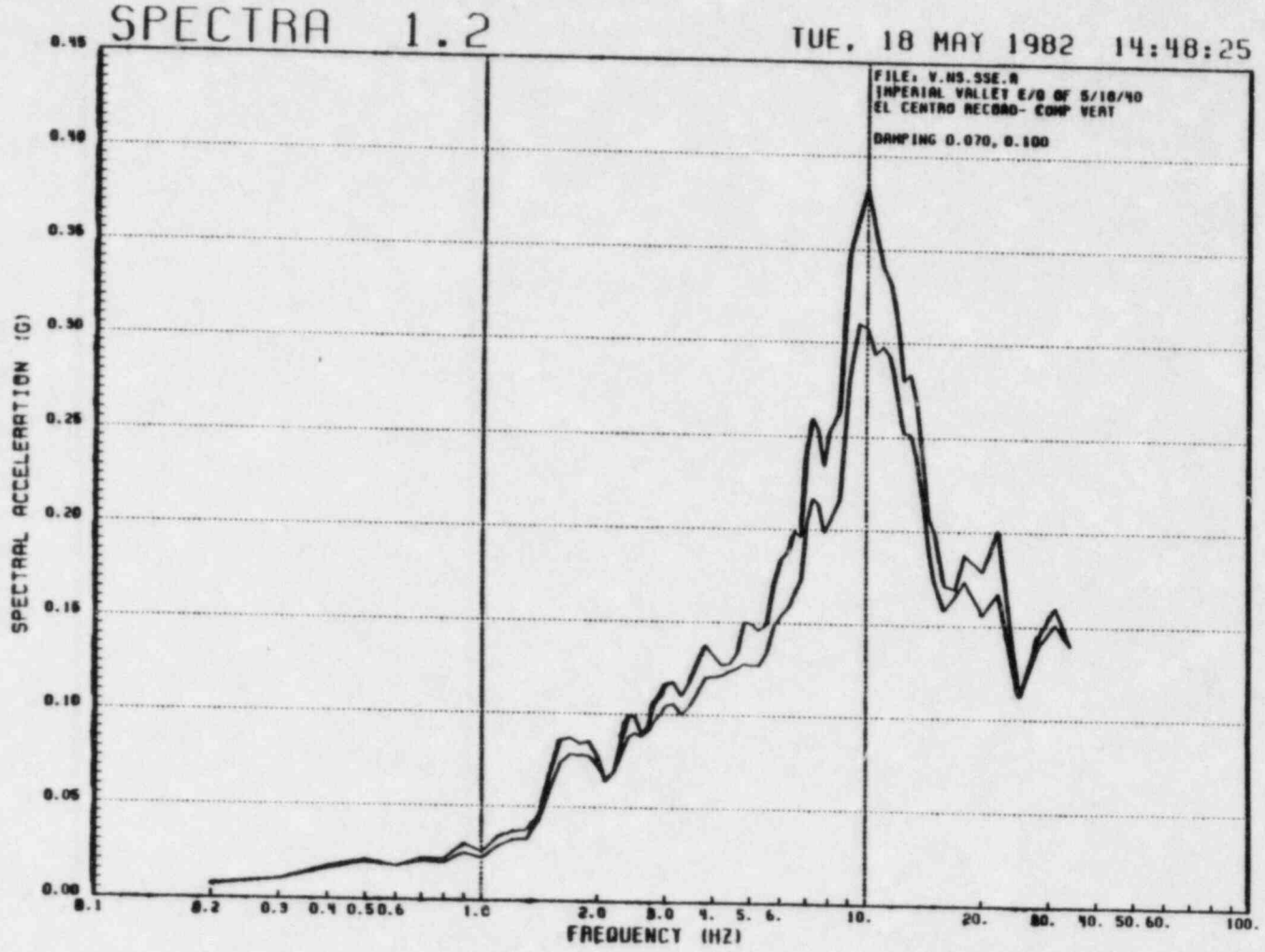

FIG. E.12 RESPONSE SPECTRUM OF EL CENTRO RECORD, VERTICAL COMPONENT, DAMPING = 0.07 AND 0.10

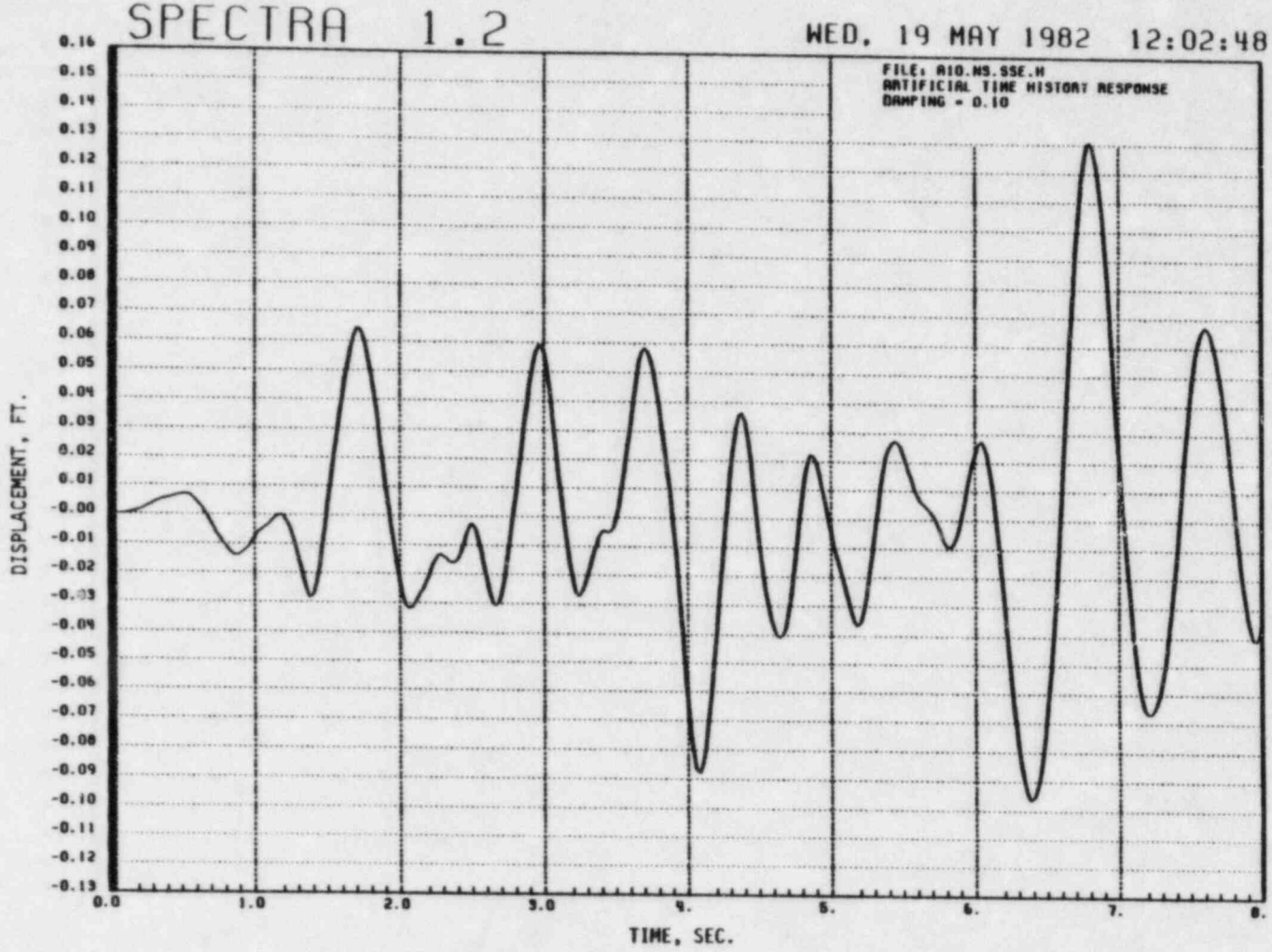

FIG. E.14 RELATIVE DISPLACEMENT RESPONSE OF NODE 7 FOR ANALYSIS CASE 'A10'

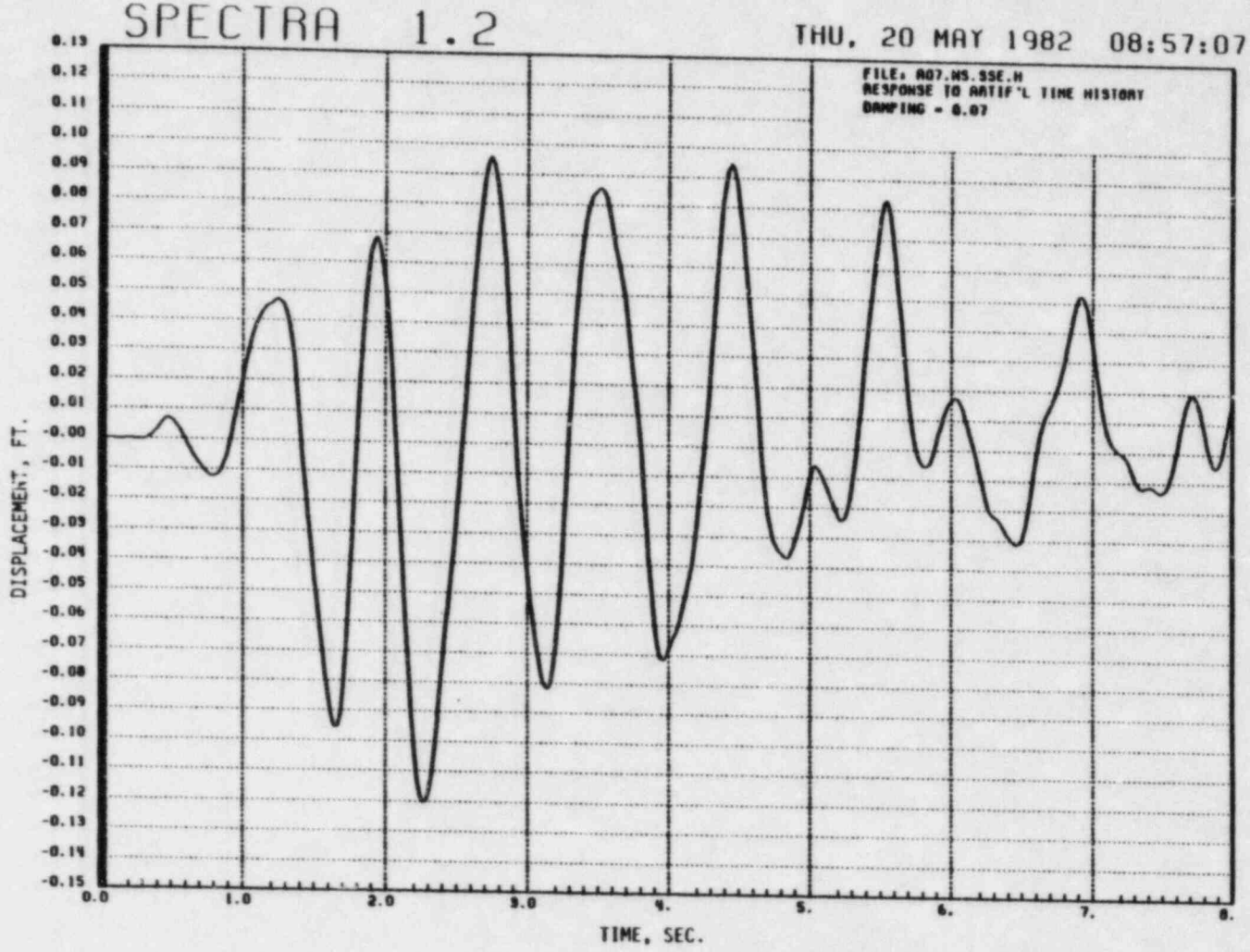

FIG. E.13 RELATIVE DISPLACEMENT RESPONSE OF NODE 7 FOR ANALYSIS CASE 'A07'

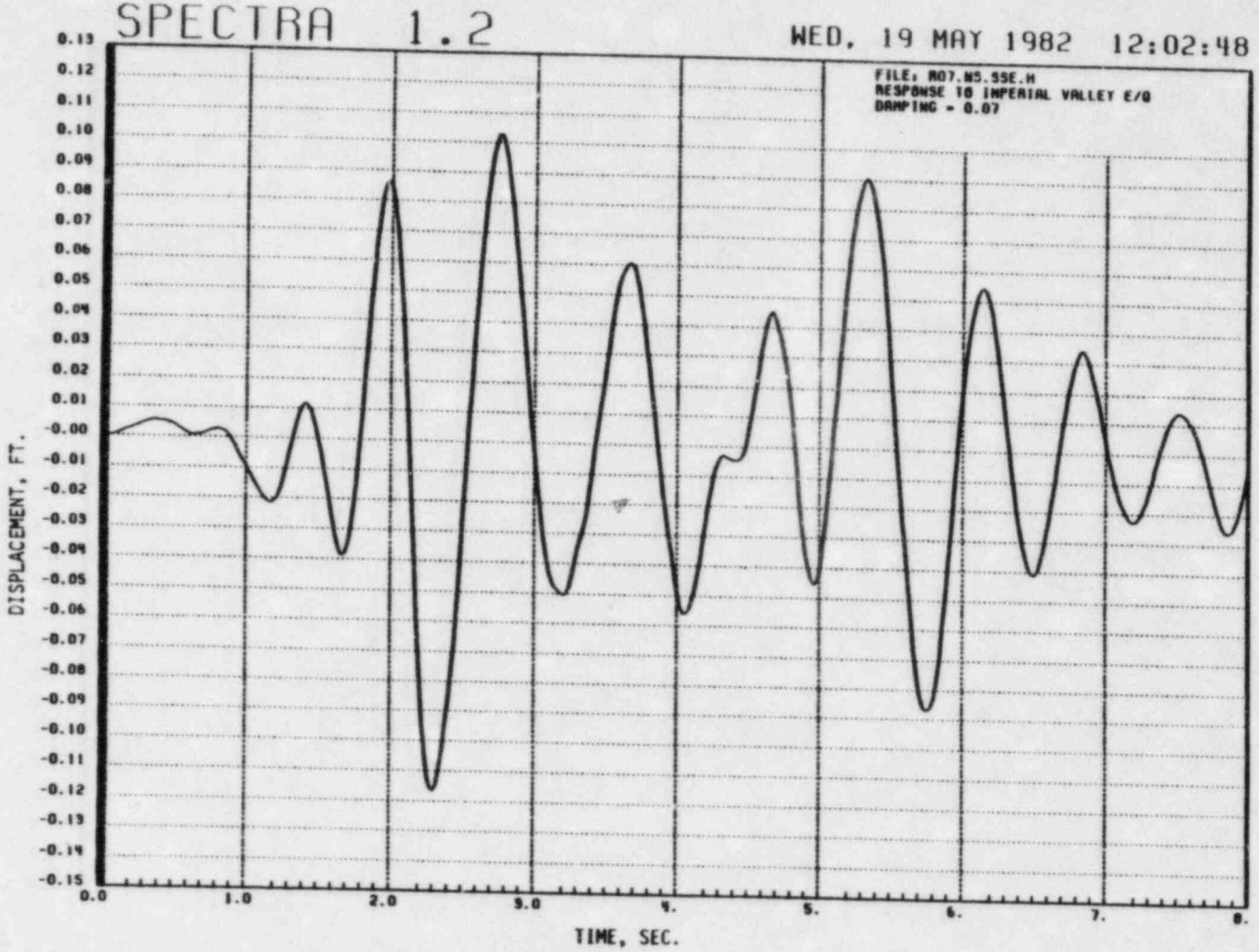

FIG. E.15 RELATIVE DISPLACEMENT RESPONSE OF NODE 7 FOR ANALYSIS CASE 'R07'

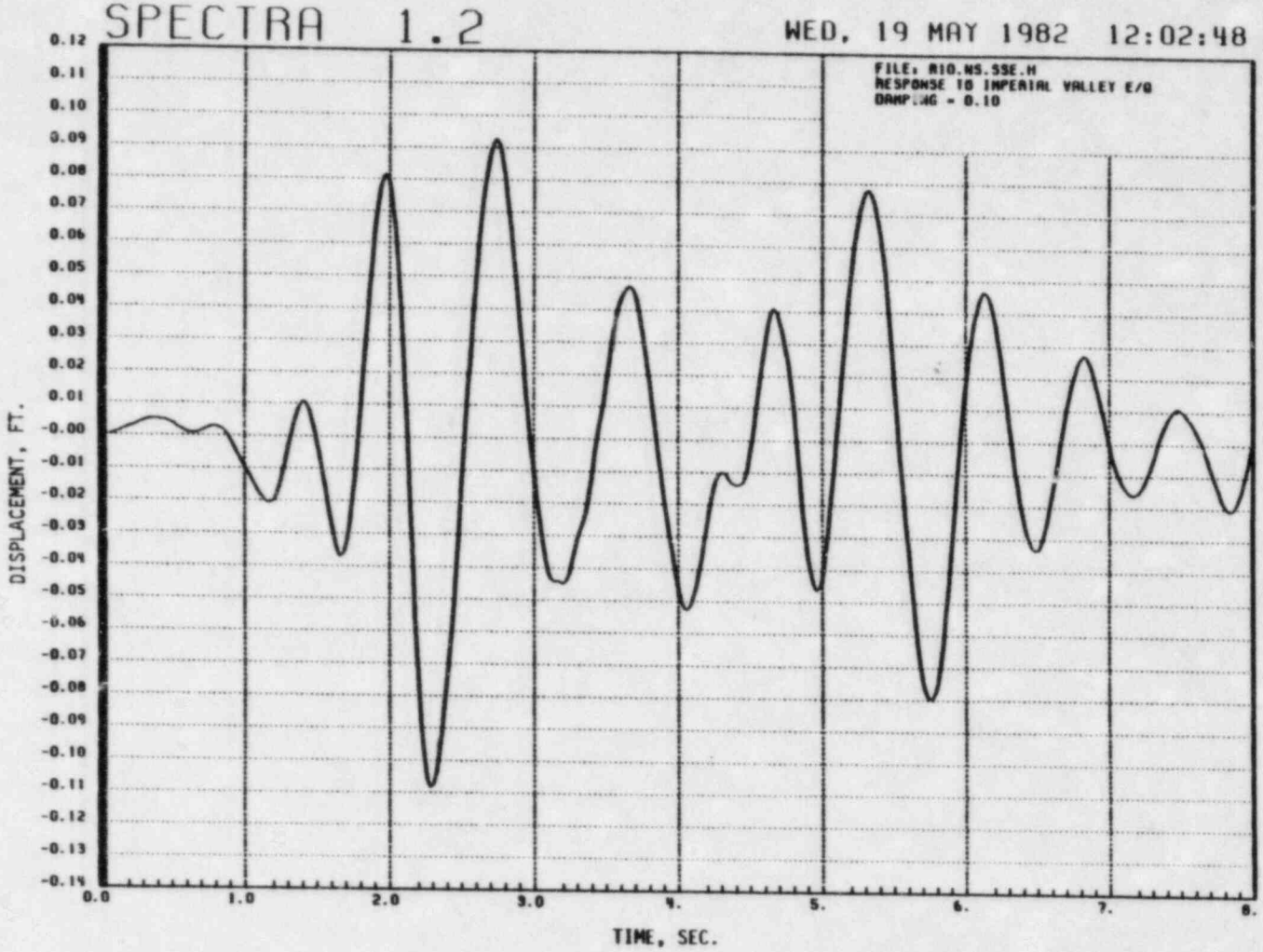

FIG. E.16 RELATIVE DISPLACEMENT RESPONSE OF NODE 7 FOR ANALYSIS CASE 'R10'

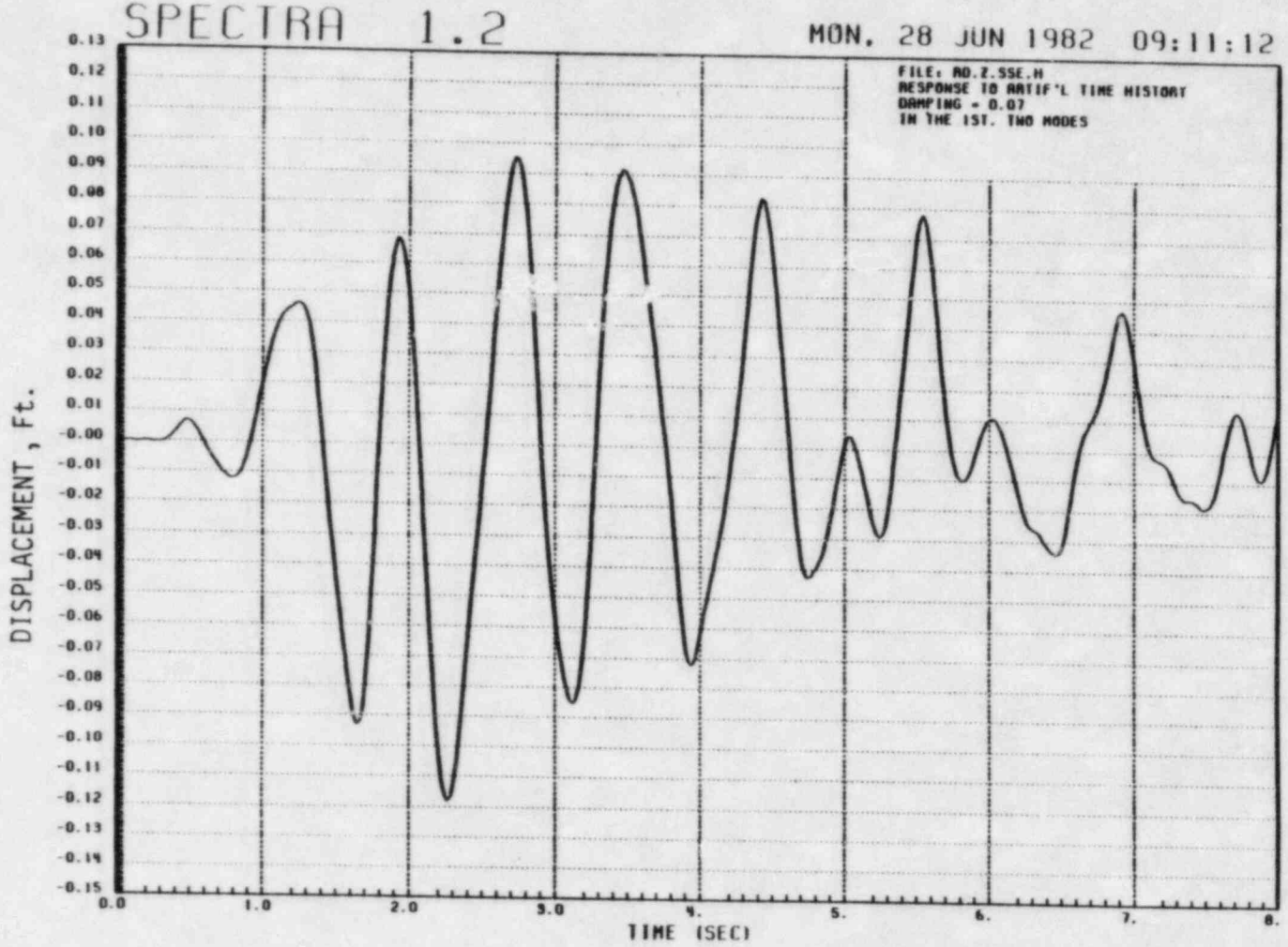

FIG. E.17 RELATIVE DISPLACEMENT RESPONSE OF NODE 7 FOR ANALYSIS CASE 'A07.1'

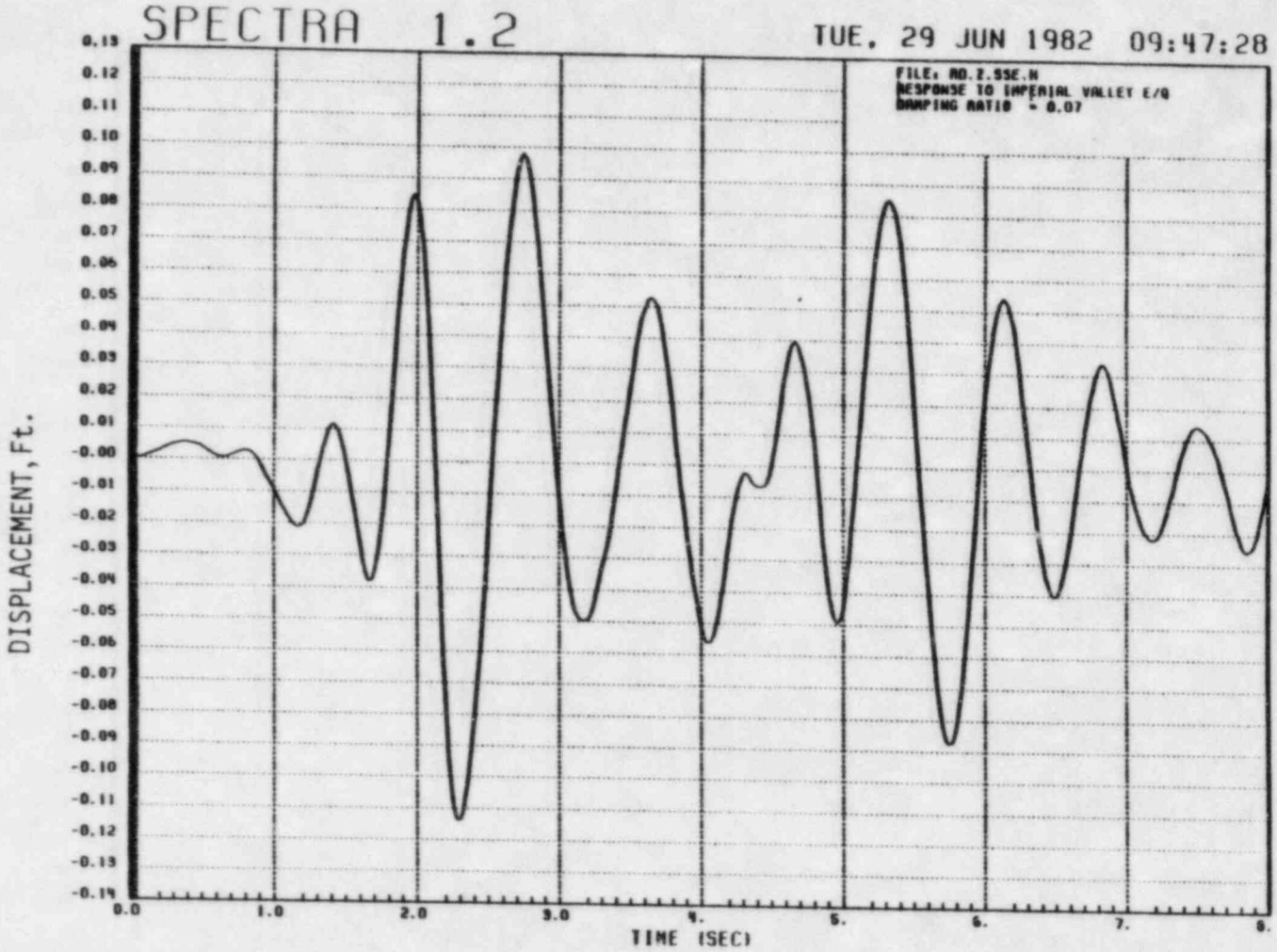

FIG. E.18 RELATIVE DISPLACEMENT RESPONSE OF NODE 7 FOR ANALYSIS CASE 'R07.1'

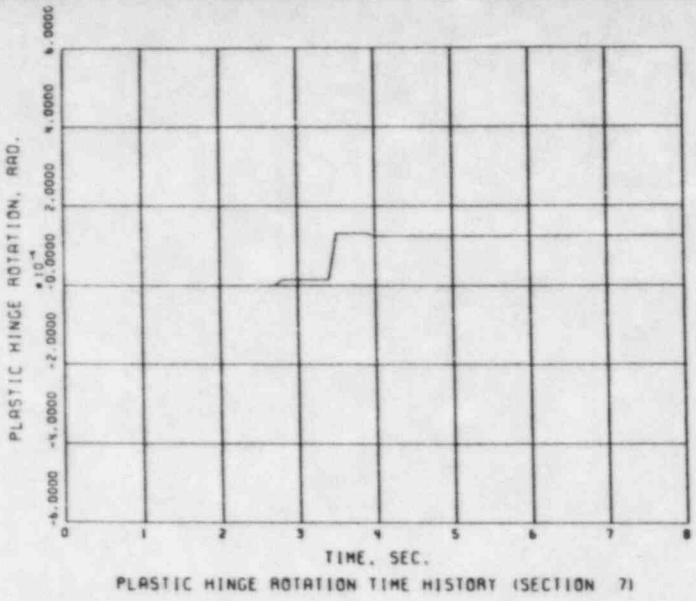

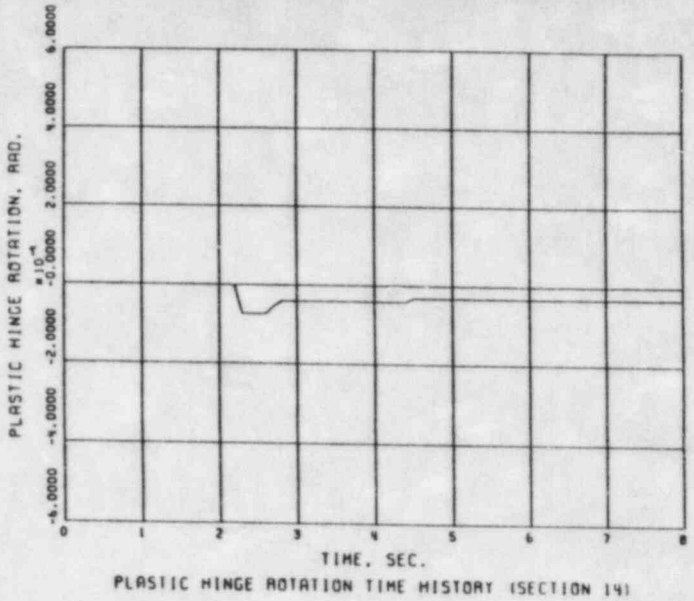

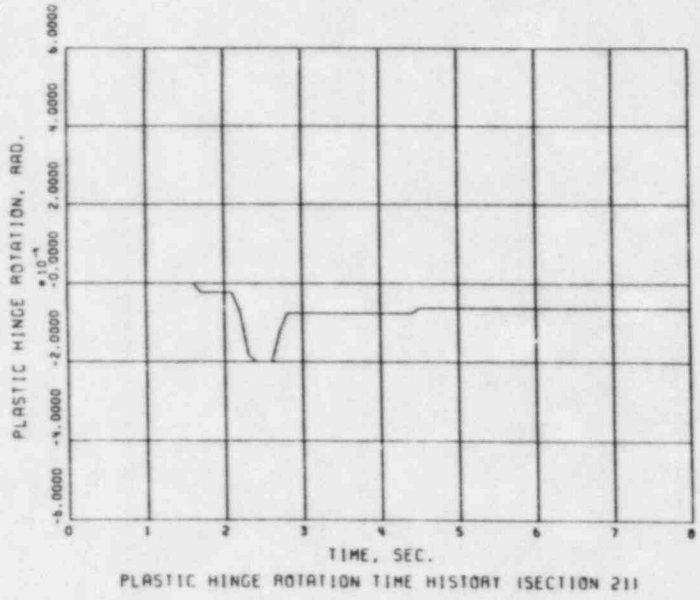

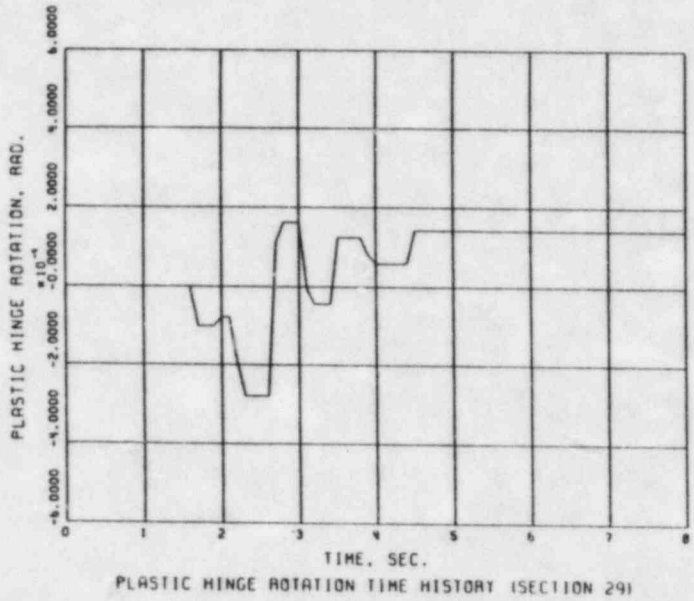

FIG. E.19 PLASTIC HINGE ROTATION TIME HISTORIES AT TOP DOWEL SECTIONS FOR ANALYSIS CASE 'A07'

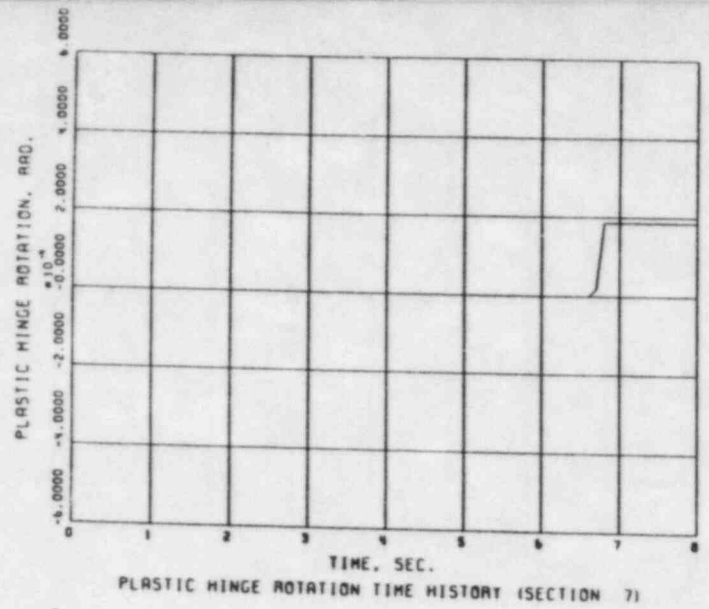

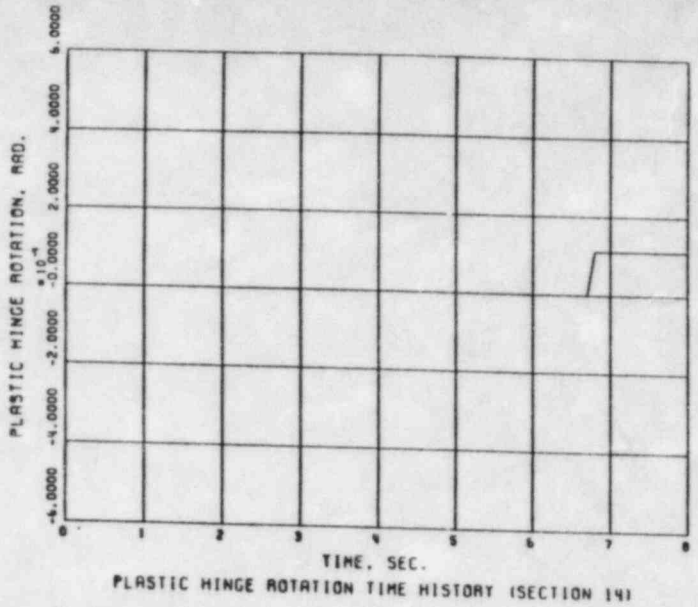

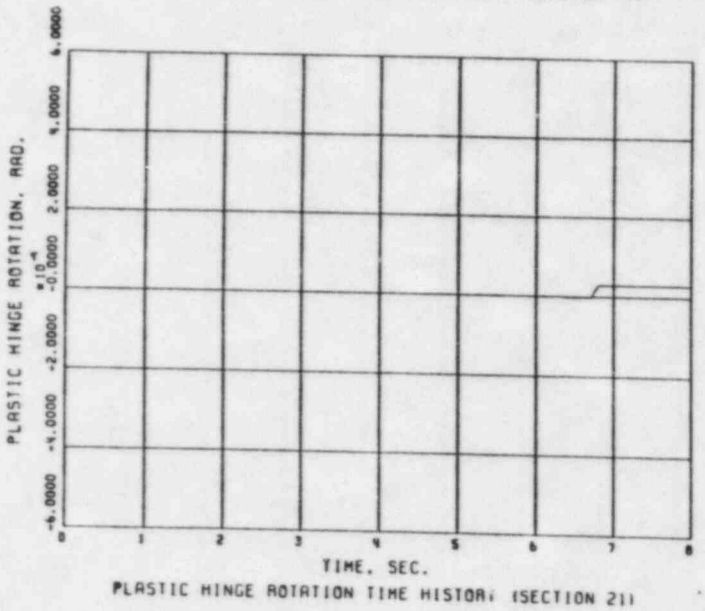

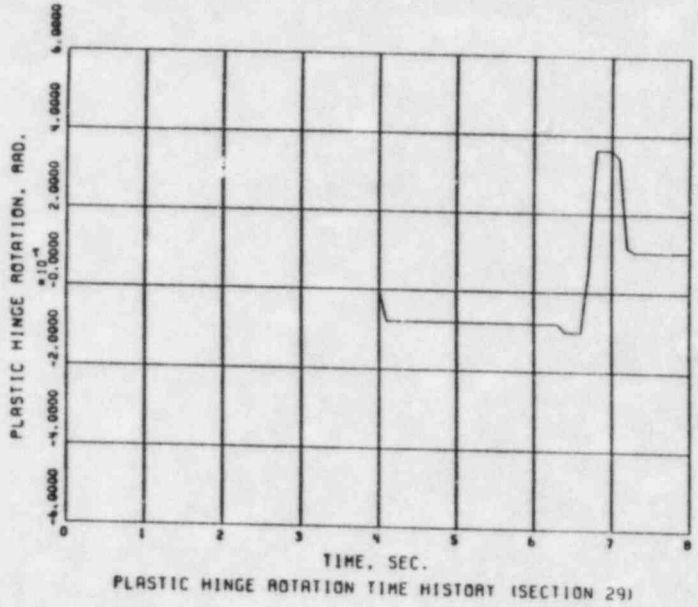

FIG. E.20 PLASTIC HINGE ROTATION TIME HISTORIES AT TOP DOWEL SECTIONS FOR ANALYSIS CASE 'A10'

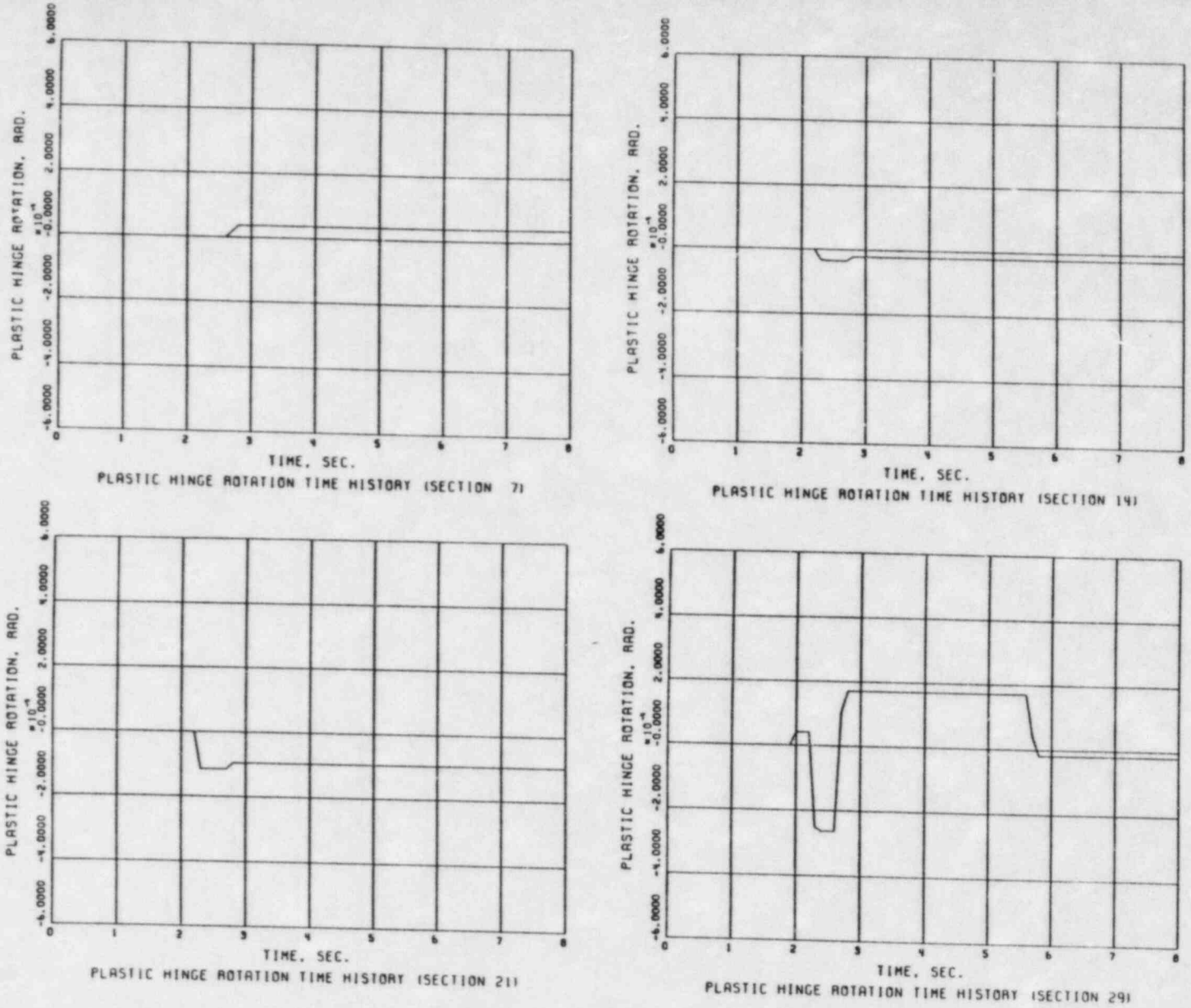

FIG. E.21 PLASTIC HINGE ROTATION TIME HISTORIES AT TOP DOWEL SECTIONS FOR ANALYSIS CASE 'R07'

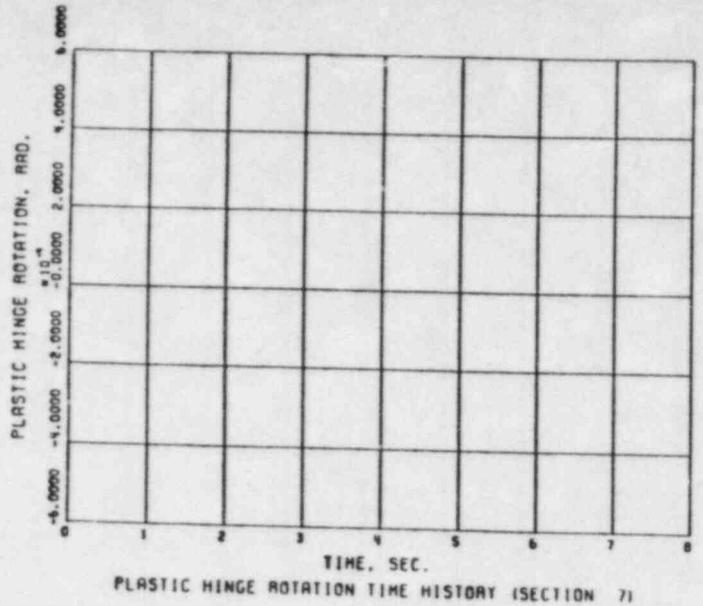

PLASTIC HINGE ROTATION TIME HISTORY (SECTION 7)

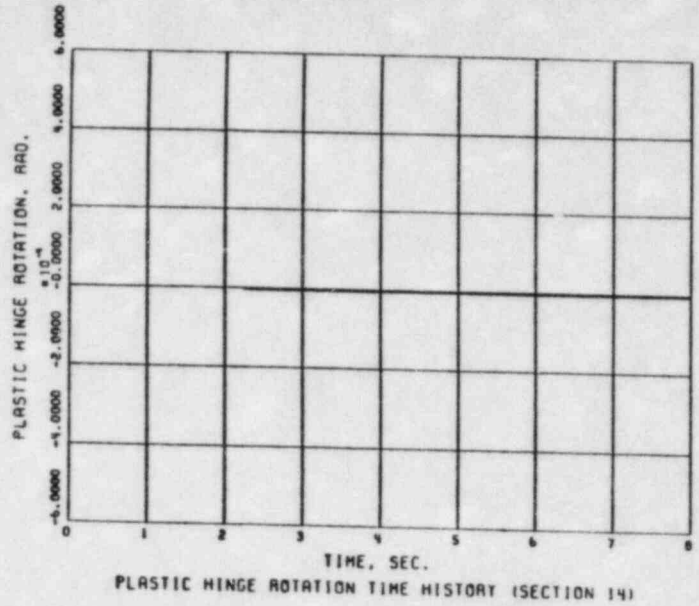

PLASTIC HINGE ROTATION TIME HISTORY (SECTION 14)

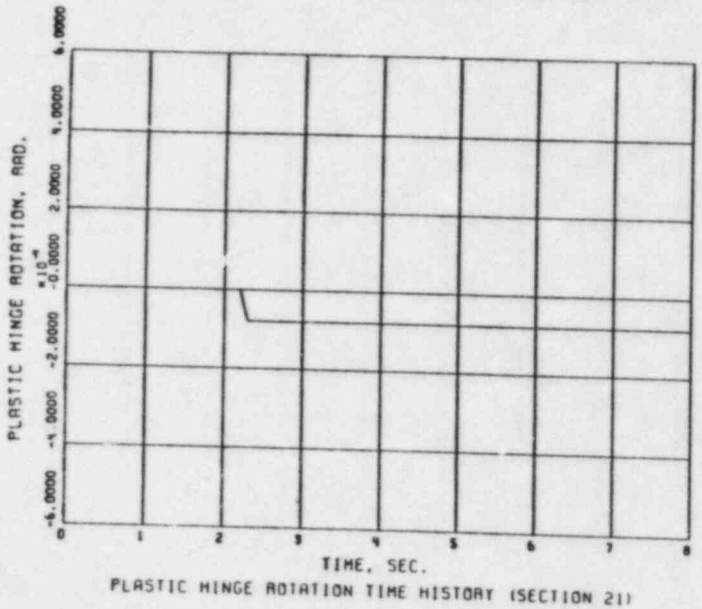

PLASTIC HINGE ROTATION TIME HISTORY (SECTION 21)

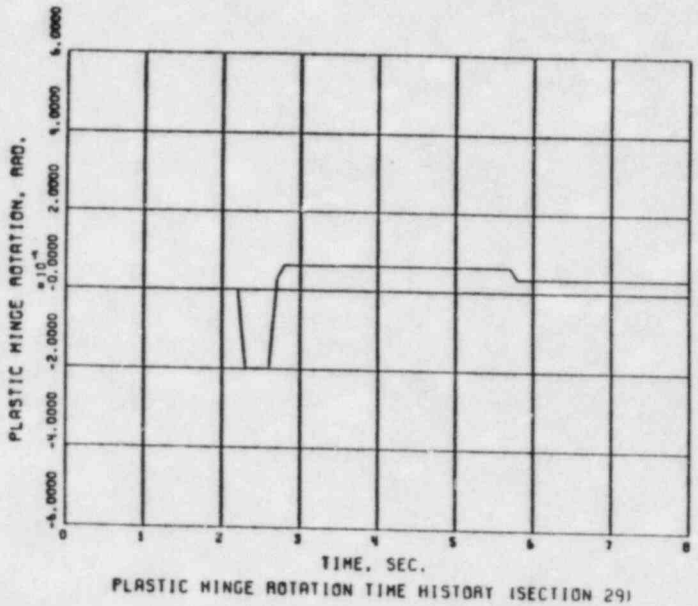

PLASTIC HINGE ROTATION TIME HISTORY (SECTION 29)

FIG. E.22 PLASTIC HINGE ROTATION TIME HISTORIES AT TOP DOWEL SECTIONS FOR ANALYSIS CASE 'R10'

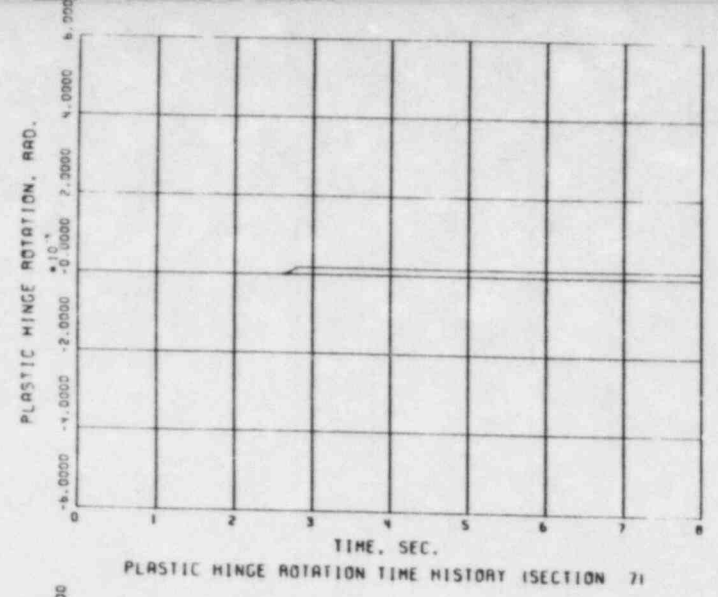

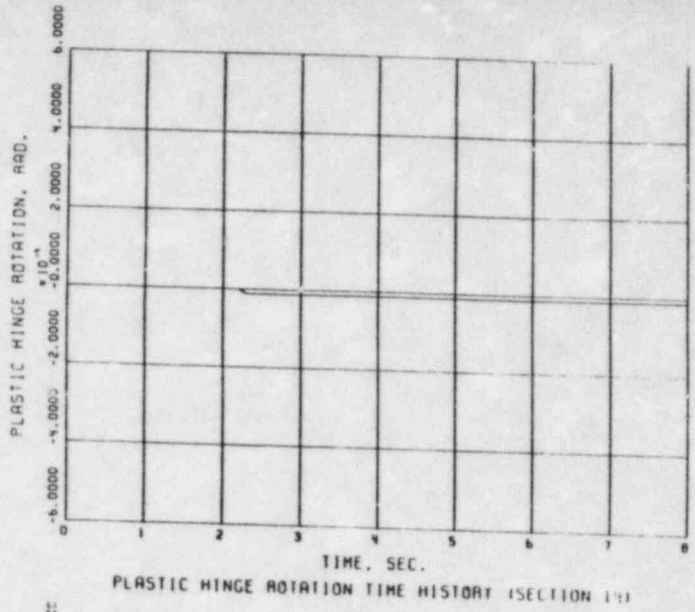

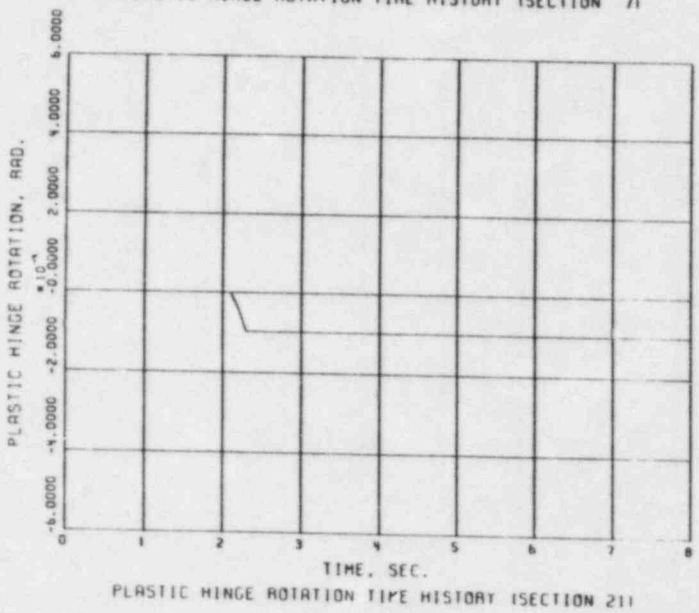

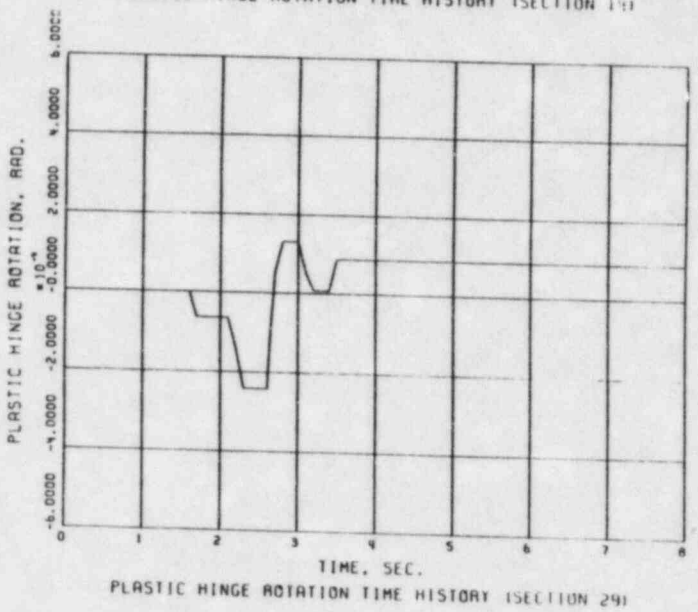

FIG. E.23 PLASTIC HINGE ROTATION TIME HISTORIES AT TOP DOWEL SECTIONS FOR ANALYSIS CASE 'A07.1'

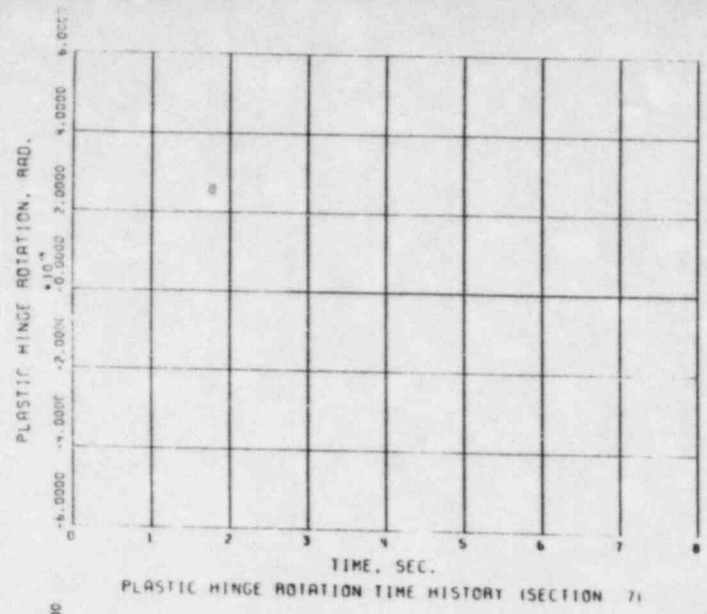

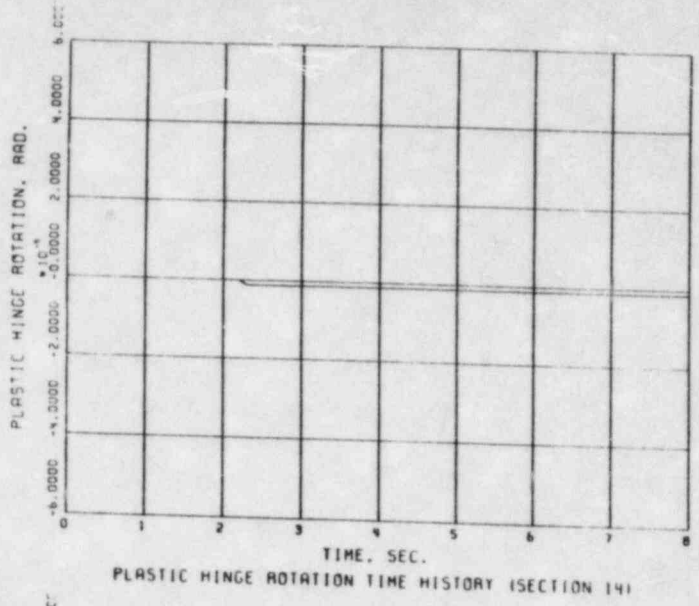

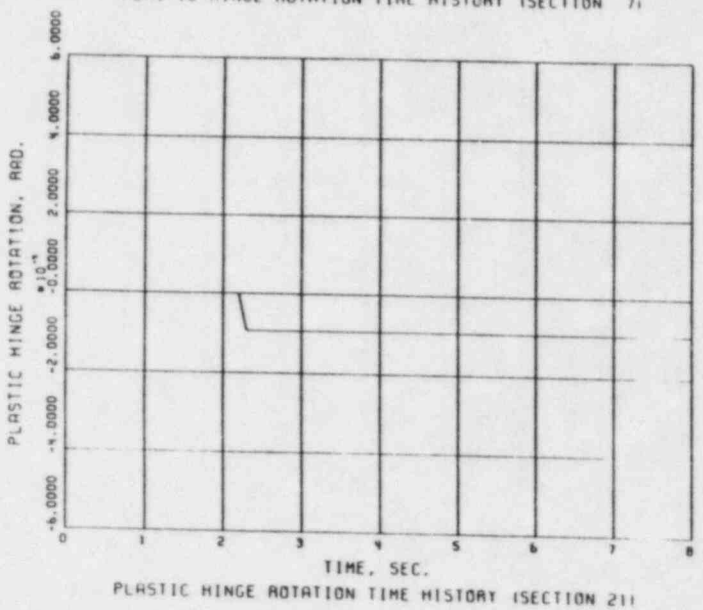

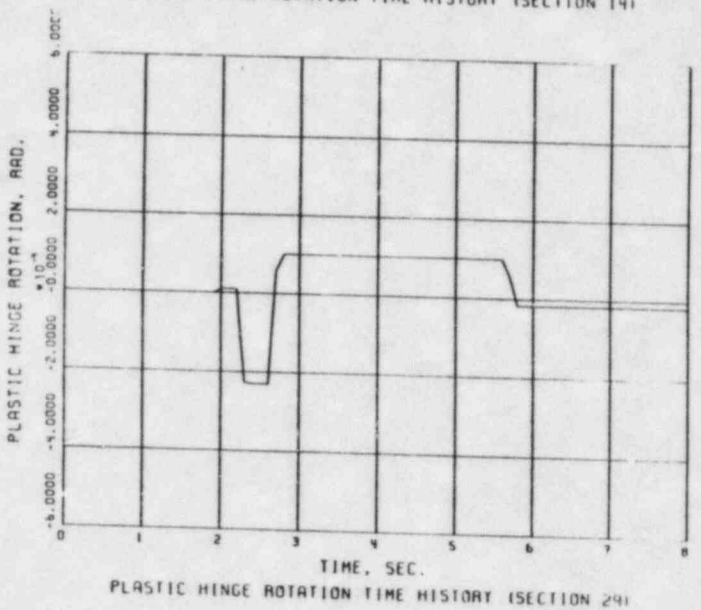

FIG. E.24 PLASTIC HINGE ROTATION TIME HISTORIES AT TOP DOWEL SECTIONS FOR ANALYSIS CASE 'R07.1'

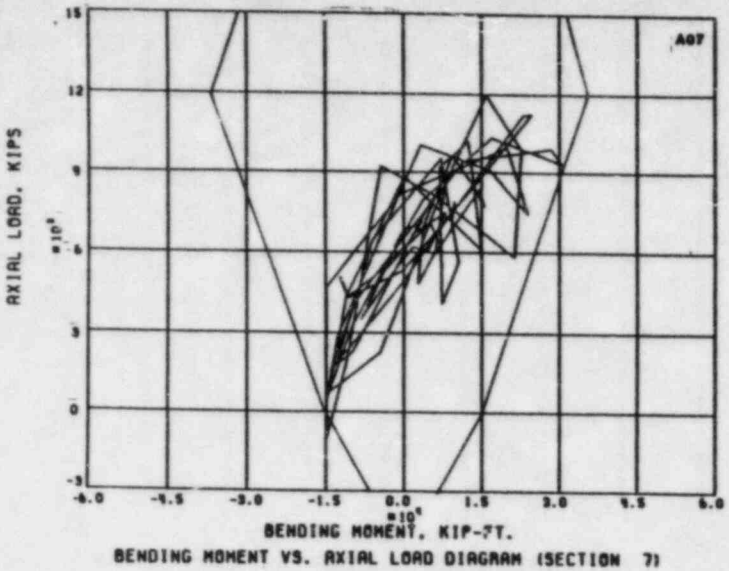

BENDING MOMENT VS. AXIAL LOAD DIAGRAM (SECTION 7)

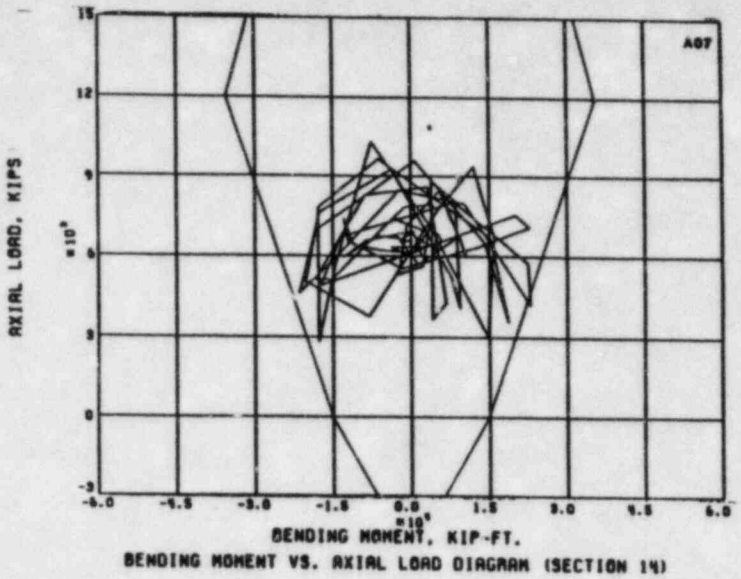

BENDING MOMENT VS. AXIAL LOAD DIAGRAM (SECTION 14)

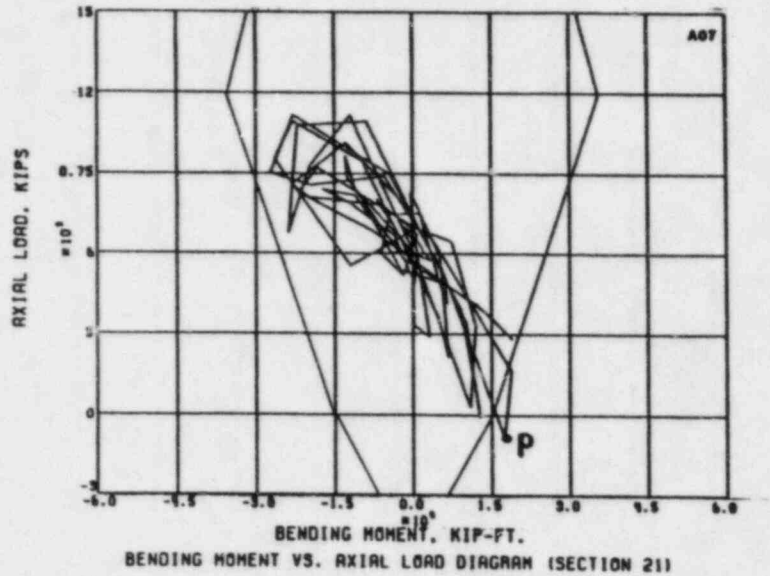

BENDING MOMENT VS. AXIAL LOAD DIAGRAM (SECTION 21)

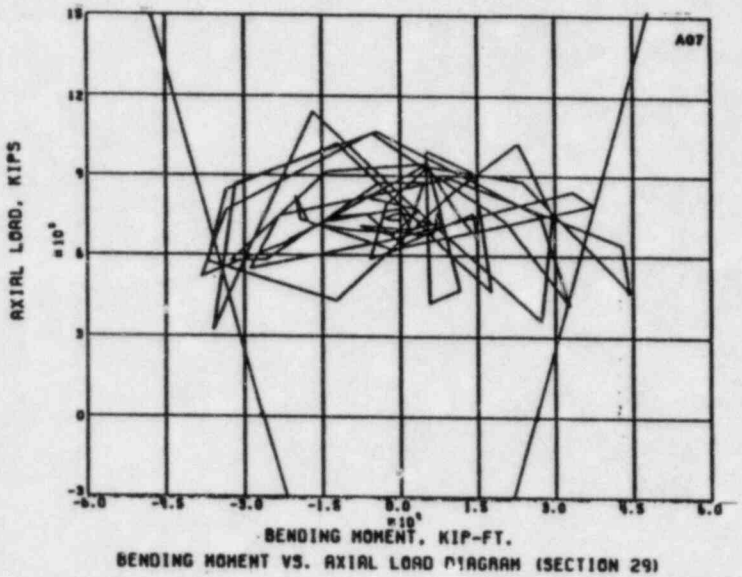

BENDING MOMENT VS. AXIAL LOAD DIAGRAM (SECTION 29)

FIG. E.25 AXIAL FORCE - BENDING MOMENT INTERACTION AT TOP DOWEL SECTIONS FOR ANALYSIS CASE 'A07'

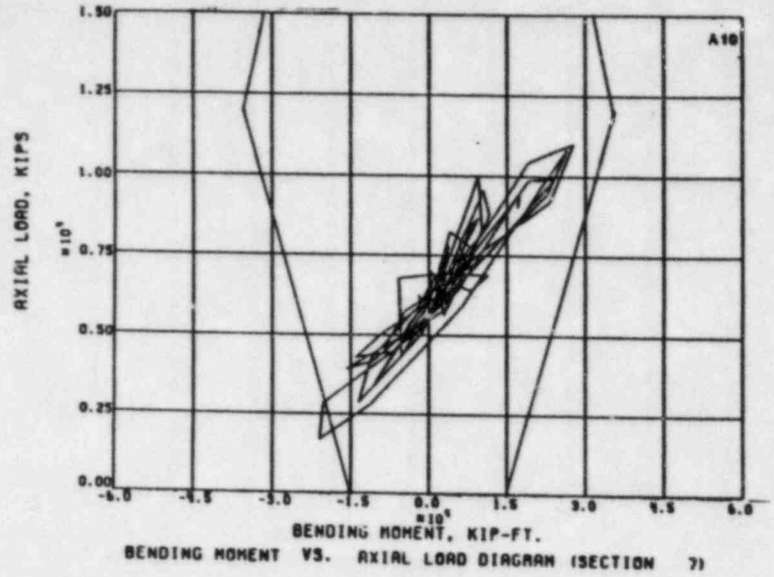

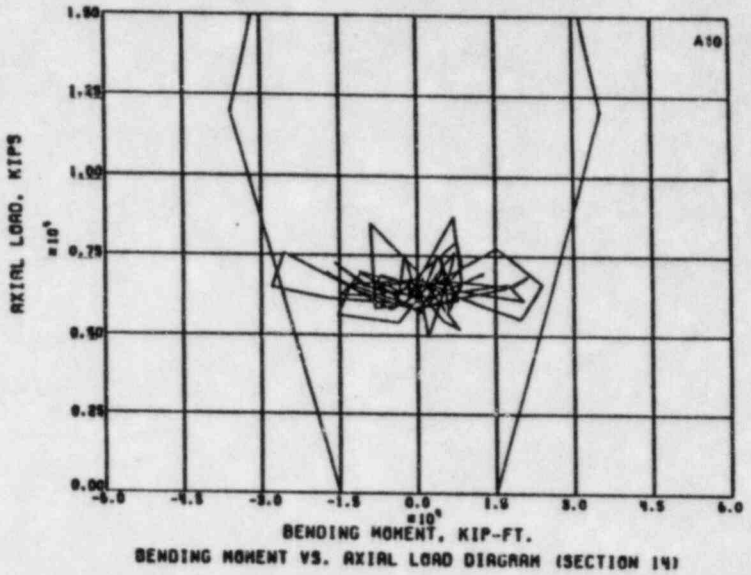

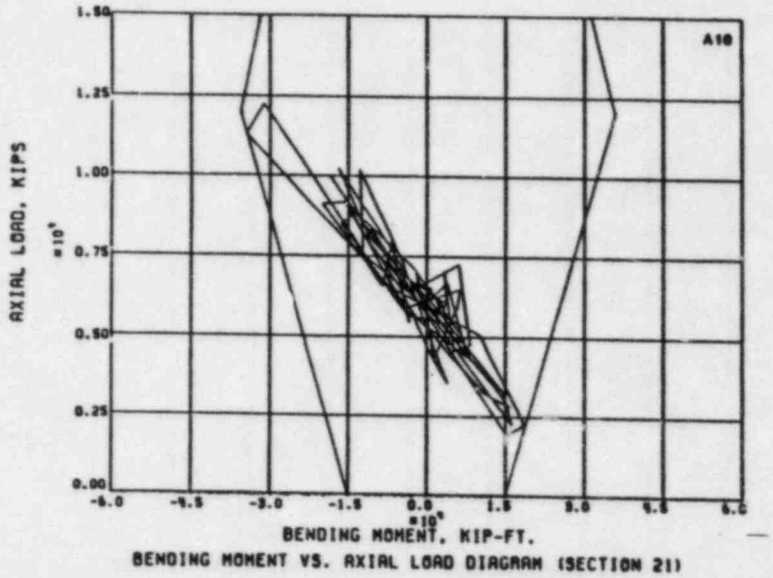

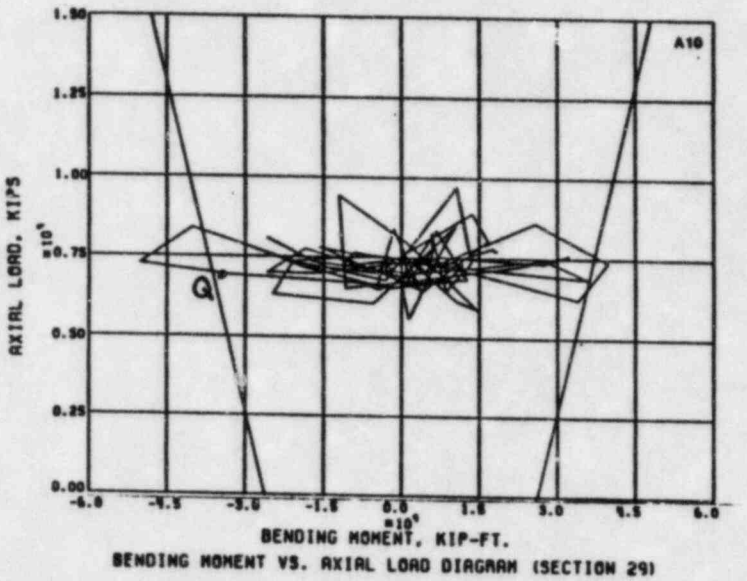

FIG. E.26 AXIAL FORCE - BENDING MOMENT INTERACTION AT TOP DOWEL SECTIONS FOR ANALYSIS CASE 'A10'

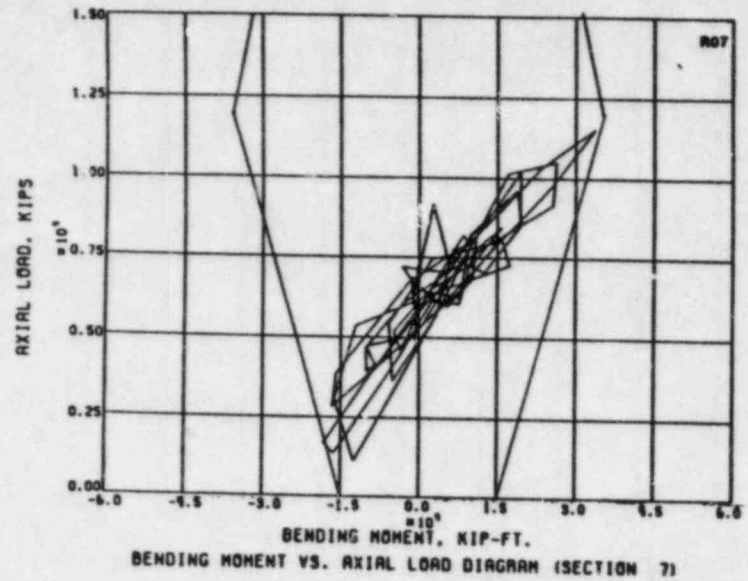

BENDING MOMENT VS. AXIAL LOAD DIAGRAM (SECTION 7)

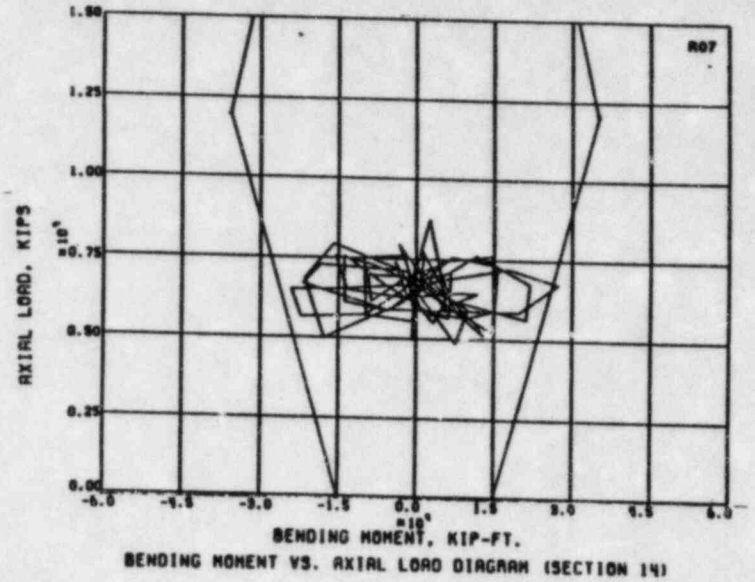

BENDING MOMENT VS. AXIAL LOAD DIAGRAM (SECTION 14)

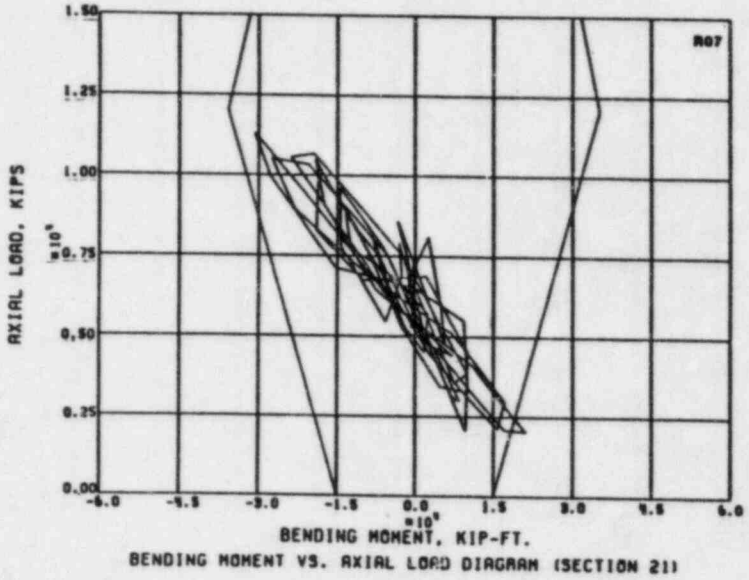

BENDING MOMENT VS. AXIAL LOAD DIAGRAM (SECTION 21)

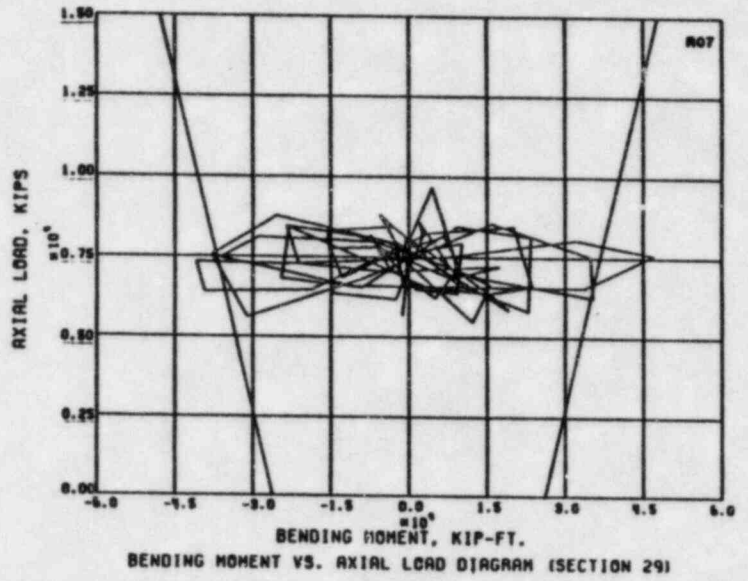

BENDING MOMENT VS. AXIAL LOAD DIAGRAM (SECTION 29)

FIG. E.27 AXIAL FORCE - BENDING MOMENT INTERACTION AT TOP DOWEL SECTIONS FOR ANALYSIS CASE 'R07'

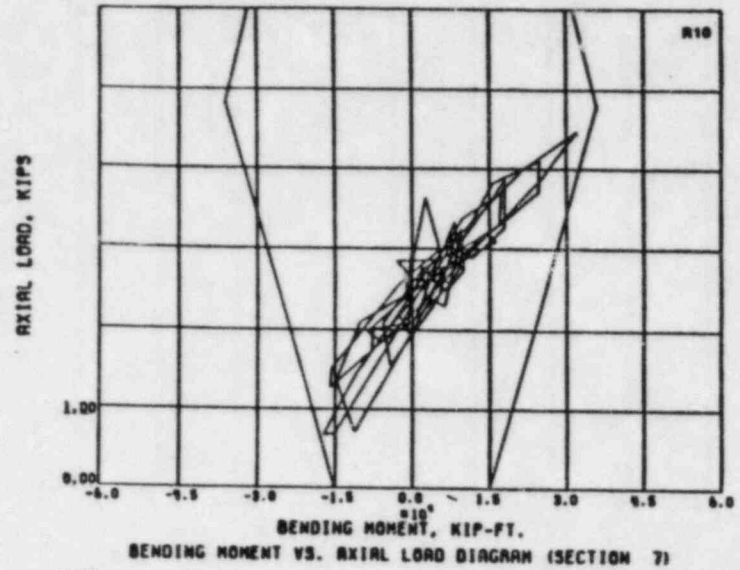

BENDING MOMENT VS. AXIAL LOAD DIAGRAM (SECTION 7)

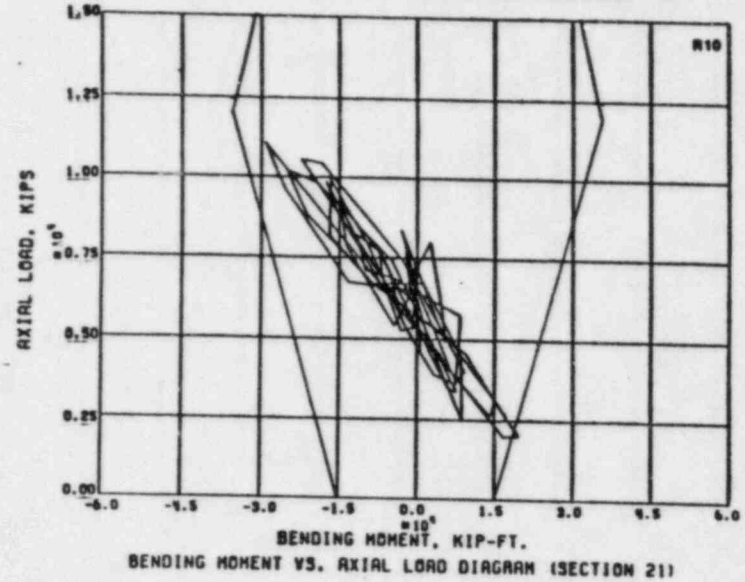

BENDING MOMENT VS. AXIAL LOAD DIAGRAM (SECTION 21)

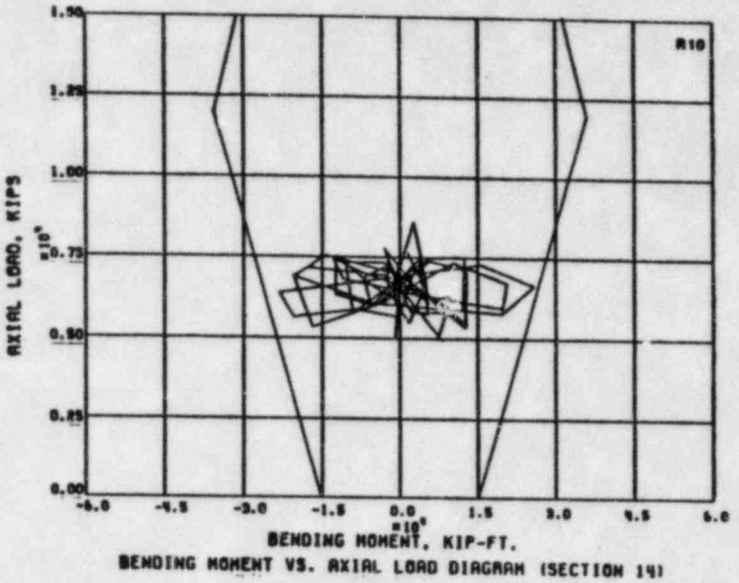

BENDING MOMENT VS. AXIAL LOAD DIAGRAM (SECTION 14)

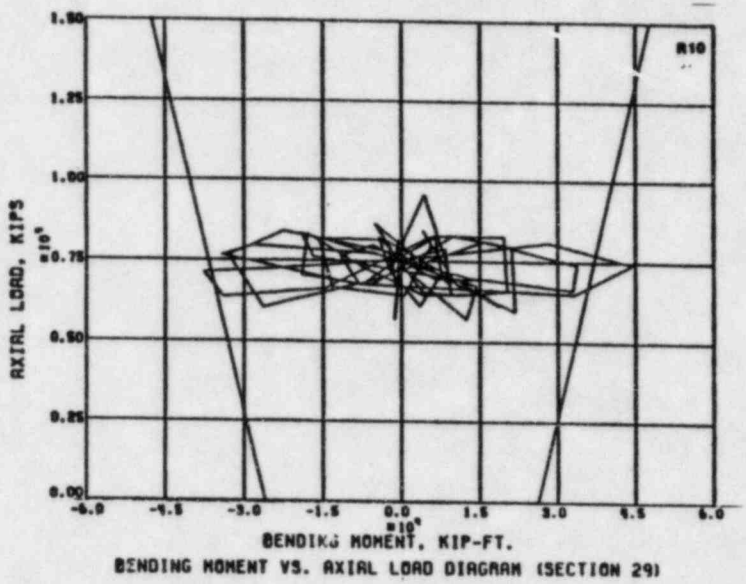

BENDING MOMENT VS. AXIAL LOAD DIAGRAM (SECTION 29)

FIG. E.28 AXIAL FORCE - BENDING MOMENT INTERACTION AT TOP DOWEL SECTIONS FOR ANALYSIS CASE 'R10'

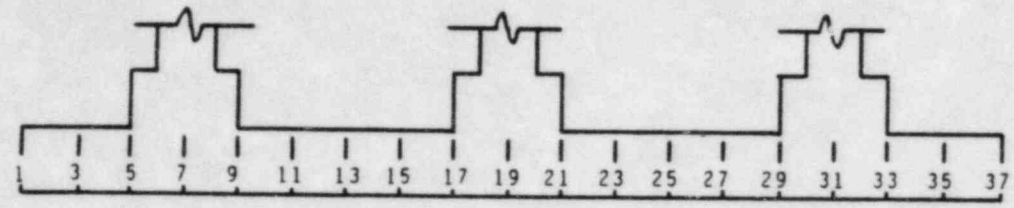

NODE NUMBER

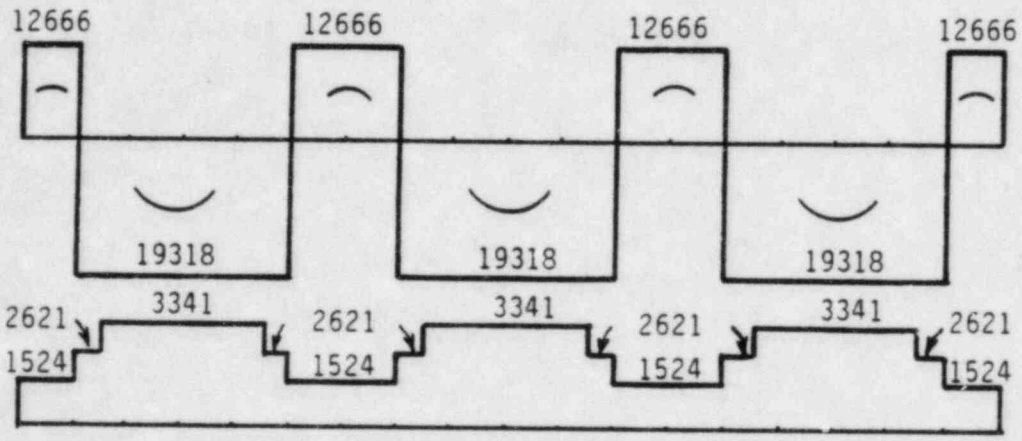

FLEXURAL CAPACITY
(K-FT)

SHEAR CAPACITY
(Torsion=0)
(K)

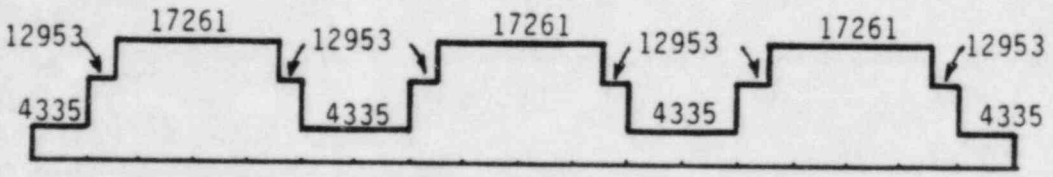

TORSIONAL CAPACITY
(Shear=0)
(K-FT)

FIG. E.29 CAPACITY OF RING FOUNDATION

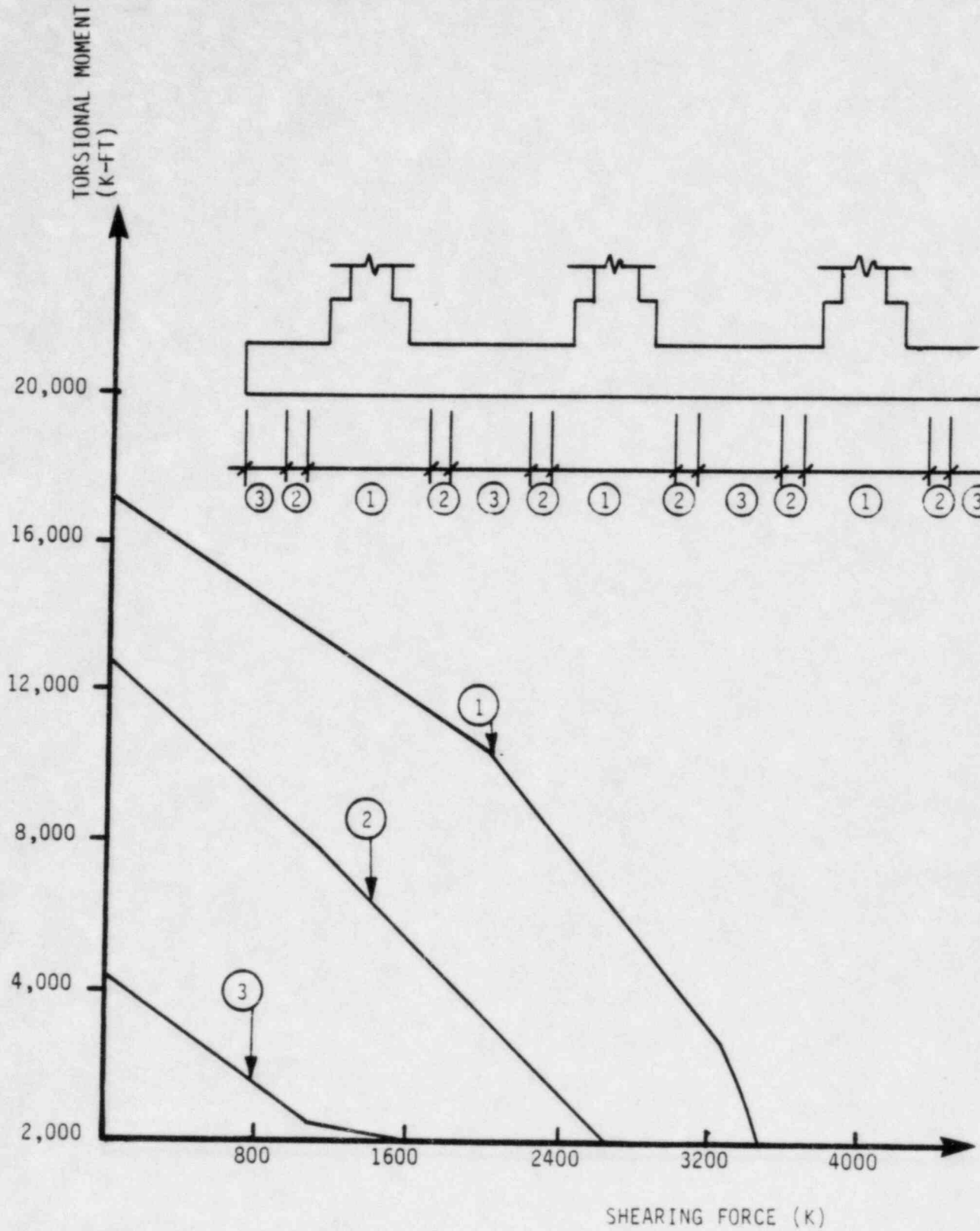

FIG. E.30 TORSION - SHEAR INTERACTION
DIAGRAM OF RING FOUNDATION

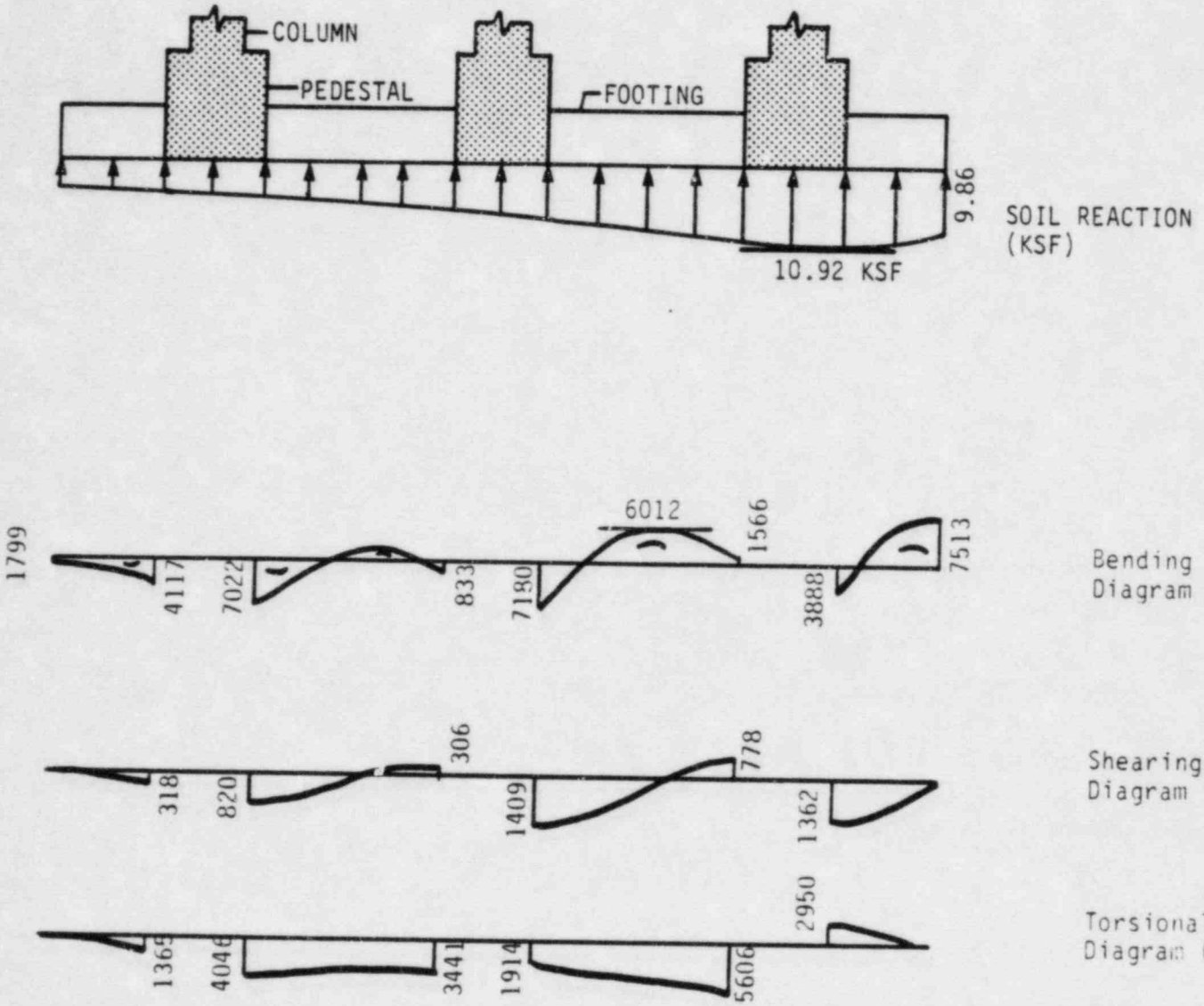

FIG. E.31 CASE 1: DEAD LOAD PLUS YCS HORIZONTAL AND VERTICAL (UPWARD) LOADS

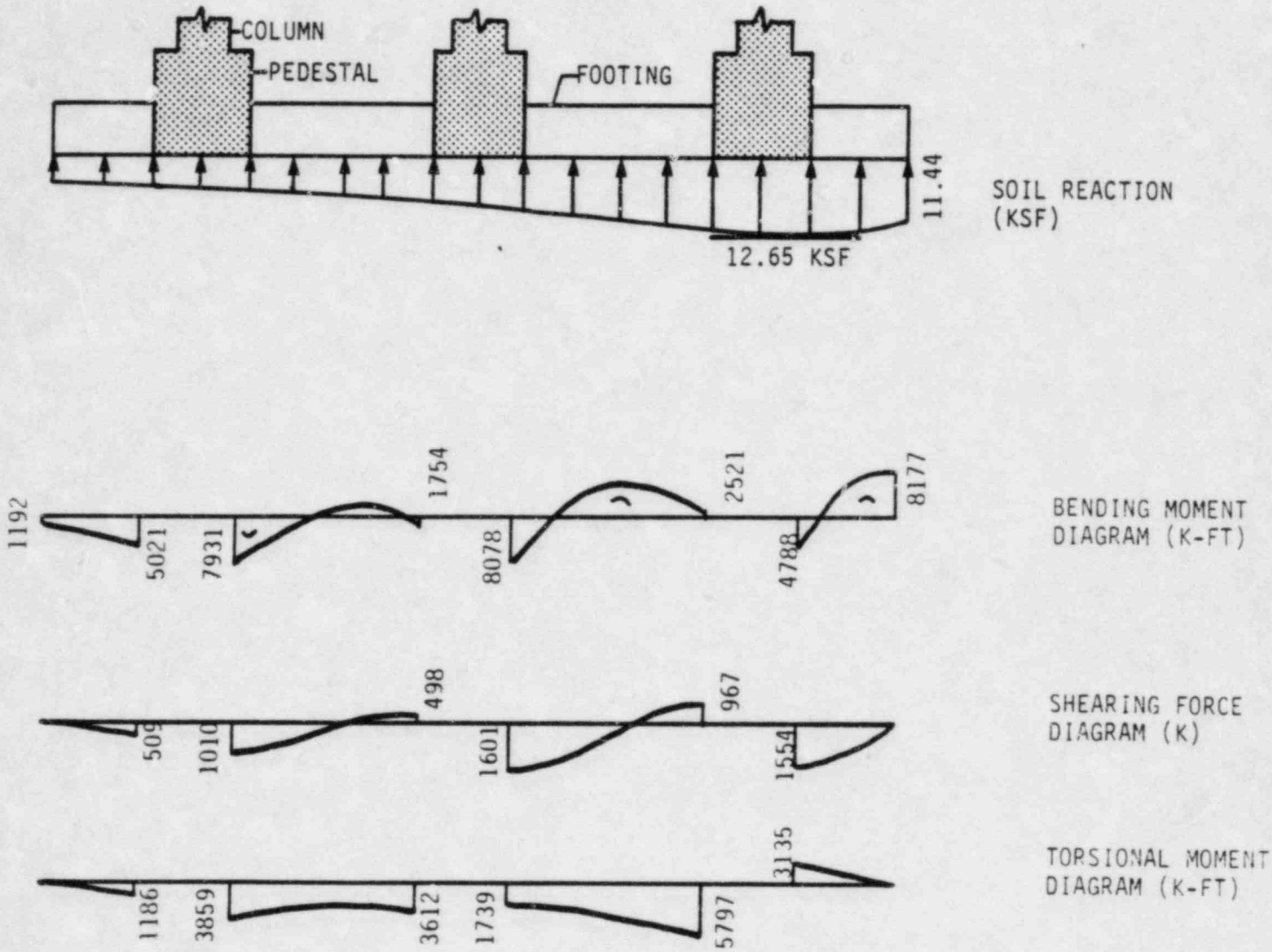

FIG. E.32 CASE 2: DEAD LOAD PLUS YCS HORIZONTAL AND VERTICAL (DOWNWARD) LOADS

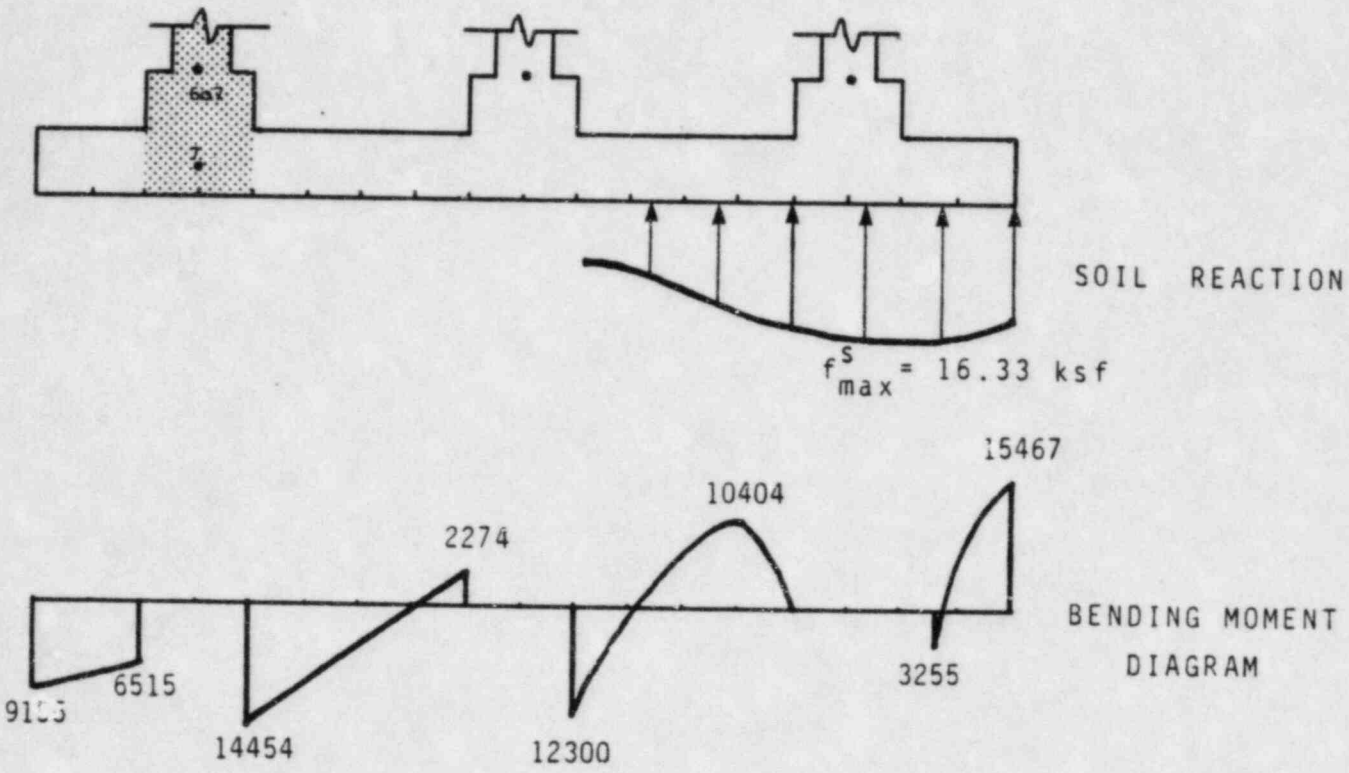

FIG. E.33 CASE 3: DEAD LOAD PLUS NRC HORIZONTAL AND VERTICAL (UPWARD) LOADS

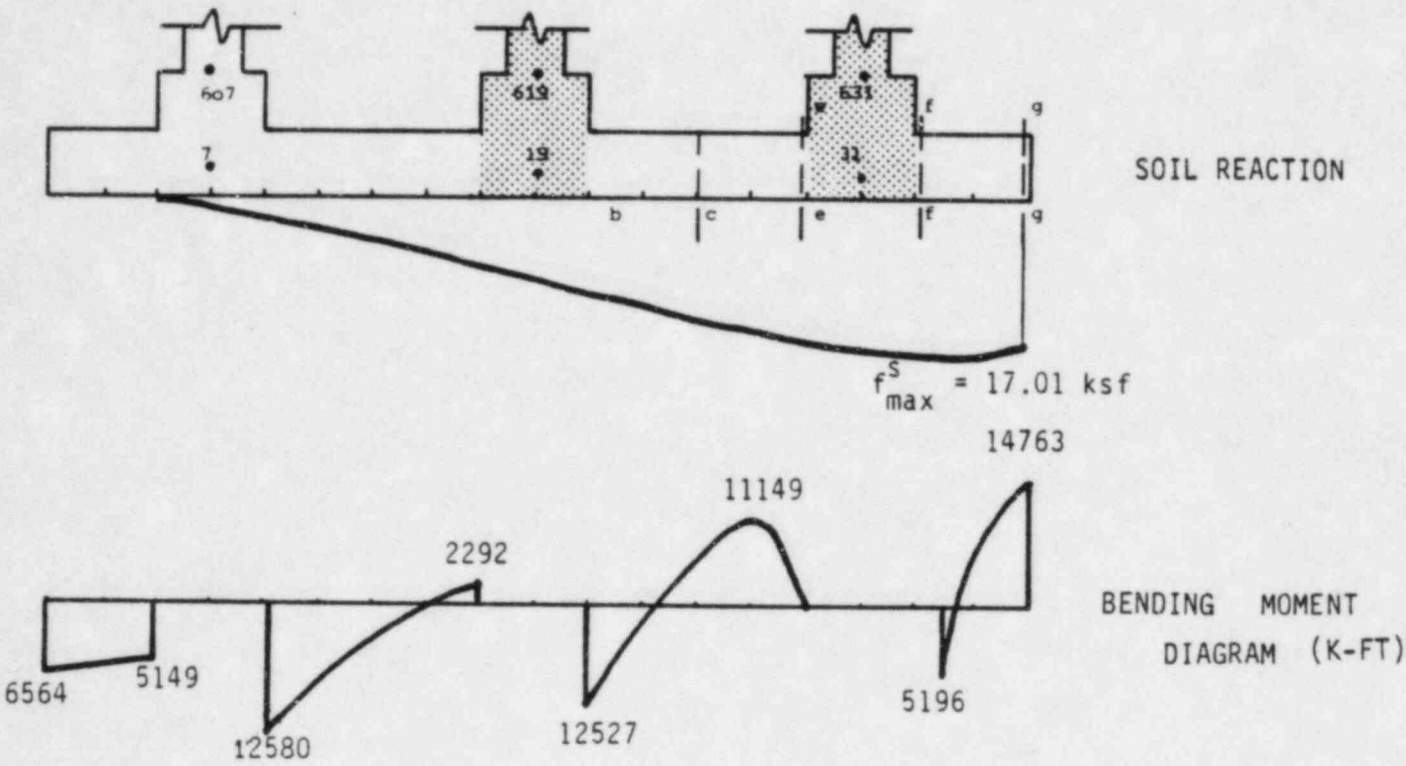

FIG. E.34 CASE 4: DEAD LOAD PLUS NRC HORIZONTAL AND VERTICAL (DOWNWARD) LOADS

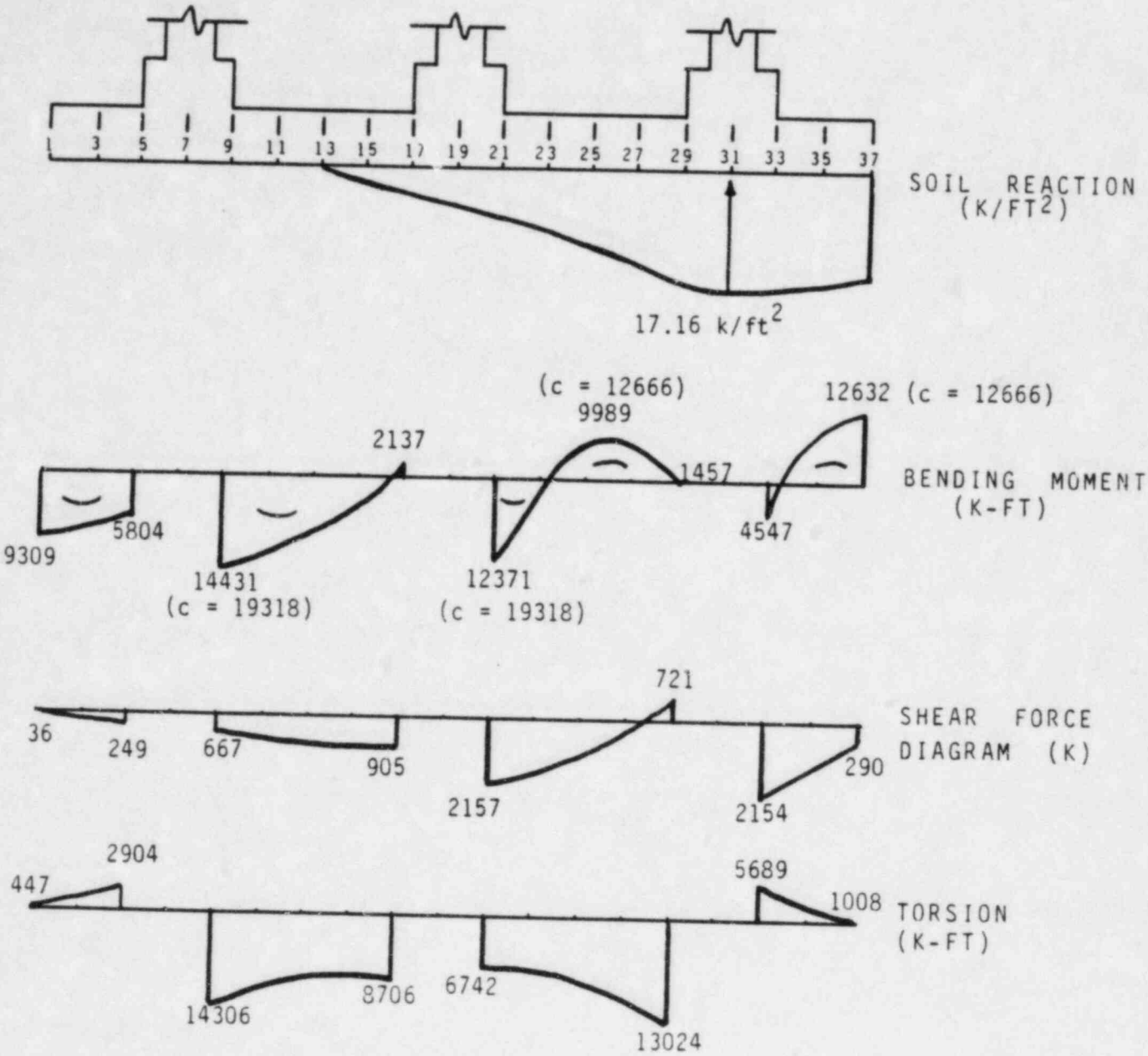

FIG. E.35
CASE 5: DEAD LOAD PLUS NRC HORIZONTAL AND VERTICAL (UPWARD) LOADS - WITH PLASTIC HINGE AT NODE 37

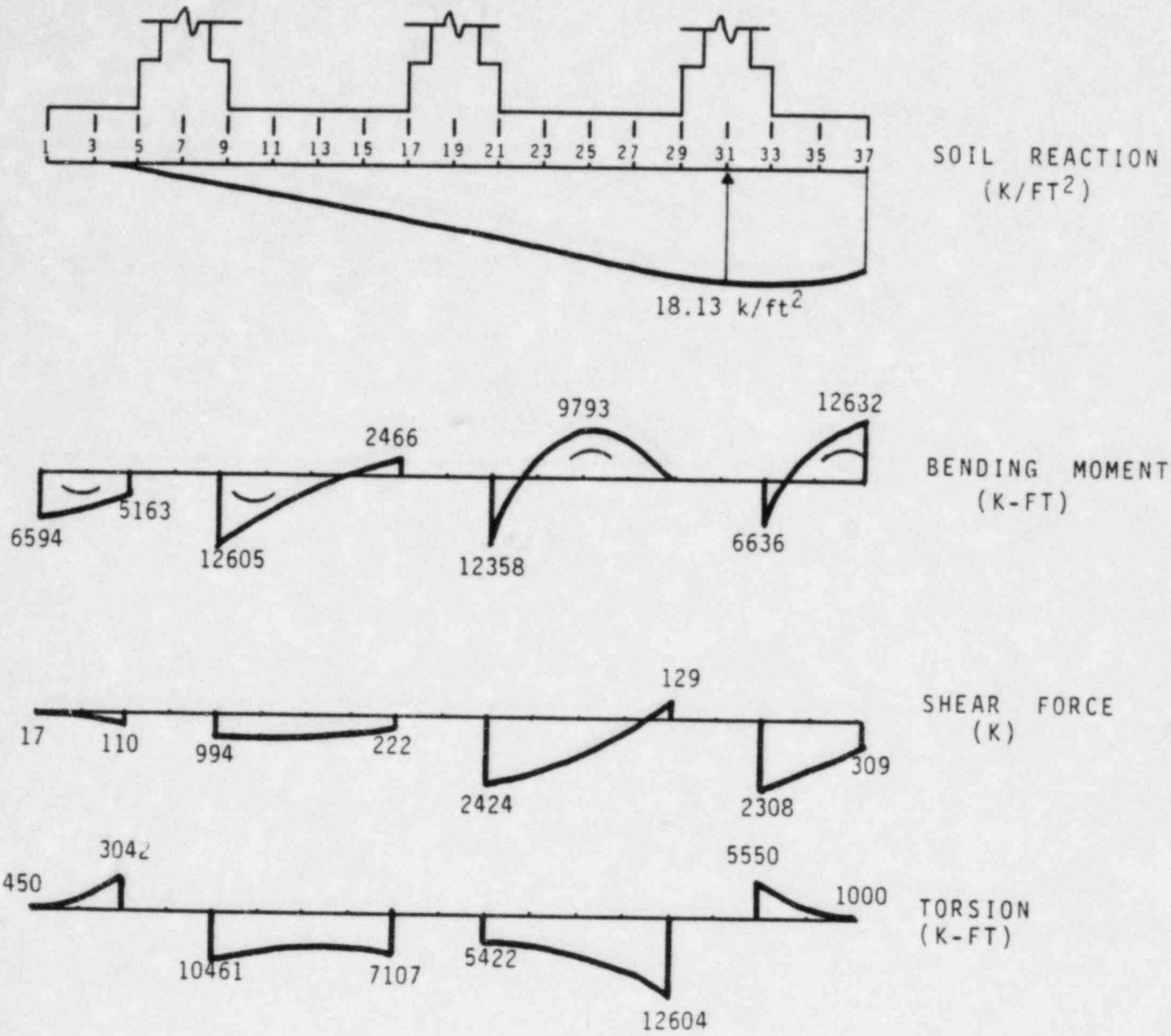

FIG. E.36
CASE 6: DEAD LOAD PLUS NRC HORIZONTAL AND VERTICAL (DOWNWARD) LOADS - WITH PLASTIC HINGE AT NODE 37

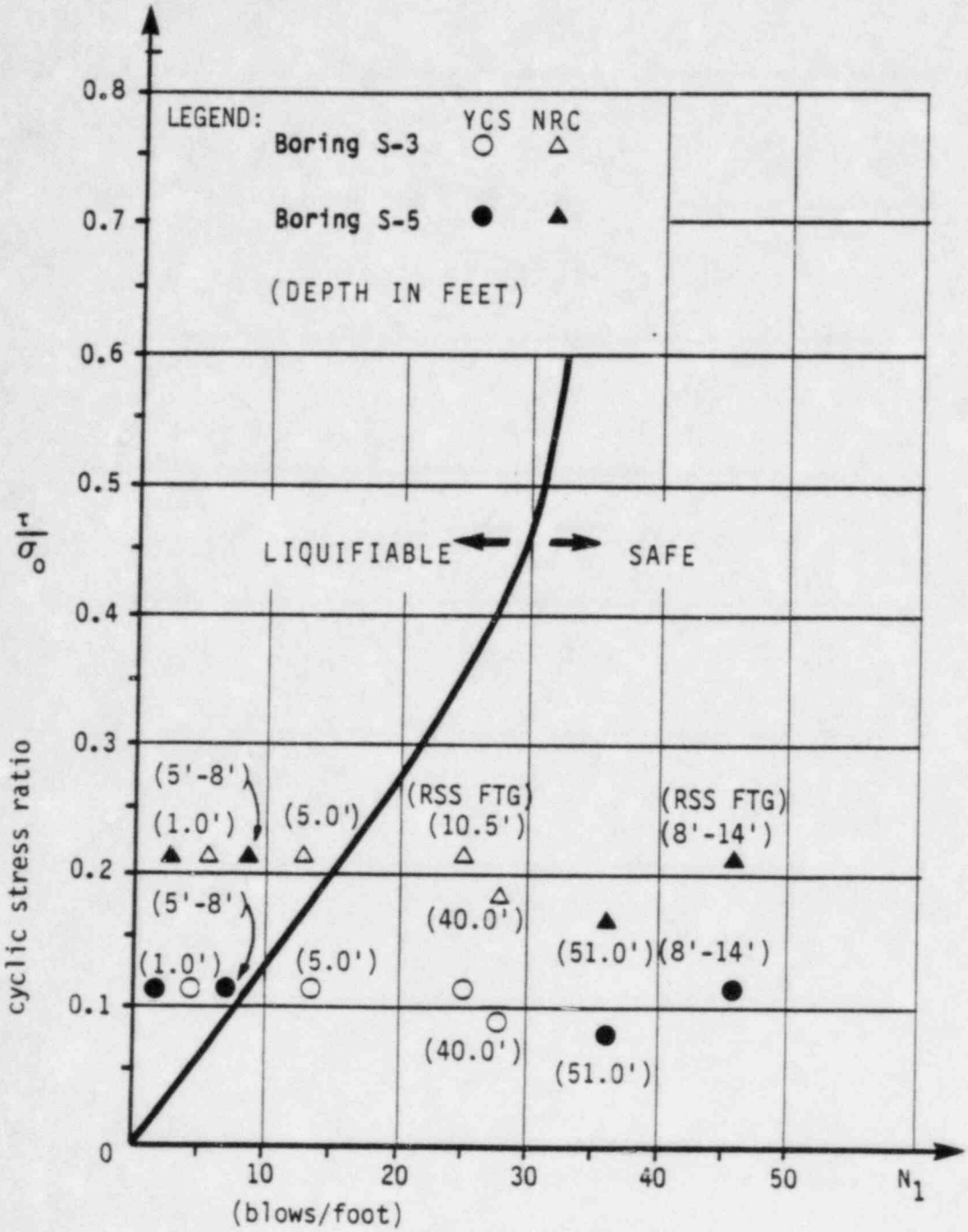

FIG. E. 37
LIQUEFACTION POTENTIAL - YANKEE ROWE NUCLEAR POWER STATION
WATER TABLE AT GROUND LEVEL

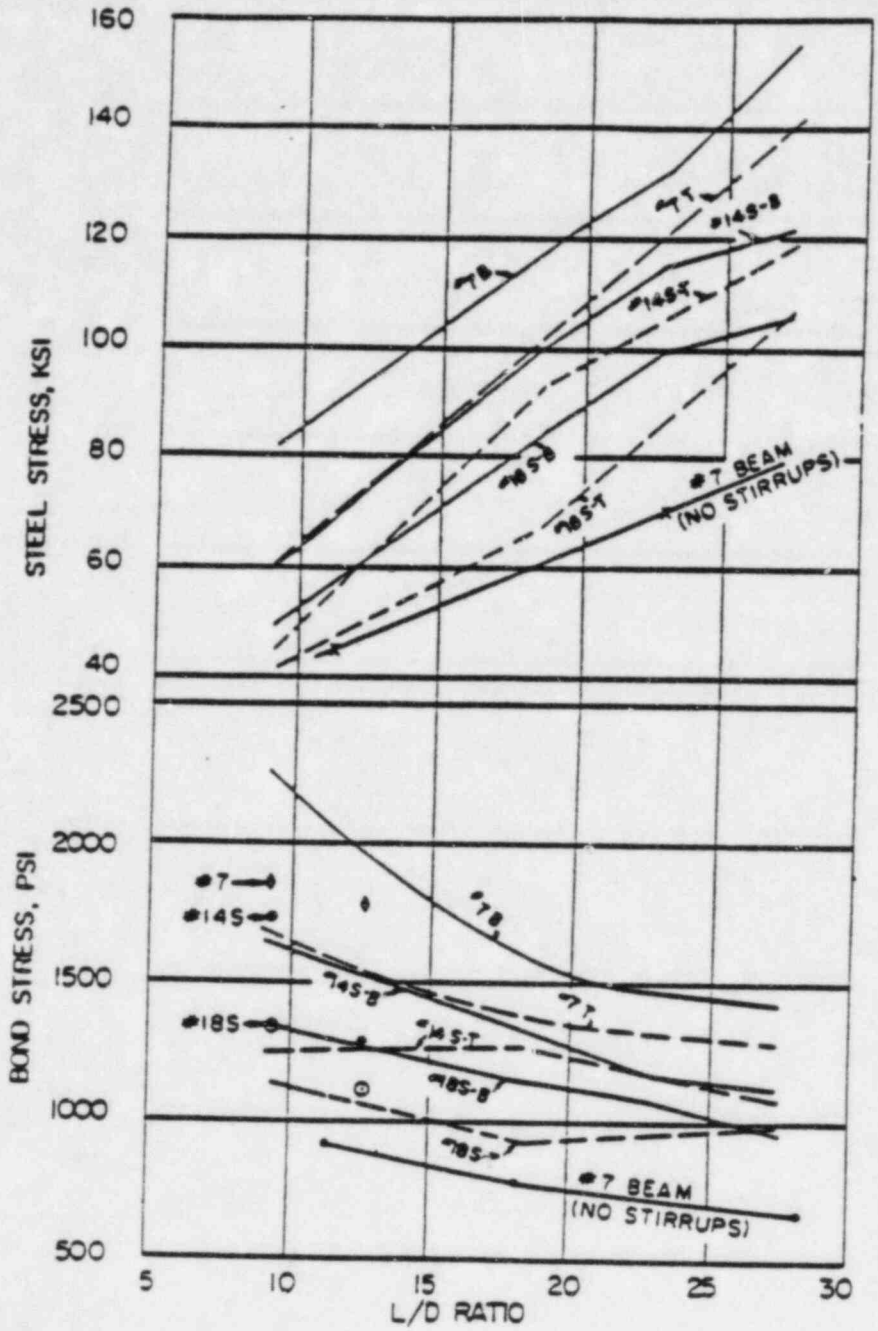

FIG. E. 38 ULTIMATE BOND AND STEEL STRESSES (f_c = 3750 psi) [12]

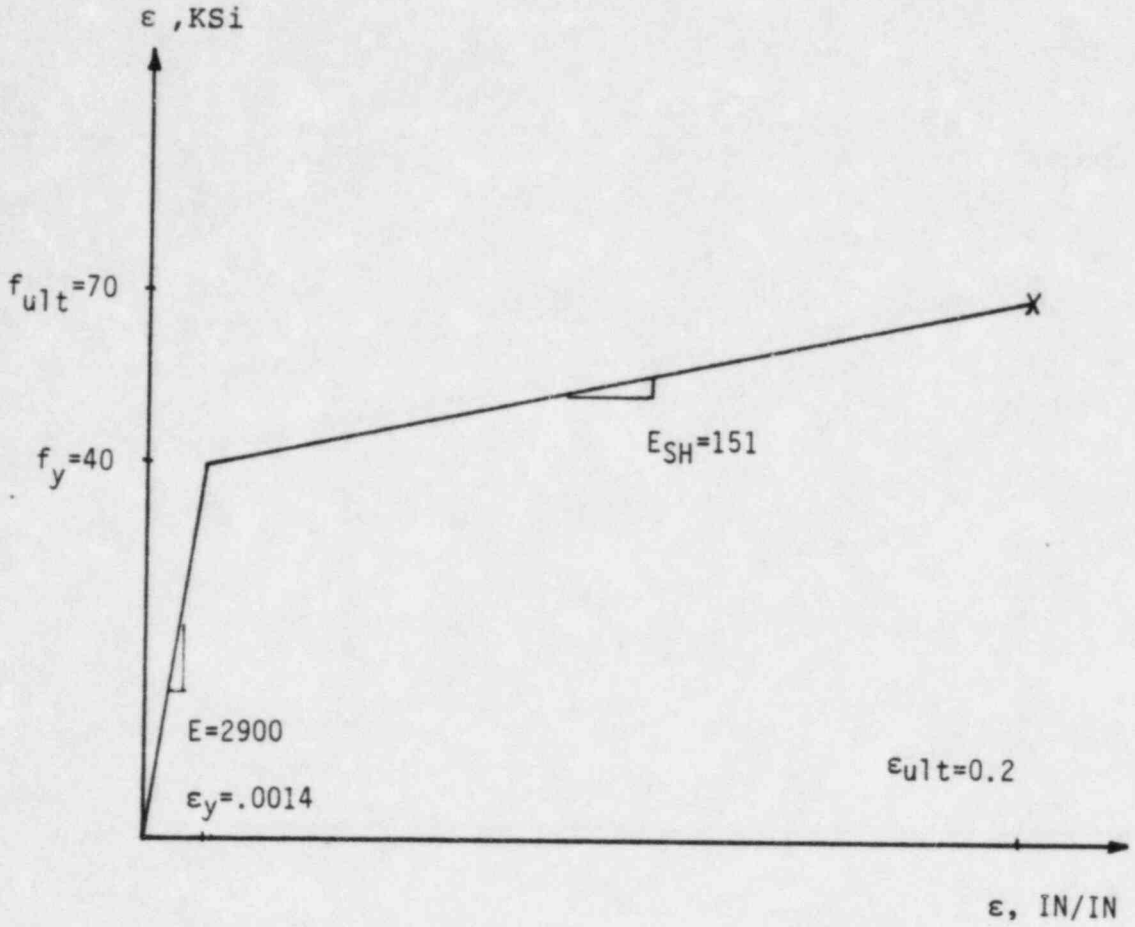

FIG. E. 39 DOWEL BILINEAR STRESS - STRAIN RELATIONSHIP

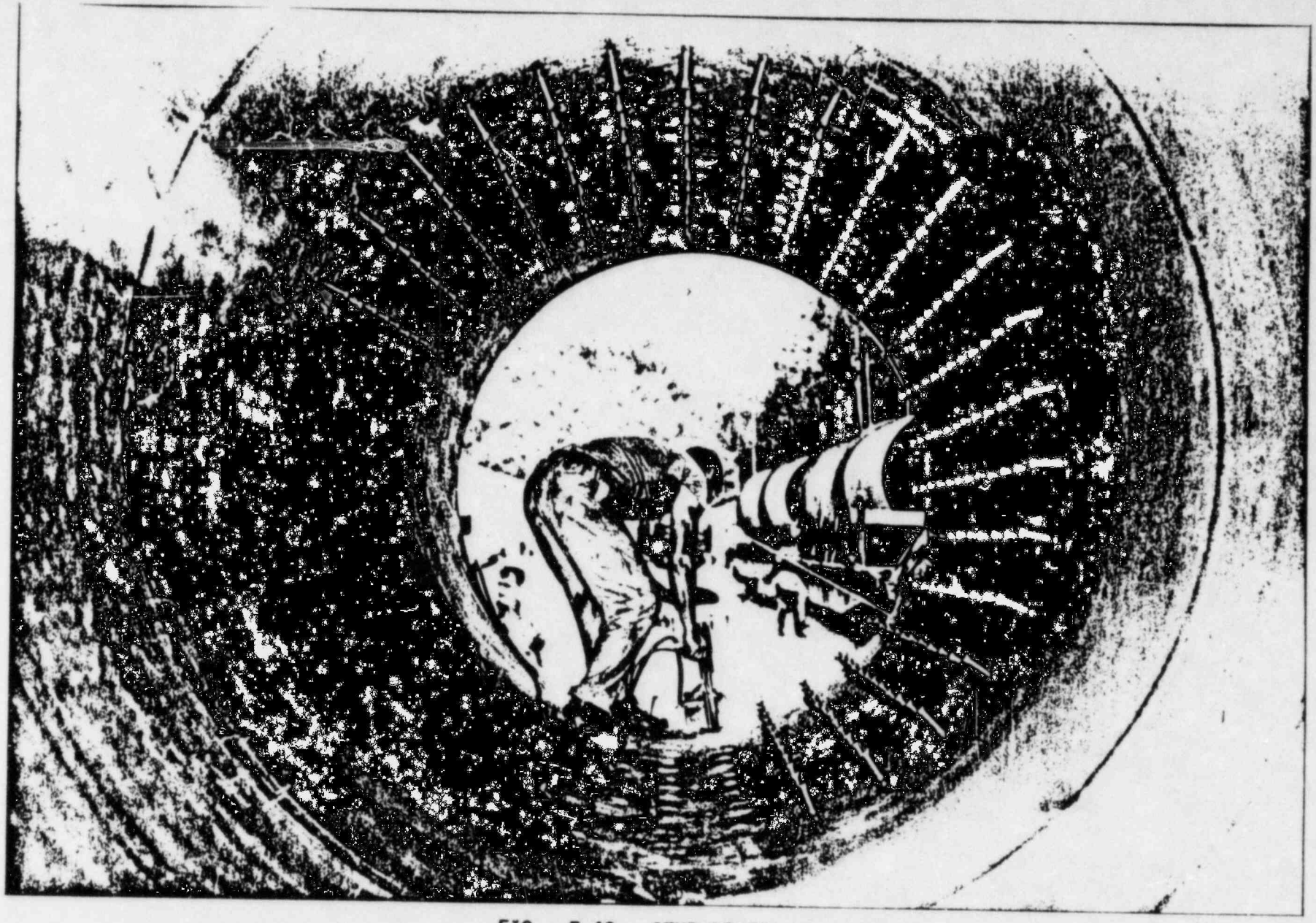

FIG. E.40 STUD BOLTS

APPENDIX F

PLOTS OF AMPLIFIED RESPONSE SPECTRA

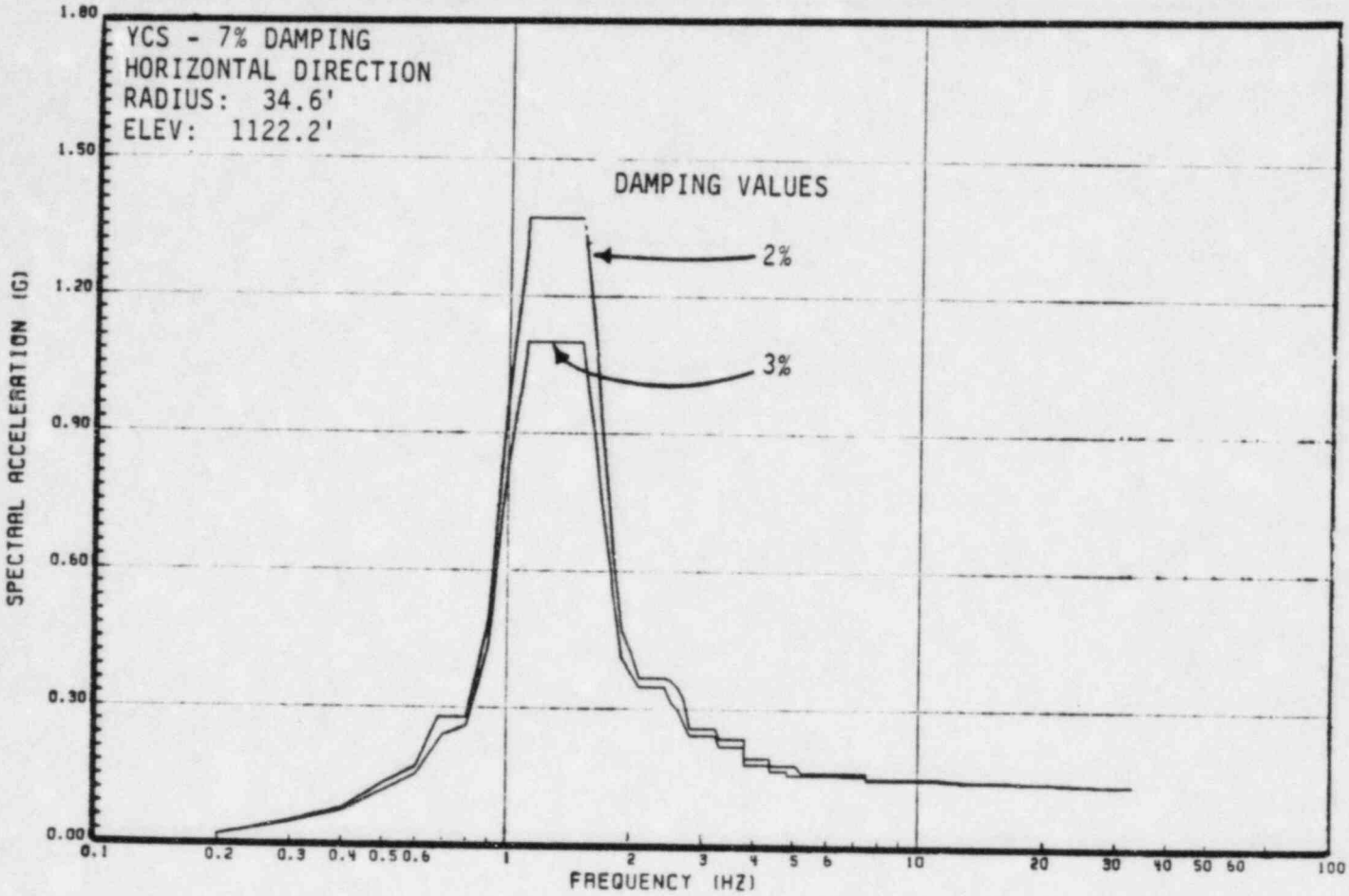

FIG. F.1 HORIZONTAL ARS AT ELEV. 1122.2' OF RSS DUE TO YCS

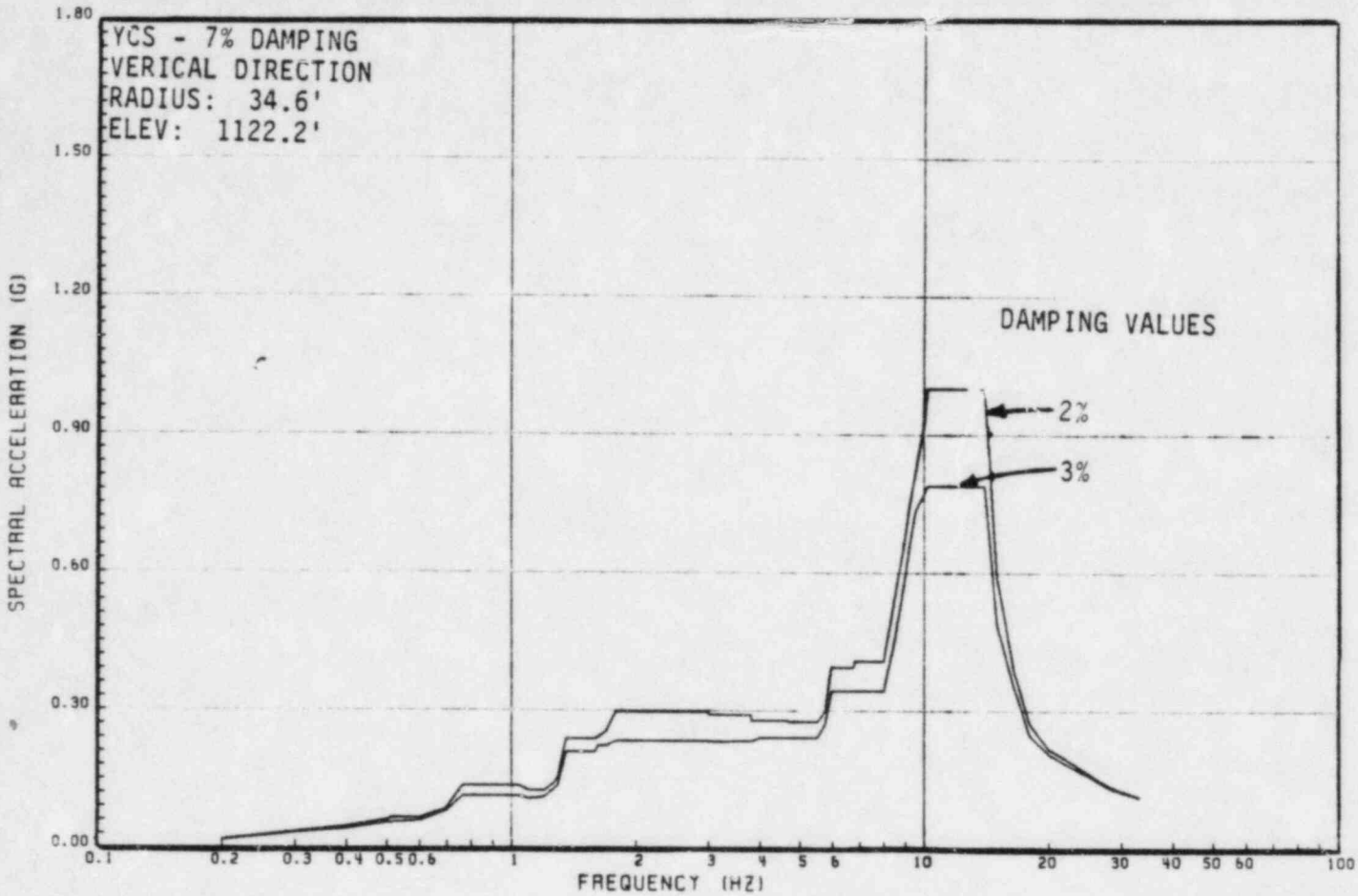

FIG. F.2 VERTICAL ARS AT ELEV. 1122.2' OF RSS DUE TO YCS

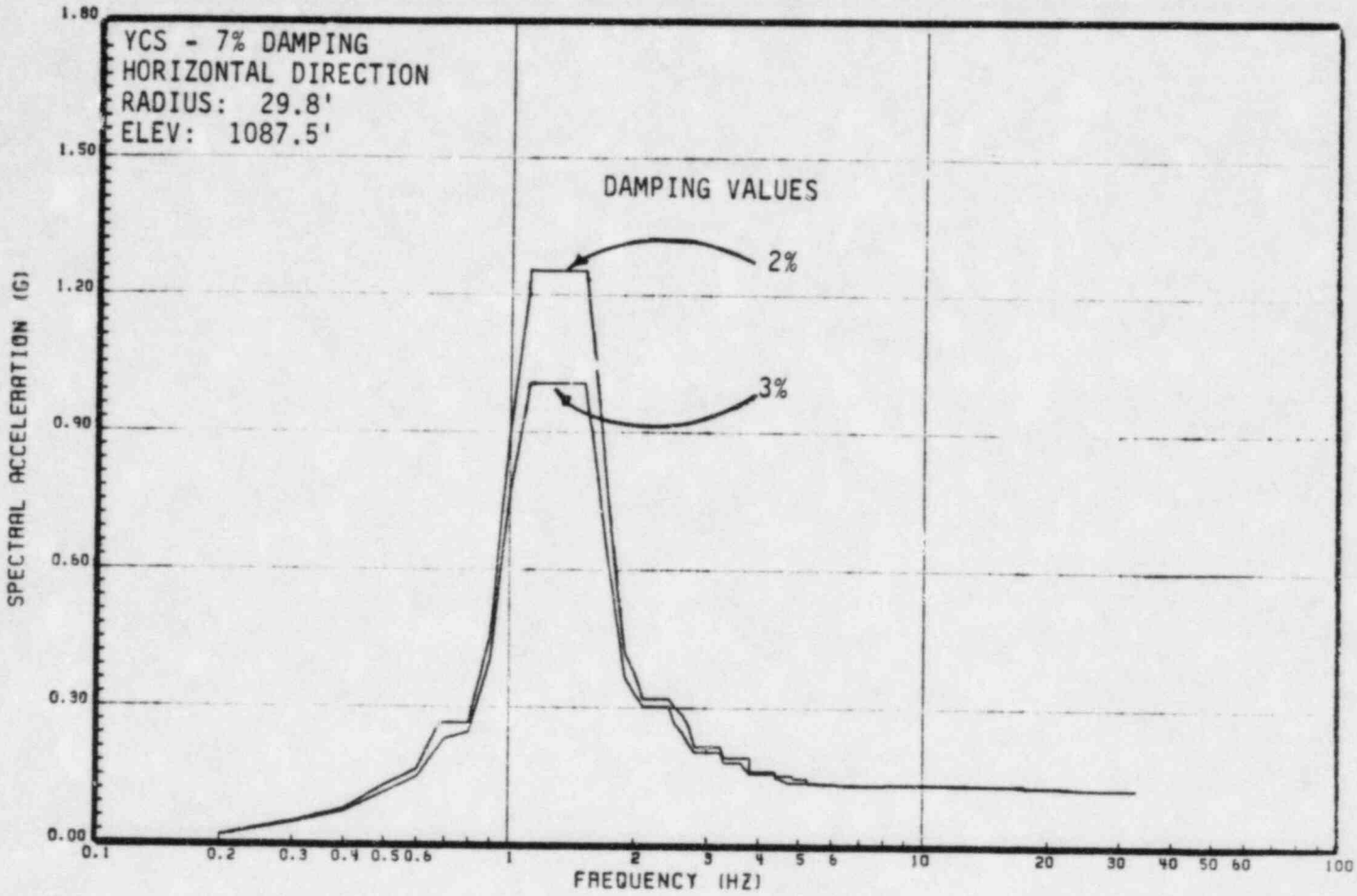

FIG. F.3 HORIZONTAL ARS AT EL. 1087.5' OF RSS DUE TO YCS

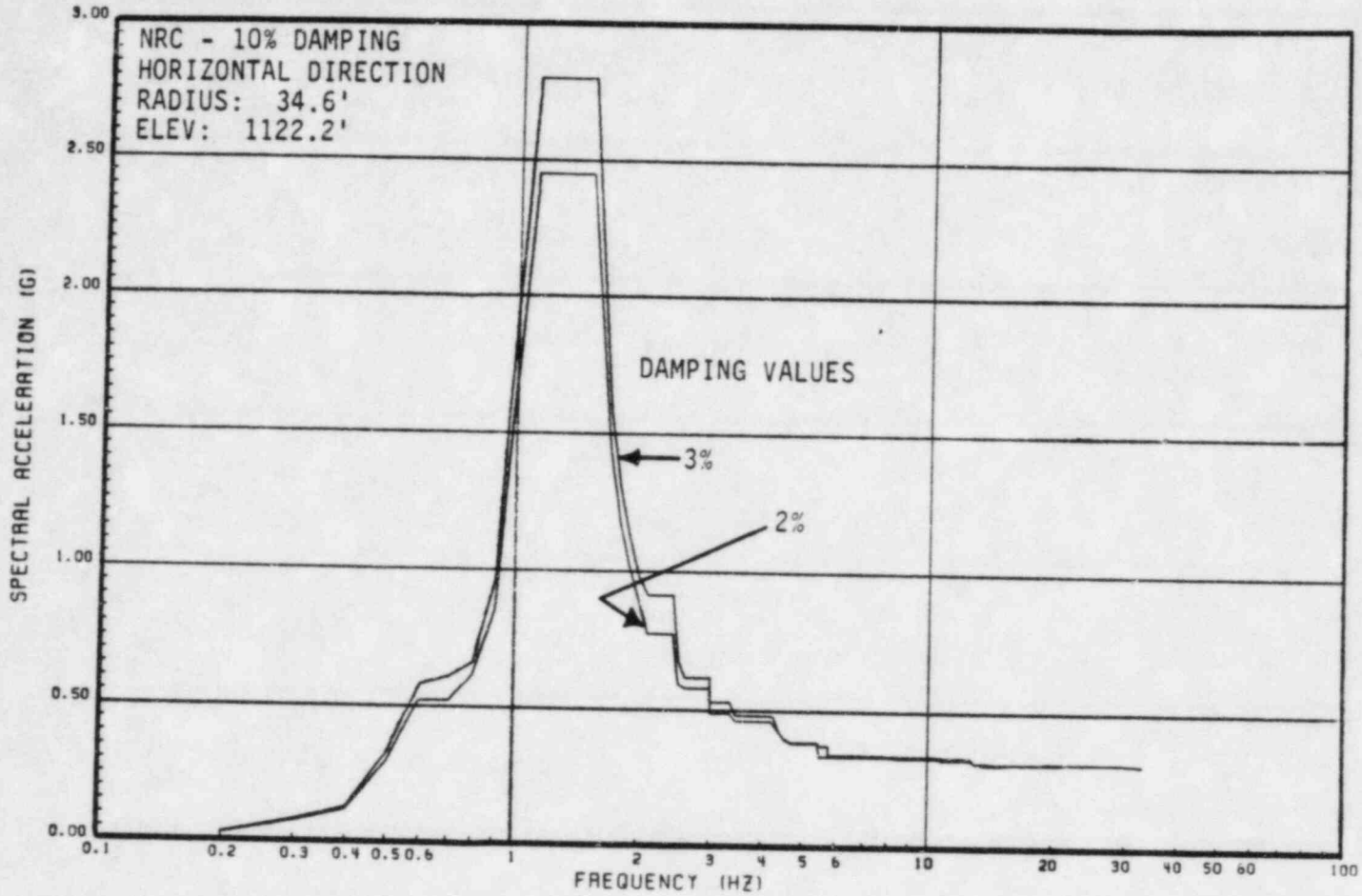

FIG. F.4 HORIZONTAL ARS AT ELEV. 1122.2'

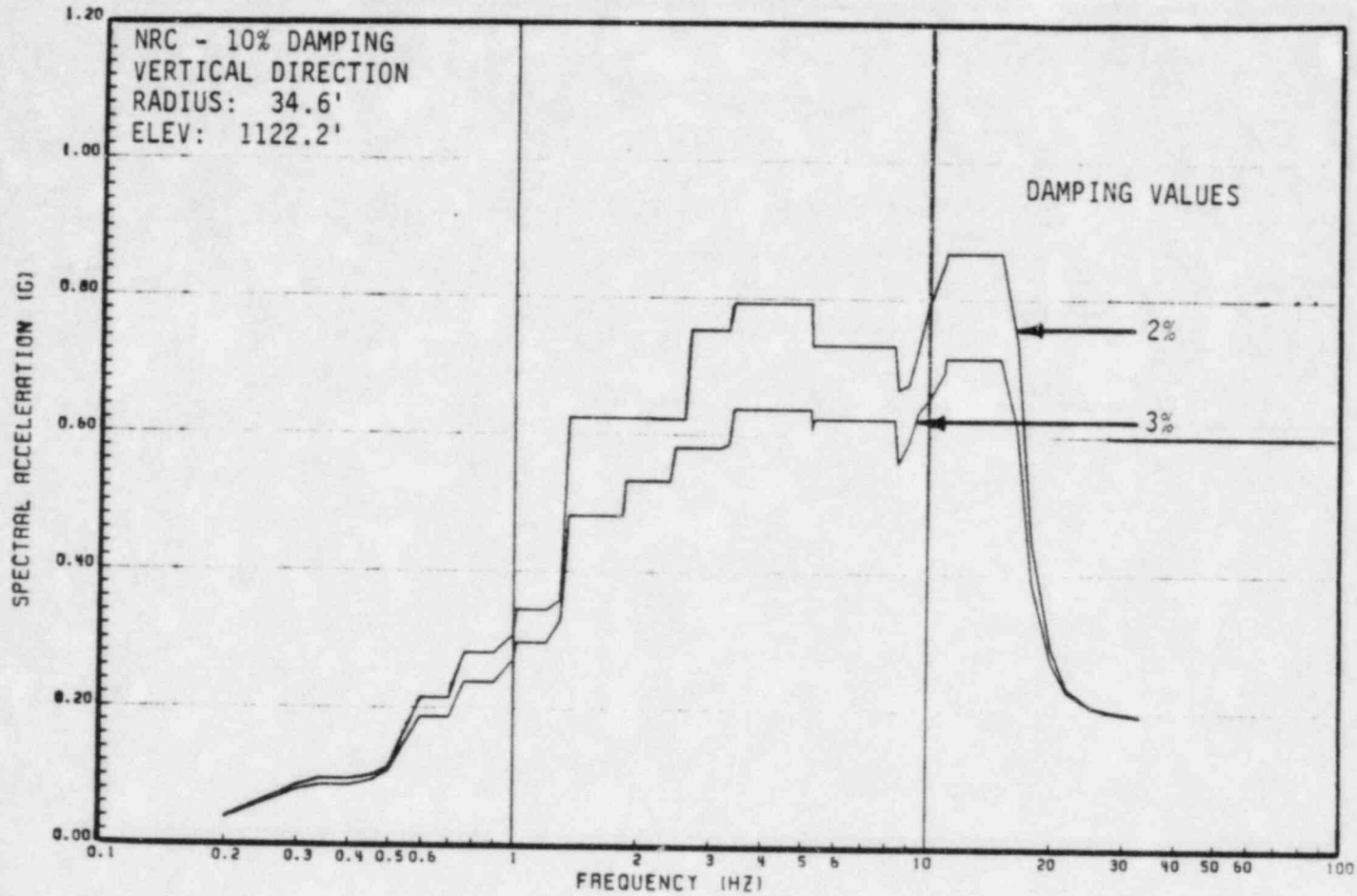

FIG. F.5 VERTICAL ARS AT ELEV. 1122.2'

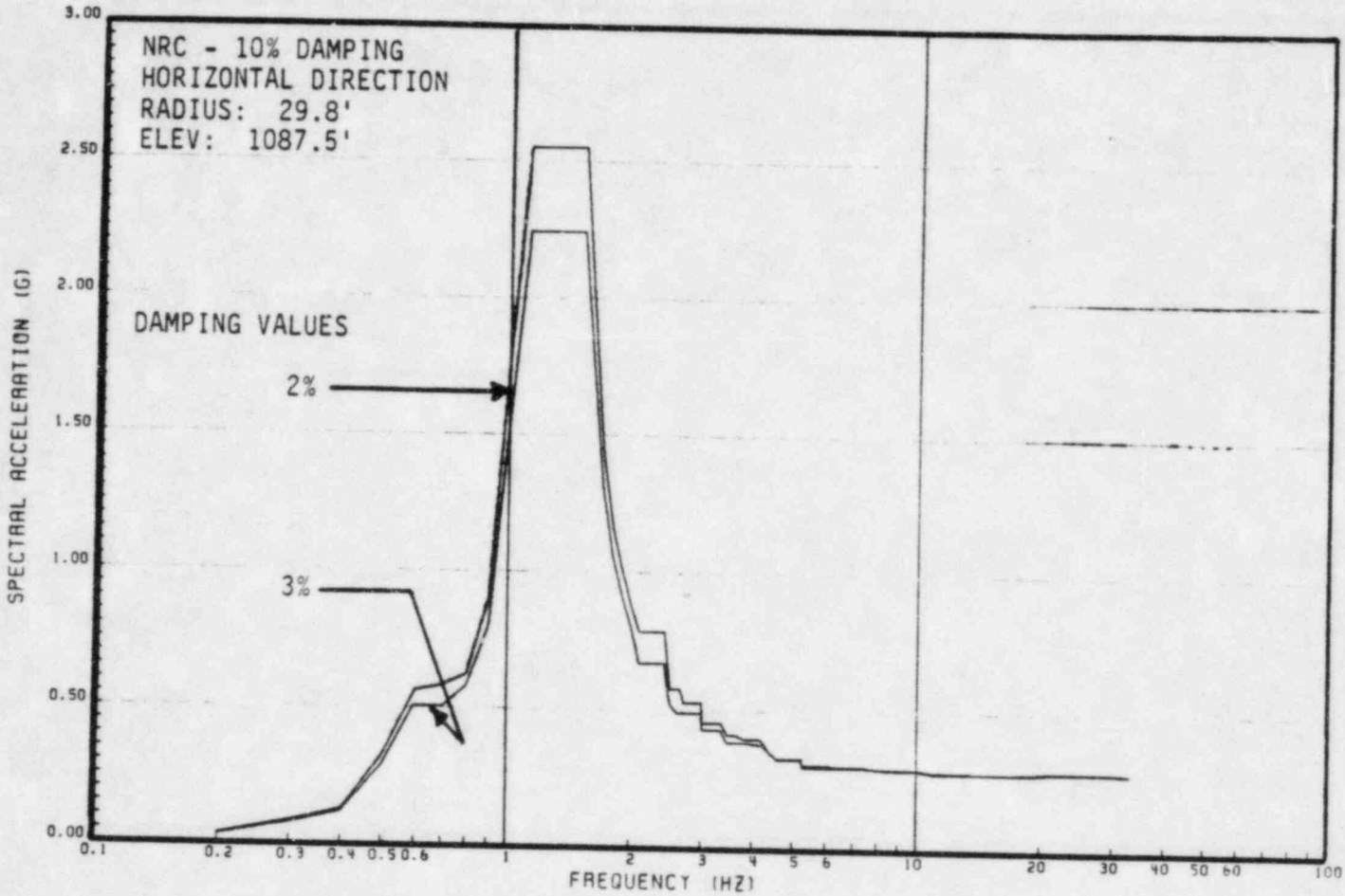

FIG. F.6 HORIZONTAL ARS AT ELEV. 1087.5'

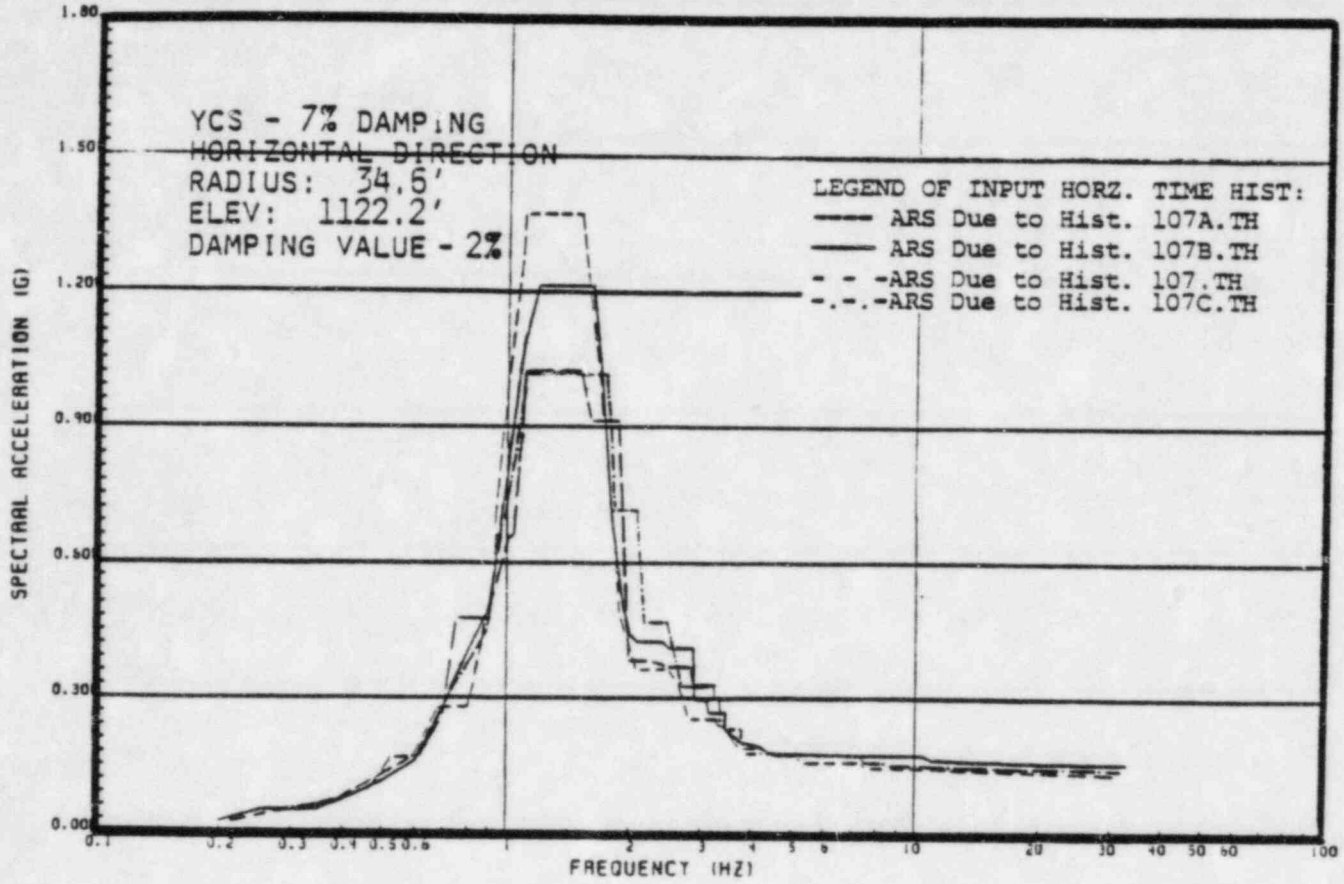

FIG. F.7 COMPARISON OF RESPONSE SPECTRA

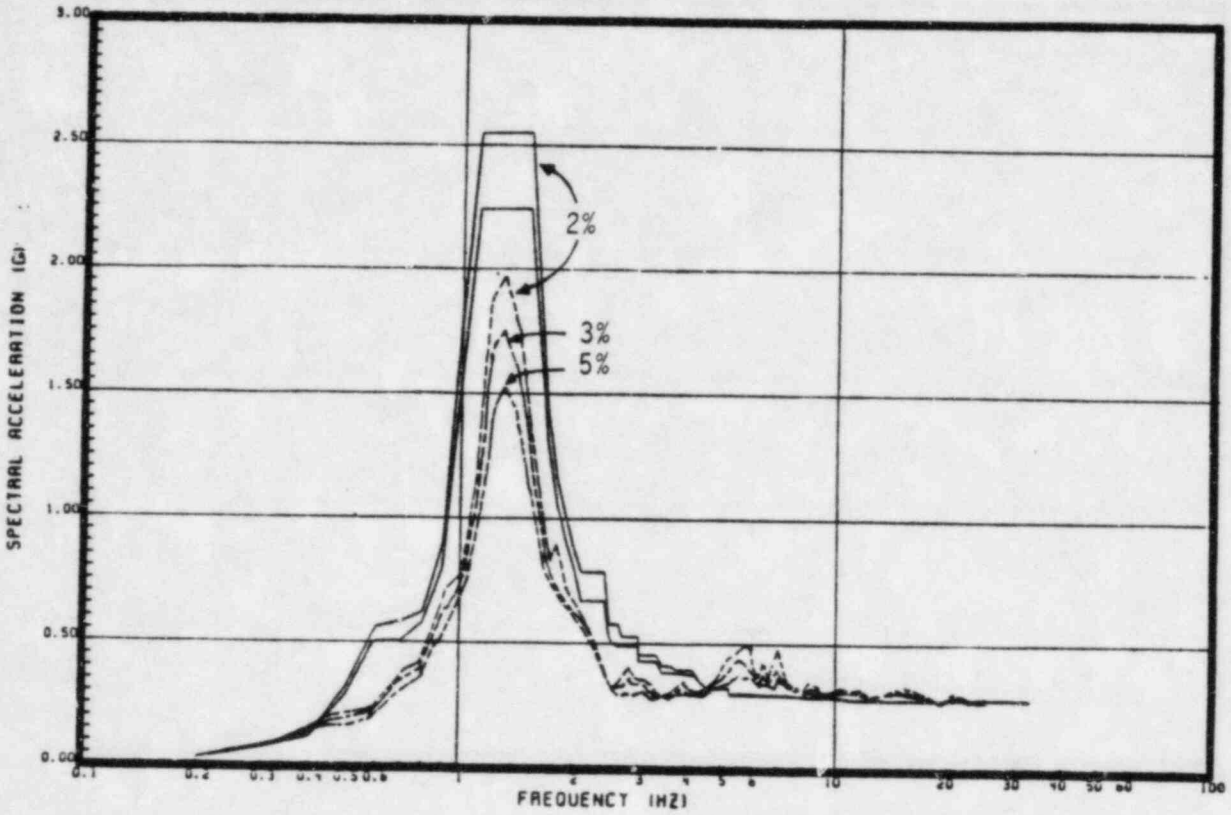

—— LLL/TERA -10% Damping Linear Analysis

------ Artificial Time History 7% Damping Nonlinear Analysis

FIG. F.8 HORIZONTAL ARS AT ELEV. 1087.5'

APPENDIX G

REFERENCES

APPENDIX G

REFERENCES

1. "Seismic Reevaluation and Retrofit Criteria for Yankee Nuclear Power Station, Rowe, Massachusetts," Cygna Energy Services, August, 1982.

2. Newmark, N.M., and W.J. Hall, "Development of Criteria for Seismic Review of Selected Nuclear Power Plants," NUREG/CR-0098, May, 1978.

3. Newmark, N.M., and E. Rosenblueth, "Fundamentals of Earthquake Engineering," Prentice-Hall, Inc., Englewood Cliffs, NJ, 1971.

4. Manin, S.A., and V.V. Bertero, "RCCOLA, A Computer Program for Reinforced Concrete Column Analysis," Department of Civil Engineering, University of California at Berkeley, August, 1977.

5. DeSalvo, G.J., and J.A. Swanson, "ANSYS Engineering Analysis System, Users Manual," Rev. 3, Swanson Analysis Systems, Inc., July 1, 1979.

6. "PRA User's Manual," Earthquake Engineering Systems, Inc., 1979.

7. Ozdemir, H., and P. Lau, "MOST, A Computer Program for Mode Superposition Time-History Analysis," Rev. 2, Earthquake Engineering Systems, Inc., October, 1980.

8. Ozdemir, H., and P. Lau, "INSPEC, A Computer Program for Calculating Spectra," Earthquake Engineering Systems, Inc., November, 1979.

9. DeSalvo, G.J., and J.A. Swanson, "ANSYS Engineering Analysis System, Users Manual," Rev. 4, Swanson Analysis Systems, Inc., February 1, 1982.

10. Kennedy, R.P., "Peak Acceleration as a Measure of Damage," 4th International Seminar on Extreme-Load Design of Nuclear Power Facilities; Paris, France, August 1981.

11. "Bearing Capacity Calculations of Spread Foundations in the Case of Eccentrical and Inclined Application of Load; Recommendations," DIN 4017, September 1970, page 2.

12. Ferguson, P.M., J.E. Breen and J.N. Thompson, "Pullout Tests on High Strength Reinforcing Bars," Journal of the ACI Proceedings, V. 62, No. 8, August 1965.

13 Viwathanatepa, S., E.P. Popov and V.V. Bertero, "Effects of Generalized Loadings on Bond of Reinforcing Bars Embedded in Confined Concrete Blocks," Earthquake Engineering Research Center, University of California, Berkeley, Report No. EERC-79/22, August 1979.

14. Cowell, A.D., E.P. Popov, V.V. Bertero, "Effects of Concrete Type and Loading Conditions on Local Bond Slip Relationships," Earthquake Engineering Research Center, University of California, Berkeley, Report No. VCB/EERC-82/17, September 1982.

15. "Building Code Requirements for Reinforced Concrete," ACI Standard 318-77, Detroit, Michigan.

16. Purchase Order No. LO-49, "Steel Reinforcing Bars for Concrete, Yankee Atomic Electric Plant," February 3, 1958.

17. YAEC letter to Cygna on "Yankee Nuclear Power Station RSS: Soil Mechanics Investigation," January 31, 1983.

18. Stevenson, J.D., "Structural Damping Values as a Function of Dynamic Response, Stress and Deformation Levels," Transactions of the 5th International Conference of Structural Mechanics in Reactor Technology, Session K11, West Berlin, August 1979.

19. Letter to Thomas Cheng of NRC SEP branch on "Bond Stresses, Yankee Nuclear Power Station," by Wiss, Janney, Elstner and Associates, Inc., January 10, 1983.

20. "Liquefaction Potential Evaluation at Yankee Rowe Nuclear Power Station," Report in Preparation, Cygna Energy Services, March 1983.

21. "PCI Design Handbook," Prestressed Concrete Institute, 1971 edition.

APPENDIX H

BOND AND ANCHORAGE OF REINFORCING BARS UNDER CYCLIC LOADINGS - LITERATURE REVIEW

APPENDIX H

BOND AND ANCHORAGE OF REINFORCING BARS UNDER CYCLIC LOADINGS

LITERATURE REVIEW

In general, pull-out tests of deformed bars show that the ultimate bond strength of bars embedded in a block of concrete in which splitting failure is prevented is considerably higher than the ultimate bond strength developed in beam tests. The basic development length values specified by ACI Code 318-71 are based upon the results of beam tests. Ferguson, et al. [H1], reports results of test on No. 14 reinforcing bars, clearly indicating that the bars were able to develop average ultimate bond stresses greater than 1000 psi. The same tests indicate that reinforcing bars having the same lug pattern and lug height as those tested, and having an embedment length of 2'-6" ($\cong$ 17 bar diameter) are able to develop an axial stress considerably higher than 40 ksi without pulling out. Note that test specimens of Ferguson, et al., have a concrete cylinder strength of f'_c = 3750 psi, while the cylinder strength of concrete in the RSS, specified as 4000 psi at 28 days, is believed to have reached about 5500 psi at present. Ferguson, et al., proposed factoring their observed bond and steel stresses by $(f'_c/3750)^{1/2}$ for a concrete strength of f'_c.

While tests of Ferguson, et al., are the only reinforcing bar pullout tests encountered that involve No. 14 bars, there are other tests using smaller diameter bars that may provide information on the behavior of the top dowel sections of the RSS Columns. A review of four of them follows.

Viwathanatepa, et. al. [H2], reports results of tests of 17 specimens of single bars, embedded in well confined concrete, simulating beam reinforcing

bars of beam column connections. Of the 17 specimens tested, 16 were "push-pull" specimens where the reinforcing bar was subjected to push at one end of the bar and simultaneous pull at the other end. In the remaining specimen test, the reinforcing bar was loaded at one end only. Monotonic as well as cyclic loadings were applied to the specimens under "push-pull" loading. Bar sizes No. 6, No. 8, and No. 10 were tested. Embedment lengths were either 15", 20", or 25". For cyclic loading it was found that increasing the load intensity and the number of cycles applied leads to a decrease in strength as well as an increase in displacement of the rebar. Cones form and fracture away at both ends of the specimen, causing a small reduction in the anchored length. The maximum bar stresses for Nos. 6, 8, and 10 bars under cyclic "push-pull" loading were 67, 72 and 68 ksi, respectively.

The only specimen tested under "push-only" loading was subjected to a monotonic load. Viwathanatepa's study does not include tests on specimens acted upon on only one side and subjected to cyclic conditions similar to those in the RSS.

The investigation started by Viwathanatepa, et al. was continued on specimen of similar properties by Cowell [H3] at the University of California at Berkeley. Cowell reports results of one test specimen subjected to cfull-reversal cyclic loading applied at one end only. While the recorded portions of the investigation do not include intensive loading it is reported that unrecorded loading well into the inelastic range was performed without significant bond degradation or failure.

Hassan and Hawkins [H4] report tests involving high intensity cyclic loading of No. 10 reinforcing bars in 13 specimens simulating beam-column connections. Bending moments simulating column and beam moments also acted on the specimens. The displacement causing pull-out of the bar under monotonic loading corresponds to a displacement ductility ratio of more than 10 for the simulated beam-column connection. Under cyclic conditions with full

reversals, specimens were found to sustain displacement ductility ratios of about 5 for at least four reversals. The response of the bar proved to be sensitive to the loading history. The worst deterioration of anchorage was obtained by applying cycles of load reversal that produced equal displacements of the bar end for both pull and push.

Based on their test results, Hassan and Hawkins developed an empirical relationship between the failure of anchorage of the reinforcing bar and the load history applied to the bar. Load history is defined by the number of inelastic half cycles, and history of applied displacement ductility ratios.

Morita and Kaku [H5] postulate that large bar diameter and the existence of transverse shear results in earlier bond failure. Tests were performed on 38 specimens using 2" nominal diameter deformed bars. The test arrangement was such that the stress distribution existing in the shear zone of beams was simulated. Specimens were subjected to either monotonic or cyclic loading with reversals. They concluded that cyclic reversals seemed to have little influence on bond deterioration. Cyclic specimens behaved in a ductile manner provided that excessively high shear stresses did not exist in that concrete.

References

[H1] Ferguson, P.M., J. E. Breen and J. N. Thompson, "Pullout Tests on High Strength Reinforcing Bars," Journal of the ACI Proceedings, v.62, No. 8, August 1965.

[H2] Viwathanatepa, S., E. P. Popov and V. V. Bertero, "Effects of Generalized Loadings on Bond of Reinforcing Bars Embedded in Confined Concrete Blocks," Earthquake Engineering Research Center Report No. EERC-79/22, University of California, Berkeley, 1979.

[H3] Cowell, A., "Results of Test of a No. 8 Reinforcing Bar Embedded in Concrete and Subjected to Axial Cyclic Loading with Reversals," Personal Communication, 1981.

[H4] Hassan, F.M. and N.M. Hawkins, "Anchorage of Reinforcing Bars for Seismic Forces," ACI Special Publication SP-53-5, 1978.

[H5] Morita, S. and T. Kaku, "Splitting Bond Failures of Large Deformed Reinforcing Bars," Journal of the ACI Proceedings, V. 76, No. 1, January 1979.